Programmable multistage drug delivery to lymph nodes

Supplementary Materials and Methods

Chemicals

Pluronic F127, hydroxyethylpiperazineethanesulfonic acid (HEPES) (Sigma), 2,2'-dipyridyl disulfide (Aldrithiol-2, Aldrich), fluorescamine, 0.5 M NaOMe in methanol, propylene sulfide, 1,8-diazabicyclo[5.4.0]undec-7-ene (DBU), Tris(2-carboxyethyl)phosphine hydrochloride (TCEP·HCl), iodoacetamide, potassium hydroxide, CaH_2 (Aldrich), dithiothreitol (DTT) (Biorad), Sepharose CL-6B (Sigma), Ellman reagent (Pierce), cysteamine hydrochloride, potassium carbonate, mercaptopropionic acid methyl ester, triphenylphosphine, acetic acid, methanesulfonyl chloride, sodium hydroxide, potassium thioacetate (KTA), pentaerythritol tetrabromide (PTB), N-(3-dimethylaminopropyl)-N′-ethylcarbodiimide (EDC), N-hydroxysulfosuccinimide sodium salt (sulfo-NHS), sodium sulfate, and morpholineethanesulfonic acid (MES) (Calbiochem) were used as received. Diethyl ether, methanol, dimethylformamide (DMF), dichloromethane, and toluene were used as received and were dried over molecular sieves. Dimethyl acetylenedicarboxylate (DMAD) was purified prior to use by passing a 50% (v/v) solution in CH_2Cl_2 through a column of normal phase silica gel (60 mesh), eluting with CH_2Cl_2 and condensing under reduced pressure. Water was distilled twice using a Milli-Q water system. Unless specified otherwise, all reactions were performed under argon atmosphere.

Compound characterization

Compound purity and identity were assessed by NMR and high-resolution mass spectroscopy (HRMS). High-resolution mass spectra (HRMS) measurements were obtained on an Agilent 6230 LC-TOF mass spectrometer in positive ion mode by direct infusion of samples in MeCN. Routine mass spectra were obtained on an Advion Compact Mass Spectrometer (G1946D) ESI-MSD instrument, using direct sample infusion followed with 9:1 CH_3CN:H_2O containing 0.1% formic acid as mobile phase. ^{1}H and ^{13}C NMR spectra were recorded on Varian-400 MHz, or Bruker AMX-400 DRX-500 spectrometers at either 298 K or 338 K in deuterated solvents, and are presented in ppm, referencing to signals of residual protium in the NMR solvent, unless specified otherwise.

Propylene sulfide polymerization initiator synthesis

Initiator *S*,*S*'-(2,2-bis((acetylthio)methyl)propane-1,3-diyl) diethanethioate was synthesized by reaction between KTA (278 mmol., 2.2 equiv) and PTB (31 mmol,) in DMF (150 mL) at 25^{o}C. After 60 hours of reaction the solution was concentrated under vacuum and then dissolved in CH_2Cl_2. The CH_2Cl_2 solution was rinsed with water and then dried with sodium sulfate and filtered. The solution was again concentrated under vacuum and the initiator was recovered by recrystallization in methanol. (10.1 g obtained, 87% yield).[1] ^{1}H NMR (400 MHz, $CDCl_3$) δ 3.03 (s, 8H, –C**H$_2$**–), 2.35 (s, 12H, –C**H$_3$**).

Carboxylate-Pluronic F127 Synthesis

Carboxylate-Pluronic F127 was synthesized as previously reported.[2] Briefly, Pluronic F127 (1.86 mmol) was activated with methanesulfonyl chloride (18.6 mmol, 10 equiv) in toluene (volume) with triethylamine (18.6 mmol). The solution was filtered, concentrated under vacuum, and then precipitated in ether. The Pluronic mesylate (1.65 mmol) was then reacted with mercaptopropionic acid methyl ester (16.5 mmol, 10 equiv) in DMF (100 mL) with potassium carbonate (16.5 mmol, 10 equiv). The solution was cleaned with activated carbon, filtered, concentrated under vacuum, and then precipitated in ether. The Pluronic thioether methyl propionate was then hydrolyzed with sodium hydroxide in water (14.1 mmol, 5 mL), dialyzed (against 5 L Milli-Q), and then lyophilized to provide Pluronic F127 carboxylate (12.2 g, 95% yield). ^{1}H NMR was 95%. NMR ($CDCl_3$): δ = 3.59−3.63 (m, CH_2, PEG), 3.46−3.58 (m, CH_2, PPO), 3.35−3.44 (m, CH, PPO), 2.83 (t, *J* = 6.4 Hz, -O-CH_2-C<u>H</u>$_2$-S-), 2.73 (t, *J*= 6.8 Hz, -S-C<u>H</u>$_2$-CH_2-CO-), 2.50, (t, *J* = 6.8 Hz, -CH_2-CO-), 1.13−1.16 (CH_3, PPO).

Pyridyl disulfide cysteamine HCl salt synthesis

Pyridyl disulfide cysteamine HCl salt was synthesized as previously reported.[2] Briefly, cystemaine HCl (0.5 mmol) was reacted with aldrithiol (15.0 mmol, 30 equiv) in methanol (10 mL), precipitated in ether and then dried to yield pyridyl disulfide cysteamine HCl salt. ^{1}H NMR (DMSO-d_6): δ = 8.51−8.50 (m, 1H), 8.30 (bs, 3H), 7.86−7.82 (m, 1H), 7.75 (d, 1H), 7.31−7.28 (m, 1H), 3.13−3.05 (m, 4H). HRMS $[M + H]^+$ calculated for $C_7H_{10}N_2S_2$ 187.0364, found 187.0358.

Pyridyl disulfide NP (PDS-NP) synthesis and stability

Pluronic pyridyl disulfide were created *in situ* on the NPs post synthesis. The pH of the aqueous solution of Pluronic F127 carboxylate NP was brought to pH 6-7 (adjusted with 10x PBS buffer and 2N HCl) and then 100 mg of iodoacetamide was added to cap the core thiols. Following core thiol capping MES was added to a final concentration of 100 mM and pH of 4-5. 180 mg of NHS was added along with 180 mg of pyridyl disulfide cysteamine HCl salt, and followed by 150 mg of EDC. The PDS-NP solution was then dialyzed against 4x5 L of Milli-Q water.

Dynamic light scattering

Data were obtained on a Malvern Nanoseries Zetasizer instrument using polystyrene cuvettes by diluting NP solutions 1:20 with PBS (10 mM, pH 7.4). Sizes are given in nanometers and are obtained as the Z-average by fitting the correlation function using the cumulant method.

Transmission electron microscopy

5 µL of undiluted, post-synthesis NP solution was placed onto carbon coated 400 mesh copper grids (Agar Scientific, Stansted, U.K.). After 60 s, the grid was washed with water and then 5 µL of 2% phosphotungstic acid was added for 45 s. After 30 s, the stain was removed and allowed to dry for 5 min at room temperature before analysis. Microscope images were acquired on a Tecnai G2 F30 S-TWIN 300 kV (Thermo Fisher Scientific, MA, USA). Images were captured using a Gatan OneView 4K camera (Gatan Inc., Grandchamp, France) and processed using Adobe Photoshop software (Adobe

Systems, San Jose, CA). TEM images were analyzed with Scion image analysis software.

OND linker conjugation design

OND linkers undergo relatively rapid Michael addition with thiols to produce adducts that fragment at predetermined rates by a retro-Diels-Alder mechanism (Figure 1a, main text). In previous work, we identified a number of control elements that enable programmability of adduct half-lives by changing functional groups that are present on the OND (Figure 1a). These functional group modifications vary in the strength of their effect on adduct stability, producing a range of adduct half-lives that can be tuned to meet the requirements of a given system (Figure 1a).[3-5] For example: epoxidation of the electron-rich alkene produces thiol-reactive 5,6-epoxyoxanorbornenes, EONB (**5-Dn**) that do not undergo retro-Diels-Alder fragmentation, and which we have used as a non-cleavable control in the present study.

Fluorogenic Dansyl (Dn) modified OND **1-5** were reacted with free thiols on NP to determine their conjugation efficiency and reaction rate. Conjugation of Dn-modified OND to NP was monitored by following the increase fluorescence emission (ex. = 345 nm, em. = 510 nm) over the course of the reaction (Figure 1d).[5, 6] Reactions were performed at OND:thiol mole ratios ranging from 1:3.5 to 1:28, giving the average observed reaction rates for each of the OND variants (Supplementary Table 1). As expected, based on our previous work, OND derivatives exhibited somewhat different rates of conjugate addition. Second order rate constants ranging between 5–61 $M^{-1}s^{-1}$ were observed, with 1,4-dialkyl OND **1** and trifluoromethylated **4** providing the slowest

and fastest rates of addition, respectively.[3-6] However, the reaction rates of all OND were sufficiently fast such that loading of NP was achieved in under an hour at room temperature, demonstrating that this loading approach should be applicable to a wide variety of biological applications. Following conjugation of the OND to NP, the release rates of model Dn-furan cargo from the NP-OND-Dn conjugates were determined. This was achieved by dialyzing the NP-OND-Dn adducts at 37°C against PBS and monitoring the fluorescence emission of the dialyzed sample at 510 nm over time. By following the loss of fluorescence from the dialyzed adduct solution, the fragmentation rates of OND-Dn-NP adducts were determined (Figure 1e). The rapidly fragmenting OND **1** presented a challenge since the dialysis rate of free cargo was on a similar time scale as the fragmentation of adducts of this derivative. In order to accurately capture the fragmentation rate of adducts of **1**, a solution of NO-OND-**1** was incubated at 37°C and small samples were periodically drawn and separated using size exclusion chromatography. The NP-OND-**1** fractions were collected and the fluorescence emission measured at 510 nm.

Supplementary Table 1. Rate constants for conjugate addition and fragmentation of dansyl (Dn) OND conjugates.

Electrophile	k_{con} ($M^{-1}s^{-1}$) [a]	k_{rDA} (x 10^{-4} min^{-1}) [b]	$t_{1/2}$ (hours) [c]
1-Dn	4.3 ± 0.2	411 ± 41	0.28 ± 0.03
2-Dn	29.3 ± 2.6	46.5 ± 4	2.48 ± 0.21
3-Dn	34.9 ± 3.9	11.7 ± 1.1	9.86 ± 0.91
4-Dn	47.4 ± 3.5	4.01 ± 0.87	28.8 ± 6.2
5-Dn	19.9 ± 5.4	0 [d]	

(a) Rate constants for conjugate addition to PPS NPs measured at room temperature. (b) Rate constants for retro-Diels-Alder reactions of the NP-OND conjugates, measured at 37 °C. (c) Calculated from the observed first-order rate constant at 37 °C as $t_{1/2} = \ln(2)/60k_{retro\text{-}Diels\text{-}Alder}$. (d) The small loss of fluorescence for **5-Dn** shown in Figure 1e derives from a combination of processes not involving retro-Diels-Alder fragmentation, such as dye bleaching and loss of particles in the experimental manipulations.

The OND variants exhibited the predicted wide range of half-lives from 23 min for **1**, up to a nearly permanent linkage for **5** (Extended Data Figure 1). Derivative **2** achieved release rates between those attainable with linkers **1** and **3**. Conjugate addition between NP and small molecule thiol proceeded readily for this derivative (k_{obs} = 21.1 ± 5.0 $M^{-1}s^{-1}$). In contrast to **1**, which provides predominantly the 3-exo-syn

Michael adducts, we observed two groups of products separable by chromatography on silica gel after reaction of **2** with β-mercaptoethanol.

Synthesis and characterization of OND derivatives

OND electrophiles **1**-Dn, **3**-Dn, **4**-Dn, **S1**, and **S7**, furan precursor **S6**, and rhodamine B derivative **S9**[7] and 3-azido-coumarin **S13**[8] were prepared according to literature procedures, and have been characterized previously.[4-6] In general, OND electrophiles were prepared by Diels-Alder reaction of substituted furans (1 equiv) and a slight excess (1.3 equiv) of the appropriate electron-deficient acetylene in minimal solvent at 60°C. With the exception of 5-Dn, all Dn-modified ONDs were prepared by Diels-Alder reactions between electron deficient acetylenes and N-dansyl(methylfurfuryl)amine derivatives. In the case of **5**-Dn, epoxidation of a *t*-butyl-carbamate protected OND to form the epoxyoxanorbornene EONB preceded installation of the Dn group to avoid oxidation of the fluorophore. For rhodamine (Rhod)- and coumarin (Coum)-modified electrophiles, conjugation of xanthene and coumarin dyes was performed after the formation of OND-electrophiles using amide coupling and copper-catalyzed azide-alkyne “click” chemistry, respectively. Details for the preparation of new OND electrophiles employed in the present study are shown below.

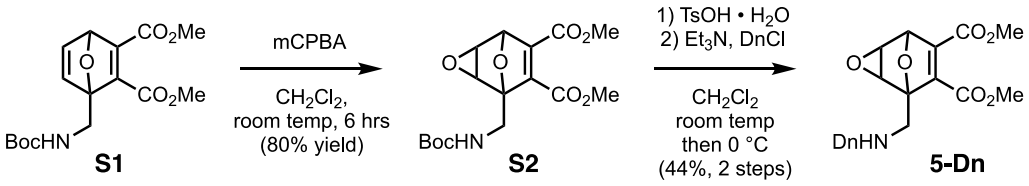

Scheme S1. Synthesis of dansyl-modified epoxyoxanorbornene, **5-Dn**.

Dimethyl 1-(((*tert*-butoxycarbonyl)amino)methyl)-3,8-dioxatricyclo[3.2.1.0^{2,4}]oct-6-ene-6,7-dicarboxylate, S2: The *tert*-butylcarbamate protected epoxyoxanorbornene **S2** was prepared by epoxidation of **S1** (prepared as previously described)[5] with *m*-chloroperoxybenzoic acid (*m*CPBA). Briefly, a solution of **S1** (834 mg, 2.46 mmol) and *m*CPBA (848 mg 70 wt% technical grade, 3.44 mmol, 1.4 equiv) in dichloromethane (5 mL) was stirred at room temperature for 5 h, at which time a precipitate of *m*-chlorobenzoic acid was observed and the OND starting material was consumed, as determined by TLC. The reaction mixture was filtered, and the filtrate was diluted with Et_2O (15 mL). The solution was washed with saturated aq. $NaHCO_3$ (4 x 15 mL), saturated aq. NaCl (15 mL), dried over anhydrous sodium sulfate, filtered, and concentrated under vacuum. The organic extract was dried to constant mass under vacuum to provide **S2** as a white solid (995 mg, >100% yield) that was used in the following step without further purification. R_f 0.26 (40% EtOAc/hexane). ^{1}H-NMR (400 MHz, $CDCl_3$) δ 5.10 (s, 1H), 4.88 (br s, 1H), 3.97 (dd, *J* = 15.1, 7.1 Hz, 1H), 3.87 – 3.72 (m, 9H), 1.43 (s, 9H). ESI-MS ($C_{16}H_{21}NO_8$) 378.1, $[M + Na]^+$.

Dimethyl 1-(((5-(dimethylamino)naphthalene)-1-sulfonamido)methyl)-3,8-dioxatricyclo-[3.2.1.0^{2,4}]oct-6-ene-6,7-dicarboxylate, **5-Dn**: Dansyl-modified epoxyoxanorbornene **5-Dn** was prepared from the *tert*-butylcarbamate-protected **S2** in a two-step, one-pot procedure as follows. **S2** (66 mg, 0.186 mmol, 1 equiv) was dissolved in CH_2Cl_2 (1 mL) at room temperature and *p*-toluenesulfonic acid monohydrate (88.4 mg, 0.464 mmol, 2.5 equiv) was added. The mixture was stirred at room temperature under nitrogen for 8 h, at which time the starting material was completely consumed, as determined by TLC analysis. The reaction mixture was chilled in a dry ice/acetone bath

at approximately -20°C and solid dansyl chloride (75 mg, 0.279 mmol, 75 mg) was added in one portion. Triethylamine (103 µL, 0.739 mmol, 4 equiv) was added dropwise to the chilled reaction mixture while stirring, and the resulting solution was stirred for 4.5 h, allowing the cooling bath to expire during this time. The mixture was then condensed under reduced pressure and purified by column chromatography on silica gel, eluting with a gradient from hexanes through 50% ethyl acetate/hexanes, to provide **5-Dn** as a yellow foam (40 mg, 44% yield over two steps). R_f 0.30 (50% EtOAc/hexanes). ^{1}H-NMR (400 MHz, $CDCl_3$) δ 8.55 (d, *J* = 8.5 Hz, 1H), 8.31 – 8.18 (m, 2H), 7.57 – 7.50 (m, 2H), 7.18 (d, *J* = 7.5 Hz, 1H), 5.23 (dd, *J* = 8.2, 4.7 Hz, 1H), 5.02 (s, 1H), 3.79 (s, 3H), 3.77 (s, 3H), 3.73 (d, *J* = 3.5 Hz, 1H), 3.73 (dd, *J* = 13.6, 8.4 Hz, 1H), 3.59 (d, *J* = 3.6 Hz, 1H), 3.40 (dd, *J* = 13.7, 4.7 Hz, 1H), 2.87 (s, 6H). ^{13}C-NMR (101 MHz, $CDCl_3$) δ 163.03, 161.93, 152.06, 148.46, 147.31, 134.18, 130.81, 129.94, 129.81, 129.62, 128.74, 123.27, 118.67, 115.46, 90.56, 78.65, 57.36, 56.12, 52.96, 52.81, 45.52, 41.29. ESI-HRMS calcd for $C_{23}H_{25}N_2O_8S_1^+$ $[MH]^+$: 489.1326, found: 489.1323.

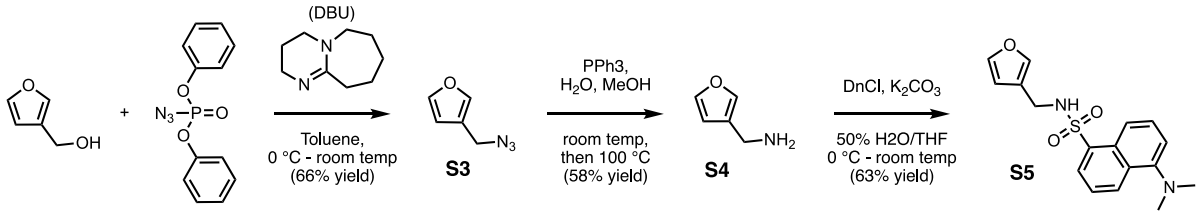

Scheme S2. Preparation of *N*-dansyl-*N*-furan-3-ylmethylamine from 3-hydroxymethylfuran.

3-(azidomethyl)furan, S3: Furan-3-ylmethanol (500 mg, 5.1 mmol, 1 equiv) and diphenyl phosphorylazide (1.318 mL, 6.1 mmol, 1.2 equiv) were dissolved in toluene (15

mL) on ice and 1,8-diazabicyclo(5.4.0)undec-7-ene (DBU, 912 µL, 6.1 mmol, 1.2 equiv) was added dropwise while stirring on ice. The cooling bath was allowed to expire and the reaction was continued at room temperature for 17 h, at which point the reaction was quenched by addition of water (10 mL) and transferred to a separatory funnel. The organic layer was separated and washed with water (10 mL) and aqueous HCl (1N, 10 mL), and then condensed under reduced pressure. The crude product was further purified by column chromatography on silica gel, eluting with a gradient of 0–7% ethyl acetate in hexanes to yield **S3** as a volatile colorless oil (413 mg, 66% yield). Note: this material should not be dried for extended periods under high vacuum. R_f 0.83 (20% EtOAc/hexanes). ^{1}H-NMR (400 MHz, $CDCl_3$) δ 7.46 (app dd, *J* = 1.5, 0.8 Hz, 1H), 7.44 (app t, *J* = 1.7 Hz, 1H), 6.42 (app dd, *J* = 1.9, 0.9 Hz, 0H), 4.20 (s, 1H).

Furan-3-ylmethanamine, S4: 3-(azidomethyl)furan **S3** (323 mg, 2.63 mmol, 1 equiv) was placed in a round bottom flask and stirred without solvent.

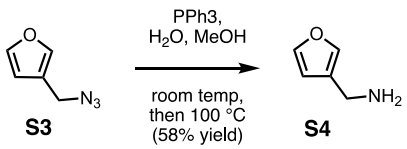

Triphenylphosphine (1 g, 3.8 mmol, 1.45 equiv) was added portionwise while stirring over 1 min and vigorous bubbling was observed within the first 10 sec of addition. Stirring was continued for 1 h, at which point the reaction mixture crystallized. Water (240 µL) and methanol (100 µL) were added, and stirring was continued for 1 h, followed by addition of a reflux condenser and heating at 100 °C for 2 h while stirring. When the reaction was complete, as indicated by TLC (1% NH_4OH in 10% MeOH/CH_2Cl_2), solvents were removed under vacuum and the crude product was purified by column chromatography on silica gel, eluting with a gradient of 0-12% methanol in dichloromethane to provide **S4** as a pale-yellow liquid (147.8 mg, 58%

yield). R_f 0.2 (1% NH_4OH in 10% MeOH/CH_2Cl_2, stains strongly with ninhydrin). ^{1}H-NMR (500 MHz, Methanol-d_4) δ 7.52 – 7.39 (m, 2H), 6.47 (dd, *J* = 1.5, 0.8 Hz, 1H). ^{13}C NMR (126 MHz, MeOD) δ 172.70, 168.98, 154.53, 139.18, 65.07.

5-(dimethylamino)-*N*-(furan-3-ylmethyl)naphthalene-1-sulfonamide, **S5**: 5-(dimethylamino) naphthalene-1-sulfonyl chloride

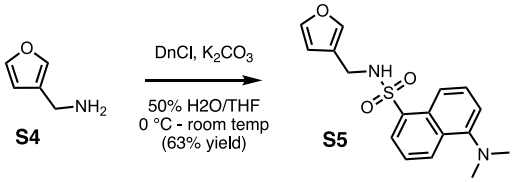

(dansyl chloride (127.9 mg, 0.474 mmol, 1 equiv) was suspended in tetrahydrofuran (0.625 mL) under nitrogen atmosphere at 4 °C and furan-3-ylmethanamine **S4** (46 mg, 0.474 mmol, 1 equiv) in tetrahydrofuran (0.625 mL) was added dropwise over 1 min while stirring. Aqueous potassium carbonate (98 mg, 0.711 mmol, 1.5 equiv in 1.25 mL deionized water) was added dropwise over 1 min and stirring was continued at 4°C, allowing the cooling bath to slowly reach room temperature overnight. The reaction was quenched by addition of deionized water (5 mL) and diethyl ether (6 mL). The layers were separated, and the organic phase was washed with 0.1 N HCl (10 mL), saturated aqueous sodium bicarbonate solution (10 mL), and brine (10 mL), dried over anhydrous sodium sulfate, filtered, and condensed under reduced pressure. The crude was further purified by column chromatography on silica gel, eluting with a gradient from 0–30% ethyl acetate/hexanes to provide a pale-yellow foaming solid (97.8 mg, 63% yield). R_f 0.5 (30% EtOAc / hexane, fluorescent under long-wave UV lamp illumination). ^{1}H NMR (500 MHz, $CDCl_3$) δ 8.53 (d, *J* = 8.5 Hz, 1H), 8.29 (d, *J* = 8.6 Hz, 1H), 8.25 (app dd, *J* = 7.2, 1.3 Hz, 1H), 7.55-7.48 (m, 2H), 7.17 (d, *J* = 7.6 Hz, 1H), 7.15 (d, *J* = 1.8 Hz, 1H), 7.09 (s, 1H), 6.02 (d, *J* = 1.9 Hz, 1H), 5.14 (br t, J = 5.8 Hz, 1H), 3.95 (d, *J* = 6.0 Hz, 2H), 2.88 (s, 6H). ^{13}C NMR (126 MHz, $CDCl_3$) δ 152.05, 143.33, 140.30, 134.62,

130.64, 129.89, 129.82, 129.69, 128.53, 123.22, 120.85, 118.73, 115.27, 109.91, 45.48, 38.40. ESI-HRMS calcd for $C_{23}H_{25}N_2O_7S_1^+$ $[MH]^+$: 473.1377, found: 473.1373.

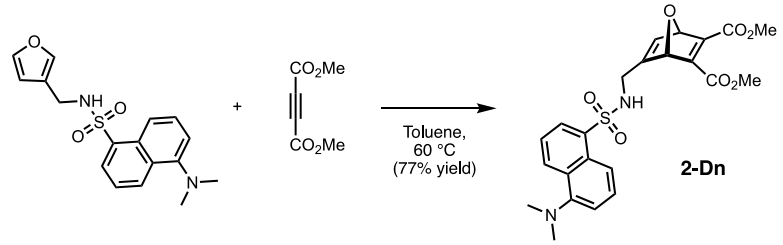

Scheme S3. Diels-Alder reaction of *N*-dansyl-*N*-furan-3-ylmethylamine and dimethyl acetylenedicarboxylate.

Dimethyl 5-(((5-(dimethylamino)naphthalene)-1-sulfonamido)methyl)-7-oxabicyclo[2.2.1] hepta-2,5-diene-2,3-dicarboxylate, **2-Dn**: Furan **S5** (97.5 mg, 0.295 mmol, 1 equiv) was combined with dimethyl acetylenedicarboxylate (DMAD, 50.7 µL, 0.413 mmol, 1.4 equiv) in toluene (295 µL) in a sealed scintillation vial and heated directly on a hot plate set at 60°C while stirring in the dark. After 5 h, an additional ~0.25 eq (10 µL) of DMAD was added, and the reaction was resumed for another 14 h. The crude reaction mixture was cooled to room temperature before purification by column chromatography on silica gel with a gradient elution of 0-40% ethyl acetate/hexanes to provide a yellow tacky solid residue (107 mg, 77% yield). R_f 0.26 (40% EtOAc/hexane). ^{1}H NMR (500 MHz, $CDCl_3$) δ 8.54 (dt, *J* = 8.6, 1.1 Hz, 1H), 8.28 (dt, *J* = 8.7, f0.9 Hz, 1H), 8.23 (dd, *J* = 7.3, 1.3 Hz, 1H), 7.55 (dd, *J* = 8.6, 7.6 Hz, 1H), 7.51 (dd, *J* = 8.6, 7.3 Hz, 1H), 7.18 (d, *J* = 7.5 Hz, 1H), 6.66 (q, *J* = 1.9 Hz, 1H), 5.54 (t, *J* = 1.8 Hz, 1H), 5.36 (t, *J* = 5.8 Hz, 2H), 5.34 (d, *J* = 1.6 Hz, 1H), 3.87 (d, *J* = 2.0 Hz, 1H), 3.88 – 3.84 (m, 4H), 3.78 (s, 3H), 2.89 (s, 6H). ^{13}C NMR (126 MHz, $CDCl_3$) δ 164.30, 162.65, 154.59, 152.86, 152.06, 137.64, 134.34, 130.81, 130.03, 130.01, 129.66, 128.60, 123.27,

118.74, 115.39, 86.41, 85.46, 52.86, 52.54, 45.52, 41.37. DEPT-135 ^{13}C NMR (126 MHz, $CDCl_3$) δ(phase): 137.35(+), 130.52(+), 129.74(+), 128.31(+), 122.98(+), 118.44(+), 115.10(+), 86.12(+), 85.17(+), 52.57(+), 52.25(+), 45.24(+), 41.08(–). ESI-HRMS calcd for $C_{23}H_{25}N_2O_7S_1^+$ $[MH]^+$: 473.1377, found: 473.1373.

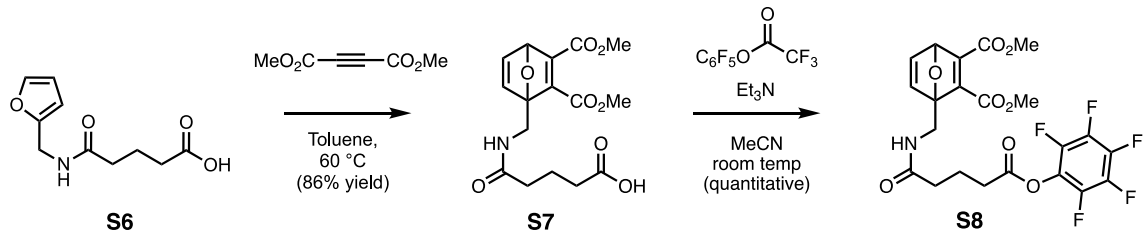

Scheme S4. Synthesis of **S8** active ester from 5-((furan-2-ylmethyl)amino)-5-oxopentanoic acid **S6** and dimethyl acetylenedicarboxylate *via* OND **S7**.

Dimethyl 1-((5-oxo-5-(perfluorophenoxy)pentanamido)methyl)-7-oxabicyclo[2.2.1]hepta-2,5-diene-2,3-dicarboxylate, **OND PFP-ester S8**: Furan and OND carboxylate precursors **S6** and **S7** were prepared as previously described in our group (Scheme S5).[4] **S7** (53 mg, 0.150 mmol, 1 equiv) was dissolved in dry acetonitrile (1.5 mL) at room temperature under air and pentafluorophenol trifluoroacetate (41 µL, 0.24 mmol, 1.6 equiv) was added, followed by triethylamine (42 µL, 0.3 mmol, 2 equiv). The reaction was stirred at room temperature for 2 h, followed by dilution with dichloromethane (20 mL). The organic solution was washed with 0.1N aqueous HCl (20 mL), saturated aqueous sodium bicarbonate (20 mL), and brine (20 mL), dried over anhydrous sodium sulfate, filtered, and condensed to produce an off-white solid which was dried under high vacuum and the crude product used in subsequent steps without further purification (78 mg, quantitative). R_f 0.55 (4% MeOH/CH_2Cl_2). ^{1}H NMR (500 MHz, $CDCl_3$) δ 7.21 (dd, *J* = 5.3, 2.0 Hz, 1H), 6.99 (d, *J* = 5.2 Hz, 1H), 5.98 (t, *J* = 5.9

Hz, 1H), 5.62 (d, *J* = 2.0 Hz, 1H), 4.17 (dd, *J* = 14.8, 6.4 Hz, 1H), 4.00 (dd, *J* = 14.8, 5.2 Hz, 1H), 3.81 (s, 3H), 3.77 (s, 3H), 2.74 (t, *J* = 7.2 Hz, 2H), 2.31 (t, *J* = 7.2 Hz, 2H), 2.08 (t, *J* = 7.2 Hz, 2H). ^{19}F NMR (471 MHz, $CDCl_3$) δ -154.15 (m), -159.37 (t, *J* = 21.7 Hz), -163.5 (m).

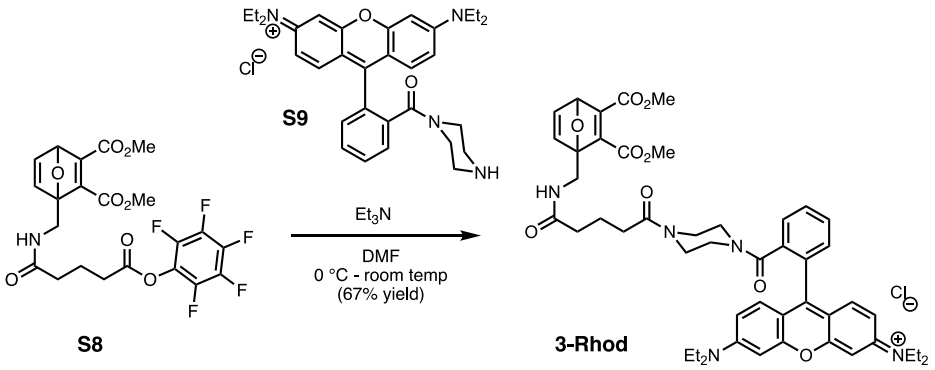

Scheme S5. Synthesis of OND **3-Rhod** by reaction between amino-rhodamine **S9** and ester **S8**.

3-Rhodamine, **3-Rhod**: Piperazine-modified rhodamine-B **S9** was prepared as previously described by Nguyen and Francis.[7] **S9** (24.8 mg, 0.045 mmol, 1 equiv) was dissolved in dry DMF (1 mL) and chilled on ice. Triethylamine (12.5 µL, 0.09 mmol, 2 equiv) was added, followed by crude active ester **S8** in one portion (26 mg, 0.050 mmol, 1.1 equiv). The resulting solution was allowed to slowly reach room temperature and stirred for 4 h, at which time 20 mL of dichloromethane. The solution was washed with 1N aqueous HCl (20 mL), saturated aqueous sodium bicarbonate (20 mL), and again with 1N HCl (20 mL). The combined aqueous phases were back-extracted once with CH_2Cl_2 (10 mL), and the combined organic phases were washed once with brine (30 mL), dried over anhydrous sodium sulfate, filtered, and condensed in vacuum. The dark fuchsia residue was purified by column chromatography on silica gel, eluting with a

gradient from 0-12% MeOH/CH_2Cl_2 to provide a pink solid residue (26.8 mg, 67% yield). R_f 0.57 (10% MeOH/CH_2Cl_2, fluorescent pink streak). NMR analysis was performed at 40 °C. ^{1}H NMR (500 MHz, 40 °C, Methanol-d_4) δ 7.80 – 7.75 (m, 2H), 7.72 – 7.68 (m, 1H), 7.57 – 7.47 (m, 1H), 7.30 – 7.22 (m, 3H), 7.15 – 7.04 (m, 3H), 6.96 (d, *J* = 2.5 Hz, 2H), 5.62 (d, *J* = 1.9 Hz, 1H), 4.14 (d, *J* = 14.8 Hz, 1H), 3.86 (d, *J* = 14.9 Hz, 1H), 3.78 (s, 3H), 3.74 (s, 3H), 3.69 (q, *J* = 7.1 Hz, 8H), 3.38 (s, 8H), 2.34 (app td, *J* = 7.3, 2.5 Hz, 2H), 2.22 (t, *J* = 7.1 Hz, 2H), 1.82 (p, *J* = 7.1 Hz, 3H), 1.31 (t, *J* = 7.1 Hz, 12H). ^{13}C NMR (126 MHz, 40 °C, MeOD) δ 175.32, 173.56, 169.61, 165.55, 164.13, 159.31, 157.31, 157.05, 155.12, 146.28, 144.37, 136.59, 136.56, 133.20, 131.75, 131.32, 131.25, 128.93, 115.47, 114.94, 114.93, 98.41, 97.42, 85.01, 52.85, 52.76, 46.92, 42.69, 38.56, 35.82, 33.04, 22.34, 13.87, 12.84. ESI-HRMS calcd for $C_{48}H_{56}N_5O_9^+$ [MH]$^+$: 846.4073, found: 846.4074.

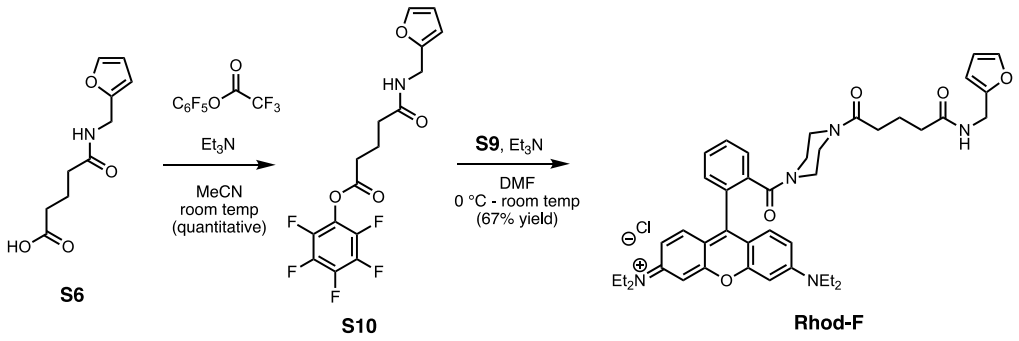

Scheme S6. Synthesis of **Rhod-F** from furan **S6** and amino-rhodamine **S9** via active ester **S10**.

Perfluorophenyl 5-((furan-2-ylmethyl)amino)-5-oxopentanoate, **furan PFP-ester S10**: **S6** (25 mg, 0.118 mmol, 1 equiv) was dissolved in dry acetonitrile (1.1 mL) while stirring and pentafluorphenol trifluoroacetate (24 µL, 0.142 mmol, 1.2 equiv) was added

in one portion, followed by triethylamine (32 µL, 0.236 mmol, 2 equiv). The mixture was stirred at room temperature for 2 h before diluting with dichloromethane (20 mL). The organic solution was washed with 0.1N aqueous HCl (20 mL), saturated aqueous sodium bicarbonate (20 mL), and brine (20 mL), dried over anhydrous sodium sulfate, filtered, and condensed to produce an off-white solid which was dried under high vacuum for 1 h and the crude product used in the following step without further purification (45 mg, quantitative). ^{1}H NMR (400 MHz, $CDCl_3$) δ 7.35 (dd, *J* = 1.9, 0.8 Hz, 1H), 6.32 (dd, *J* = 3.3, 1.9 Hz, 1H), 6.23 (dd, *J* = 3.1, 0.8 Hz, 1H), 5.78 (s, 1H), 4.46 (d, *J* = 5.5 Hz, 2H), 2.77 (t, *J* = 7.1 Hz, 2H), 2.34 (t, *J* = 7.2 Hz, 2H), 2.13 (p, *J* = 7.0 Hz, 2H).

Rhodamine-furan, **Rhod-F**: **Rhod-F** was prepared as described for **3-Rhod** from active ester **S10**. **S9** (21 mg, 0.039 mmol, 1 equiv) was dissolved in dry DMF (1 mL) and chilled on ice. Triethylamine (11 µL, 0.079 mmol, 2 equiv) was added, followed by crude active ester **S10** in one portion (17 mg, 0.045 mmol, 1.16 equiv). The resulting solution was allowed to slowly reach room temperature and stirred for 4 h, at which time 20 mL of dichloromethane. The solution was washed with 1N aqueous HCl (20 mL), saturated aqueous sodium bicarbonate (20 mL), and again with 1N HCl (20 mL). The combined aqueous phases were back-extracted once with CH_2Cl_2 (10 mL), and the combined organic phases were washed once with brine (30 mL), dried over anhydrous sodium sulfate, filtered, and condensed in vacuum. The dark purple residue was purified by column chromatography on silica gel, eluting with a gradient from 0-10% MeOH/CH_2Cl_2 to provide dark purple solid residue (16.7 mg, 77% yield). R_f 0.56 (10% MeOH/CH_2Cl_2, fluorescent pink streak). NMR analysis was performed at 40 °C. ^{1}H NMR (500 MHz, 40 °C, Methanol-d_4) δ 7.81 – 7.74 (m, 2H), 7.75 – 7.66 (m, 1H), 7.55 – 7.49

(m, 1H), 7.38 (app s, 1H), 7.33 – 7.22 (m, 2H), 7.13 – 7.04 (m, 2H), 6.96 (d, *J* = 2.5 Hz, 2H), 6.32 (app t, *J* = 2.5 Hz, 1H), 6.22 (d, *J* = 3.2 Hz, 1H), 4.32 (s, 2H), 3.69 (q, *J* = 7.1 Hz, 8H), 3.37 (s, 8H), 2.35 (t, *J* = 7.5 Hz, 2H), 2.23 (t, *J* = 7.2 Hz, 2H), 1.84 (ddt, *J* = 14.7, 10.6, 5.6 Hz, 2H), 1.31 (t, *J* = 7.0 Hz, 12H). ^{13}C NMR (126 MHz, 40 °C, MeOD) δ 175.04, 173.55, 169.62, 159.31, 157.30, 157.03, 153.20, 143.25, 136.57, 133.19, 132.26, 131.75, 131.32, 131.27, 128.93, 115.45, 114.92, 111.35, 108.04, 97.40, 46.92, 42.78, 37.09, 35.83, 33.12, 22.43, 13.86, 12.83. ESI-HRMS calcd for $C_{42}H_{50}N_5O_5^+$ $[MH]^+$: 704.3806, found: 704.3810.

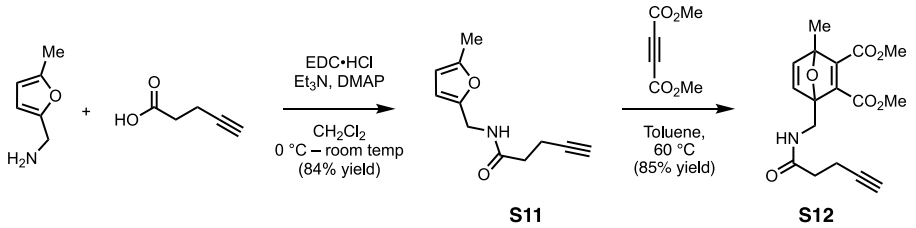

Scheme S7. Preparation of alkyne-modified 4-Me-OND **S12** via furan **S11**.

N-((5-methylfuran-2-yl)methyl)pent-4-ynamide, S11: Pentynoic acid (160 mg, 1.61 mmol, 1.1 equiv) was dissolved in dry CH_2Cl_2 (8 mL) and chilled to 4°C while stirring. N-(3-dimethylaminopropyl)-N′-ethylcarbodiimide hydrochloride (EDC•HCl, 400 mg, 2.04 mmol, 1.4 equiv) was added in one portion while stirring. After 15 min, (5-methylfuran-2-yl)methanamine (166 µL, 1.46 mmol, 1 equiv), triethylamine (224 µL, 1.6 mmol, 1.1 equiv), and 4-dimethylaminopyridine (17.80 mg, 10 mol%) dissolved in CH_2Cl_2 (1 mL) were added dropwise over 1 min and stirring was continued under nitrogen, and the reaction was allowed to reach room temperature. The reaction mixture was diluted with CH_2Cl_2 (25 mL), and washed with 1N aqueous HCl (2x20 mL), saturated aqueous sodium bicarbonate solution (20 mL), and brine (20 mL), dried over anhydrous sodium

sulfate, filtered, and condensed under vacuum to provide an off-white solid that was used in the next step without further purification (231 mg, 83% yield). R_f 0.50 (40% EtOAc/hexane).

Dimethyl 1-methyl-4-(pent-4-ynamidomethyl)-7-oxabicyclo[2.2.1]hepta-2,5-diene-2,3-dicarboxylate, **S12**: **S11** (56 mg, 0.293 mmol, 1 equiv), dimethyl acetylenedicarboxylate (DMAD, 47 µL, 0.38 mmol, 1.3 equiv), and toluene (300 µL) were sealed in a 20 mL scintillation vial and heated directly on a hot plate at 60 °C for 9 hours, at which point another aliquot of DMAD (18 µL, 0.147 mmol, 0.5 equiv) was added, and the reaction was continued for 13 h more before purifying by column chromatography on silica gel, eiluting with a gradient of 40-70% ethyl acetate/hexanes to provide a yellow sticky residue (83 mg, 85% yield). R_f 0.31 (40% EtOAc/hexane). ^{1}H NMR (400 MHz, $CDCl_3$) δ 6.96 (s, 2H), 6.08 (t, *J* = 5.6 Hz, 1H), 4.08 (dd, *J* = 5.7, 1.9 Hz, 1H), 3.79 (s, 2H), 3.76 (s, 2H), 2.50 (td, *J* = 7.3, 6.1, 2.1 Hz, 2H), 2.39 (t, *J* = 7.1 Hz, 2H), 1.96 (t, *J* = 2.6 Hz, 1H), 1.76 (s, 3H). ^{13}C NMR (101 MHz, $CDCl_3$) δ 171.00, 164.33, 163.49, 157.25, 151.58, 147.90, 144.42, 94.82, 92.75, 82.92, 69.45, 52.56, 52.45, 38.19, 35.37, 15.31, 14.92.

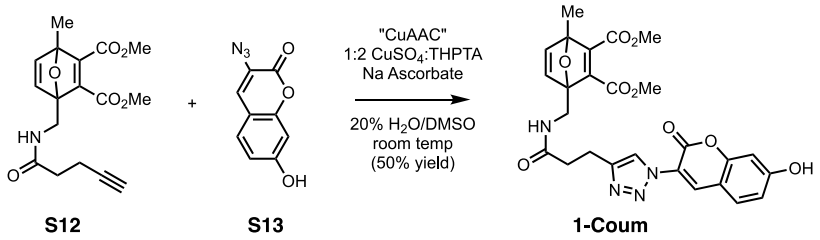

S12 **S13** **1-Coum**

Scheme S8. Coupling of coumarin cargo with OND **S12** by the ligand-accelerated copper-catalyzed azide-alkyne cycloaddition (CuAAC) reaction to form **1-Coum**.

Dimethyl 1-((3-(1-(7-hydroxy-2-oxo-2*H*-chromen-3-yl)-1*H*-1,2,3-triazol-4-yl)propanamido)methyl)-4-methyl-7-oxabicyclo[2.2.1]hepta-2,5-diene-2,3-dicarboxylate, **1-Coum**: Synthesis of the coumarin-modified OND was achieved by the ligand accelerated copper-catalyzed azide-alkyne cycloaddition reaction between alkyne-modified **S12** and coumarin-azide **S13**, the preparation of which has been described elsewhere.[8] **S12** (24.85 mg, 0.075 mmol, 1 equiv) was dissolved in DMSO (1 mL) and 300 µL of an aqueous solution of THPTA accelerating ligand (100 mM) and copper (II) sulfate (50 mM) was added, followed by an aqueous solution of 200 mM sodium ascorbate (100 µL) to produce a pale-yellow solution which was stirred at room temperature under nitrogen for 5 minutes. At this point azide **S13** was added and the reaction was stirred at room temperature under nitrogen in the dark for 3 h, at which point an additional 50 µL of 100 mM: 50 mM THPTA:Cu(II)SO_4 and 200 mM sodium ascorbate solutions were added. The reaction was stirred for another 3 h, then diluted with ethyl acetate (20 mL), washed with 1N aqueous HCl (20 mL), which was back-extracted with ethyl acetate (10 mL). The combined organic phases were washed with brine (2x20 mL), dried over anhydrous sodium sulfate, filtered, and condensed under reduced pressure. The crude was purified by column chromatography on silica gel, eluting with a gradient from 75–100% ethyl acetate/hexanes to provide a tan solid (20 mg, 50% yield). R_f 0.43 (EtOAc). NMR was performed at 40 °C. ^{1}H NMR (500 MHz, 40 °C, Methanol-d_4) δ 8.42 (s, 1H), 8.31 (s, 1H), 7.62 (d, J = 8.6 Hz, 1H), 6.98 (d, J = 5.1 Hz, 1H), 6.96 (d, J = 5.2 Hz, 1H), 6.88 (dd, J = 8.6, 2.2 Hz, 1H), 6.81 (d, J = 2.1 Hz, 1H), 4.05 (d, J = 14.8 Hz, 1H), 3.98 (d, J = 14.8 Hz, 1H), 3.74 (s, 3H), 3.73 (s, 3H), 3.08 (t, J = 7.3 Hz, 2H), 2.64 (t, J = 7.4 Hz, 2H), 1.71 (s, 3H). ^{13}C NMR (126 MHz, 40 °C, MeOD)

δ 174.55, 165.55, 165.10, 164.33, 158.12, 157.84, 156.52, 153.48, 148.84, 147.75, 145.61, 137.02, 131.81, 124.34, 120.93, 115.60, 112.01, 103.47, 96.41, 93.84, 52.73, 52.61, 38.94, 35.95, 22.48, 15.51. ESI-HRMS calcd for $C_{26}H_{25}N_4O_9^+$ $[MH]^+$: 537.1616, found: 537.1617.

Synthesis and preparation of NP-OND-CpG.

CpG-3'-NH_2 (5′-TCCATGACGTTCCTGACGTT-3'-$(CH_2)_3$-NH_2) was purchased from Eurofins Genomics on the 1 μmol scale. SPO_3-CpG (5′-SPO_3-TCCATGACGTTCCTGACGTT-3') (phosphorothioate-CpG, PTO-CpG) was purchased from Microsynth on the 1 μmol scale. The 5' was chosen for modification with phosphorothioate, while the 3' was chosen for modification with amine because the CpG can tolerate greater modification to the 3' end and still maintain immunostimulatory potency.[9]. OND-3'-CpG (OND-CpG) was installed on the CpG 3' using NHS chemistry (Scheme S9).

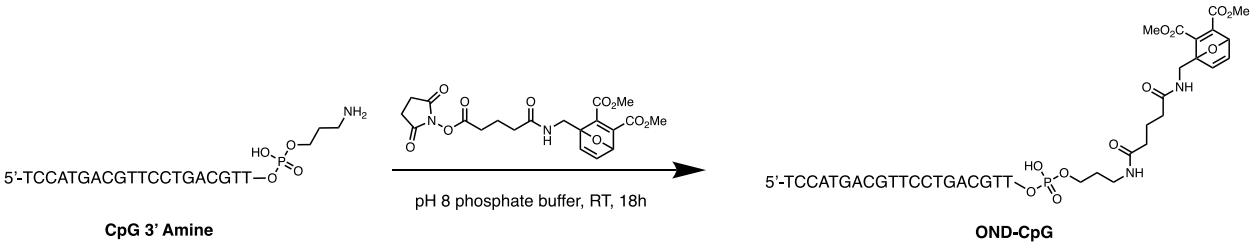

Scheme S9. Synthesis of OND-CpG from CpG 3′ amine (purchased from Eurofins Genomics).

To the CpG-3'-NH_2 (500 μM, final concentration) in a pH 8 phosphate buffer (0.1 M) was added the small molecule OND-NHS (in DMSO, 10 mM final concentration) and the reaction was left at room temperature for 18 h. The reaction was confirmed to have

gone to completion by LCMS. The OND-CpG was first purified by EtOH precipitation, where 3M NaOAc (10% v/v), pure EtOH (3× reaction vol.) and 20 μg glycogen (1 μL) were added to the reaction mixture. The resulting solution was kept at -80°C for at least an hour to allow DNA precipitation. The sample was then centrifuged for 25 min and the supernatant was removed to obtain the DNA pellet. EtOH (70% in H_2O, 400 μL) was added to the pellet, vortexed and centrifuged for 15 min. The supernatant was removed and the residual EtOH was removed on speedvac. The pellet was re-dissolved in nuclease-free H_2O and further purified on Ilustra microspin G25 column (following the manufacturer's protocols) to yield OND-CpG (4 mg/ml, 60–70% yield).

PDS-NP were synthesized as previously reported.[2] PDS-NP were thiol-activated by adding dithiothreitol (DTT) to 100 mM for 30 min. The solution was then cleaned of DTT on a PD-10 G25 column followed by collection of the NP fractions and then concentrated to 80-100 mg/mL with a 4 mL 10 kDa Amincon Spin filter at 4000 x g for 30 min and 15 min. The concentrated NP solution was then run on three 5 mL 7 kDa Zeba spin columns at 1000 x g for 2 min in 1x -/- PBS. OND-CpG was added to the NP solution at a concentration of 1 ug/15 μL NP (80 mg/mL) and reacted for 12 h. Following reaction the solution was run on a Sepharose CL6B column 1x30 cm. The fractions were assayed for NP using Iodine[10] and Gel Red for CpG.[11] The NP-OND-CpG conjugate fractions were pooled and concentrated with a 10 kDa Amicon Spin filter at 4000 x g for 30 min. Final concentration of CpG was determined using Gel Red and Iodine standard curves for CpG and NP, respectively; the average concentration of CpG was between 0.4-0.8 ug CpG/30μL NP (40 mg/mL). For disulfide-linked NP-SS-CpG, PTO-CpG was added to PDS-NP at a concentration of 1 ug/15 μL NP (40 mg/mL) and

reacted 12 h. The solution was separated using size exclusion column chromatography (Sepharose CL6B).

Characterization of NP-OND-Dn conjugation and fragmentation rates.

OND conjugation rates to NP were determined using OND-dansyl (Dn) variants due to their fluorogenic nature. The Dn fluorescence is quenched by the OND electrophile presumably by a photoinduced electron transfer mechanism, and a robust fluorescence is observed following conjugate addition.[5, 6] OND were added at 25, 50, 100, and 200 μM to NP with a thiol concentration of 700 μM (550 μM thiol was used in reactions with **2-Dn**), yielding a mole range of OND to thiol ratios of 1:3.5 to 1:28 in pH 7.4 phosphate buffered saline. Fluorescence was tracked (ex: 332 nm, em: 510 nm) over the course of conjugation until a plateau was reached. The observed rate constant was determined by nonlinear least squares fitting to the second order rate equation (Figures S1-S5). Rate constant values are reported as the average ± standard deviation from three independent trials at four different initial concentrations of OND and fixed concentration of NP thiols. Fragmentation studies were conducted using dialysis membrane cups of 20,000 MWCO that retain the NP-OND-Dn adduct but allow for the removal of fragmented OND dye cargo. OND-dansyl variants were reacted in buffer at pH 7.4 with excess NP for 1 hour and then transferred to 20,000 MWCO dialysis membrane cups at 37°C. Samples of 4x2μL were extracted to minimize reduction of dialysate volume throughout the experiment and read for fluorescence (ex: 332 nm, em: 510 nm) using a BioTek Synergy H4 Multi-Mode Microplate Reader. Size-exclusion chromatography on a PD-10 column was employed for **1-Dn** because the adduct half-life for this linker is only 17 min and is similar to the rate of dialysis of free dansyl-furan.

Samples were prepared using the staggered start method every 10 min for 2 h and incubated at 37°C prior to size-exclusion chromatography. The fluorescence of PD-10 purified NP-OND-Dn at each time point was normalized to the initial fluorescence, and Dn release rates were calculated by nonlinear least squares fitting of the decline in fluorescence over time to the first order kinetic equation ($A = A_o e^{-kt}$). Values are reported as the average ± standard deviation from ≥3 individual reactions. Half-lives were calculated from first order rate constants using the formula $t_{1/2} = \ln(2)/k$. Rate constants for conjugate addition at room temperature, Dn cargo release at 37°C, and the corresponding release half-lives for all OND-Dn derivatives are presented in Supplementary Table 1.

Area under the curve and multi-off rate studies

In order to determine which OND linker would be most useful *in vivo* we conducted area under the curve studies over 72 h. Using our mouse forearm injection model 30 µL of OND-Dn-NP solution was injected under isofluorane anesthesia intradermally into both forearms of 6-week-old female C57BL6/J mice. The mice were allowed to recover for 24 h before being sacrificed and having axillary and brachial LN excised and homogenized in 400 µL of DMSO to improve the weak fluorescence signal of dansyl furan in aqueous buffer. Using a standard curve generated in PBS we were able to calculate the percent injection at each time point for each OND linker within the LN homogenate. Using the measured half-lives from Supplementary Table 1 we were able to calculate the percent of cargo that would be free at 24 h for each OND linker.

In order to demonstrate the full advantage that different OND variants can provide, different mole ratios of OND derivatives **1-Dn**, **3-Dn**, and **4-Dn** were conjugated to the same NP solution such that the overall release rate of Dn-furan cargo would represent superposed simultaneous release profiles. For this study OND **1-Dn**, **3-Dn**, and **4-Dn** were chosen for their greatly differing half-lives. These OND variants were mixed at mole ratios of 8:1:1, 1:8:1, 1:1:8, and 1:1:1 of OND **1-Dn**:**3-Dn**:**4-Dn**, and their conjugation was monitored by measuring fluorescence emission at 510 nm (excitation at 332 nm). The conjugation fluorescence (data not shown), demonstrated that the percent of total OND conjugated from each OND variant was directly proportional to its starting percentage, since the thiol from NP are in excess. It should be noted that the fragmentation half-life for **1-Dn** is on the same time scale as that of the conjugation reaction, leaving approximately 50% of its conjugates intact by the time addition was completed, thereby limiting the final conjugated percentage of **1-Dn**. Following conjugation, the NP-OND-Dn adduct solutions were incubated at 37°C and over the course of 28 h samples were drawn and separated on a size-exclusion column. The OND-Dn-NP fraction eluting first was collected in bulk and its fluorescence emission at 510 nm was measured. Only OND-Dn-NP-conjugated cargo elutes with the NP fraction, enabling the calculation of the percent of cargo still linked to the NP carrier, and the amount that has been released. These data are shown in Supplementary Figure 1, along with model release curves created using the known fragmentation rates of adducts of **1-Dn**, **3-Dn**, and **4-Dn** and the conjugation efficiency to predict the release profile for each of the OND variant ratios.

As predicted by the model, incorporation of **1-Dn**, which has a half-life of only 17 min, led to an initial burst release of cargo and was observed for all ratios but was most prevalent for the 8:1:1 mole ratio. When **4-Dn** was predominantly incorporated, there was a much slower overall release of cargo, since its half-life is 28.8 h, as observed for the 1:1:8 mole ratio. The incorporation of **3-Dn**, which has a half-life of 9.86 h at 37°C, led to a steadier release observed over the time course of this experiment, particularly for the 1:8:1 mole ratio. When all three OND variants were in an equimolar ratio (1:1:1), the release profile exhibited a steady release rate closely resembling that predicted by the model. The described results demonstrate the capability of the OND-NP system to be programmed to release cargo on a defined time scale.

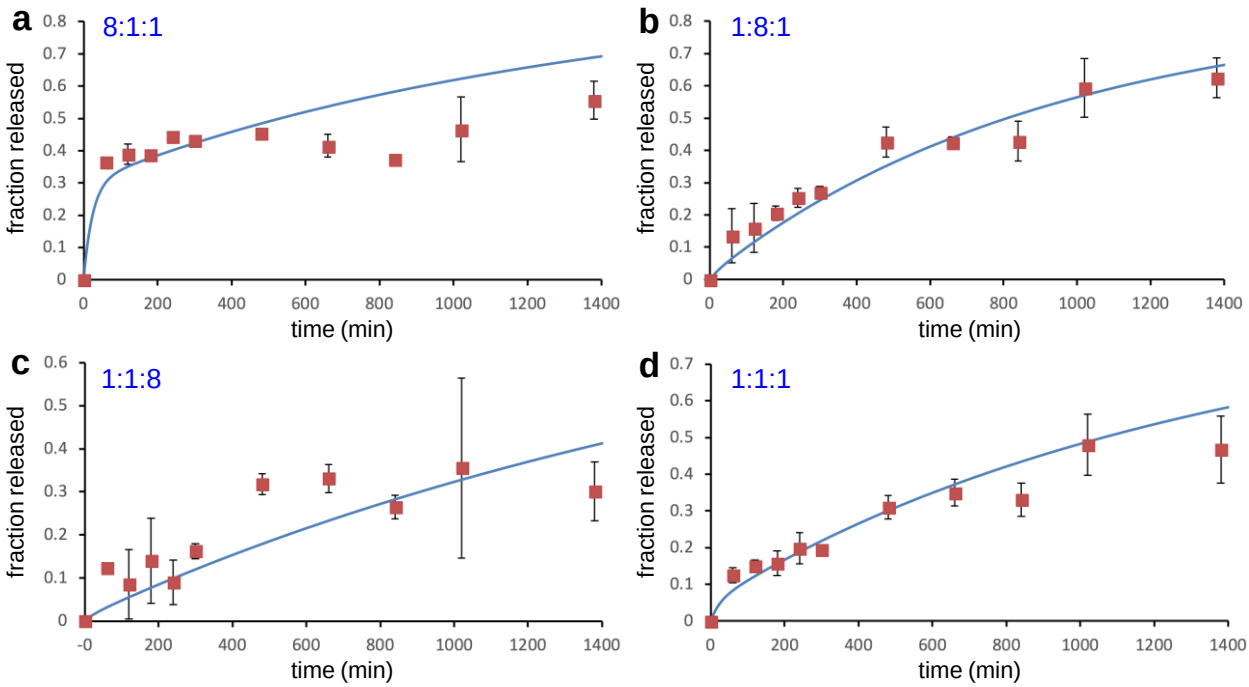

Supplementary Figure 1. Release of dansyl-furan from nanoparticles loaded with an excess of mixtures of 1-Dn+3-Dn+4-Dn in the indicated ratios. Measured data points are represented by the squares (error = standard deviation of at four replicate

experiments). The curves are calculated profiles derived from the measured rate constants for loading (conjugate addition) and release (retro-Diels-Alder) reactions of the respective OND linkers measured in Source Data Figures S1-S6, applied to each case for the ratios of dansyl-OND reagents used. For all graphs, the columns/points and error bars represent the mean + SEM.

NP biodistribution profiles

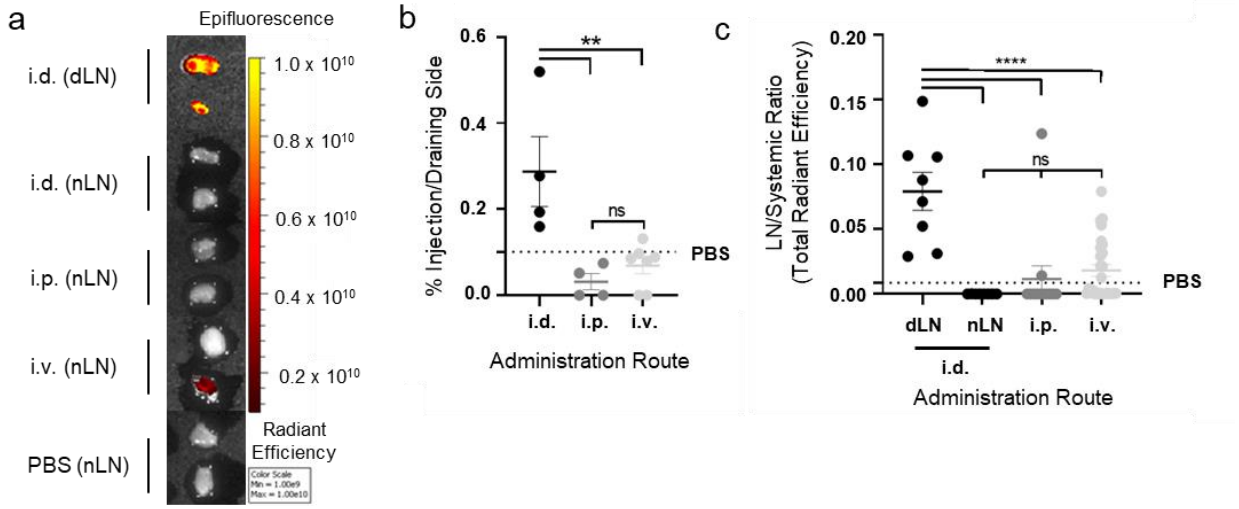

Supplementary Figure 2. **Biodistribution of 647-labeled PPS NP injected intradermal (i.d.), intraperitoneal (i.p.), or intravenous (i.v.).** dLN is the draining lymph node for the i.d. injection on the ipsilateral side. nLN is the contralateral lymph node for the i.d. injection and the lymph nodes for the other administration routes. a) Representative IVIS images of axillary and brachial LNs excised following administration of AF647 core-labelled NP through different routes. Units are in Radiant Efficiency. n=4 biological replicates per group. b) Percent of injection in pooled axillary and brachial lymph nodes. n=4 biological replicates per group. c) Ratio of the total radiant efficiency in each lymph node compared to the total of the systemic radiant

efficiency (spleen, kidney, lungs, and liver). n=8 biological replicates per group. For all graphs, the columns/points and error bars represent the mean + SEM. Statistics were performed by ordinary one-way ANOVA with Tukey's multiple comparisons test. ****=p<.0001, ***=p<.005, *=p<.05, ns=p>.05.

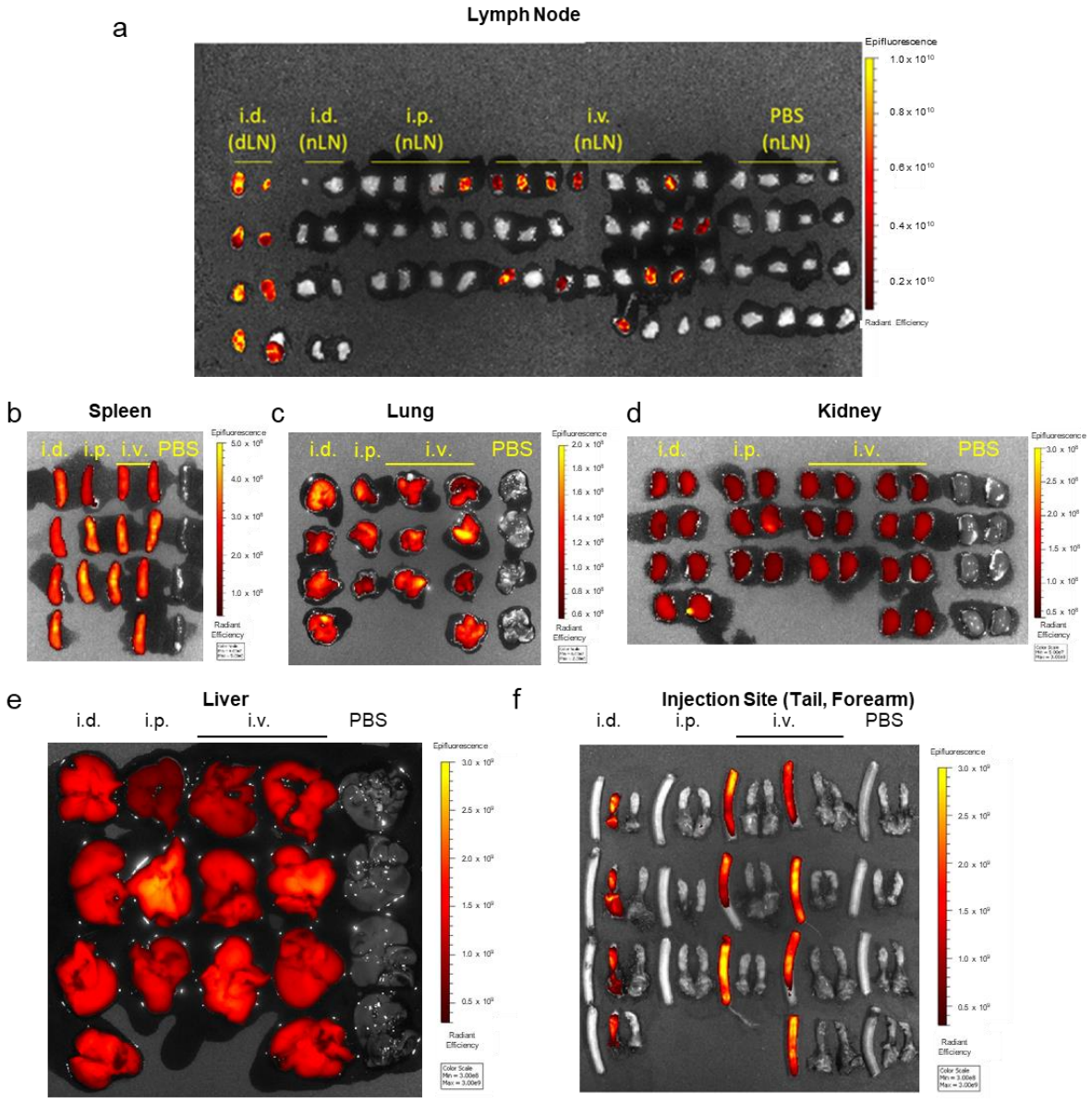

Supplementary Figure 3. IVIS imaging of tissue biodistribution of AF647 core-labelled PPS-NP injected intradermally (i.d.), intraperitoneally (i.p.), or

intravenously (i.v.). All samples in each group are presented. All units are Radiant Efficiency. a) Axillary and brachial lymph nodes. dLN is the draining lymph node for the i.d. injection on the ipsilateral side. nLN is the contralateral lymph node for the i.d. injection and the lymph nodes for the other administration routes. b) Spleens. c) Lungs. d) Kidneys, as a pair. e) Liver. f) Anatomical site of injection: tail for i.v. injection, and forelimbs for i.d. injection.

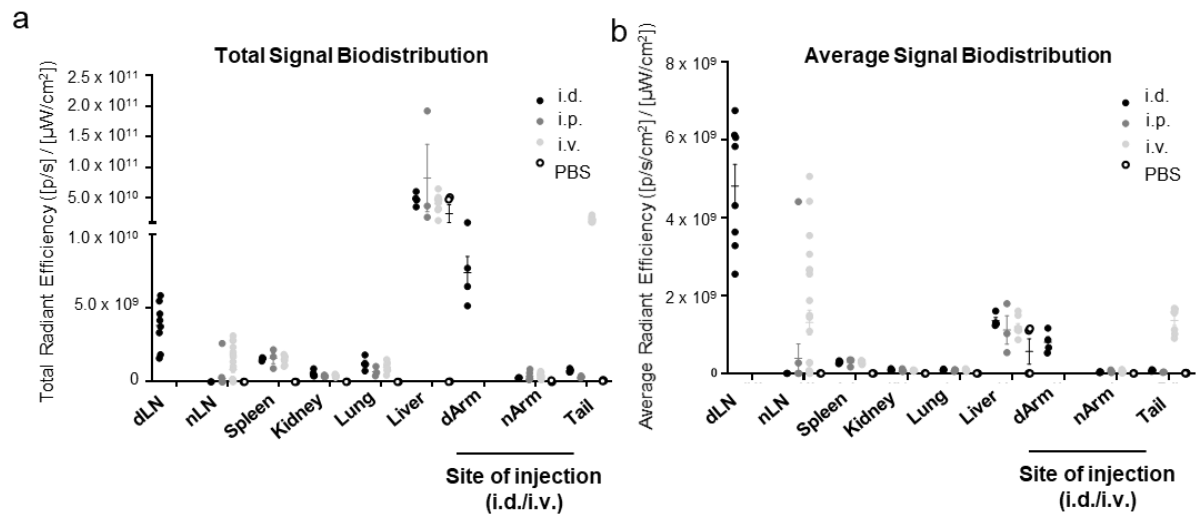

Supplementary Figure 4. Analysis of IVIS biodistribution of AF647 core-labeled PPS-NP injected intradermally (i.d.), intraperitoneally (i.p.), or intravenously (i.v.). dLN is the draining lymph node for the i.d. injection on the ipsilateral side. nLN is the contralateral LN for the i.d. injection and the LNs for the other administration routes. The dLN injection in the forearm = dArm, the contralateral arm for i.d. and forearms for all groups are nArm. a) Total radiant efficiency for each tissue and administration method. n=6 biological replicates per group. b) Average radiant efficiency for each tissue and administration method. n=6 biological replicates per group. For all graphs, the columns/points and error bars represent the mean + SEM.

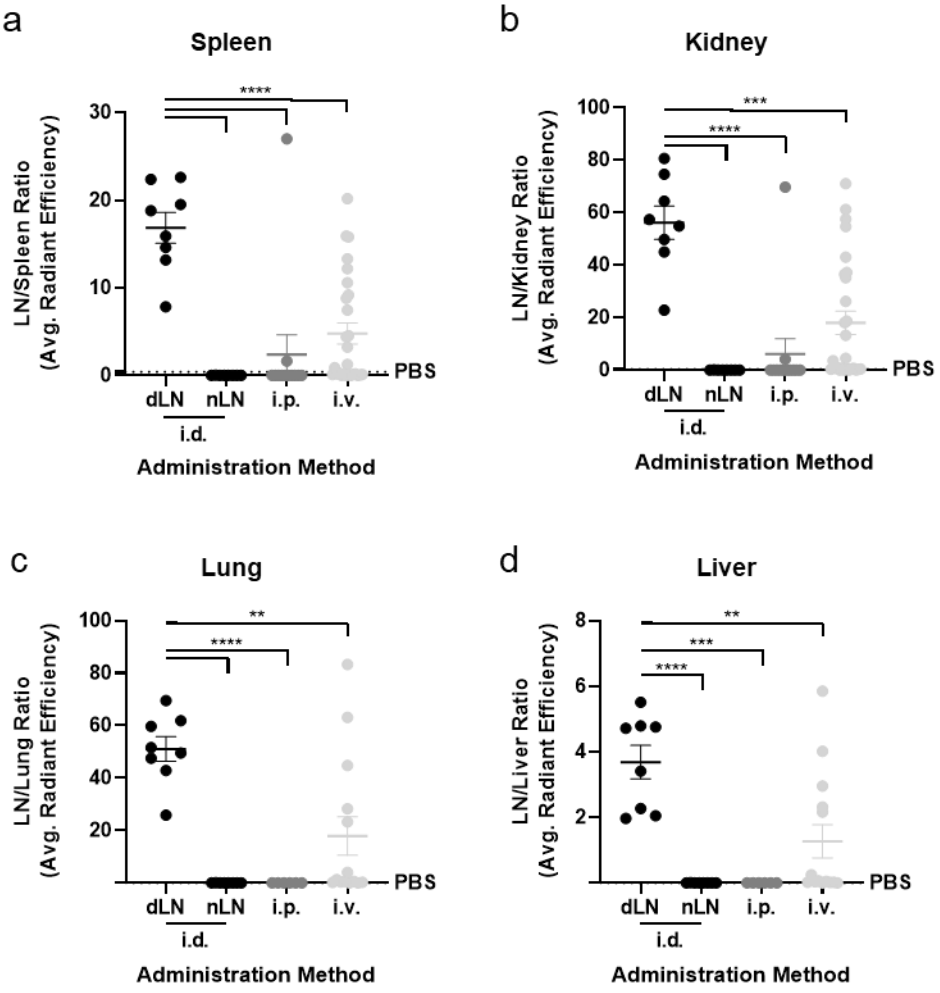

Supplementary Figure 5. **Analysis of IVIS lymph node to tissue biodistribution ratio of AF647 core-labelled PPS-NP injected intradermally (i.d.), intraperitoneally (i.p.), or intravenously (i.v.).** Average radiant efficiency for each tissue and administration method was calculated. The ratio of the lymph node to the specific systemic tissue is plotted. dLN is the draining lymph node for the i.d. injection on the ipsilateral side. nLN is the contralateral lymph node for the i.d. injection and the lymph nodes for the other administration routes. a) Ratio of average lymph node signal to average spleen signal. n=7 biological replicates per group. b) Ratio of average lymph

node signal to average kidney signal. n=7 biological replicates per group. c) Ratio of average lymph node signal to average lung signal. n=7 samples per group. d) Ratio of average lymph node signal to average liver signal. n=7 biological replicates per group. For all graphs, the columns/points and error bars represent the mean + SEM. Statistics were performed by ordinary one-way ANOVA with Tukey's multiple comparisons test. ****=p<.0001, ***=p<.005, *=p<.05, ns=p>.05.

Stability of maleimide chemistry to link fluorophores to thiols of PPS core of NPs

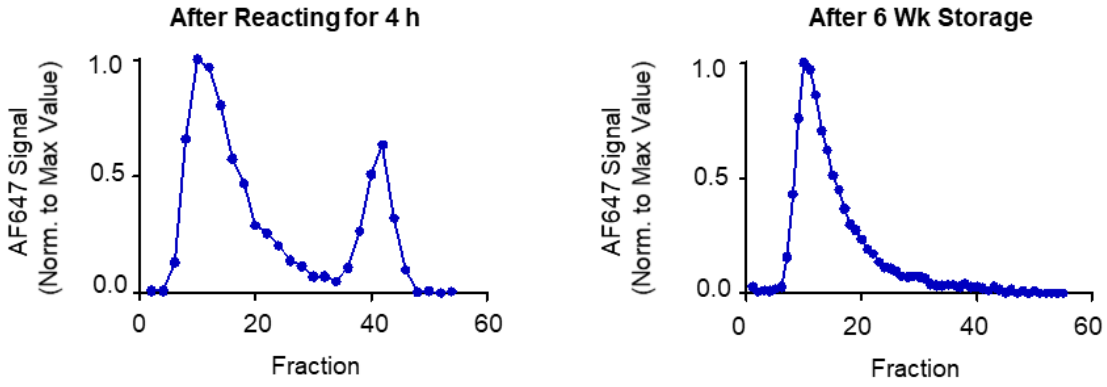

Supplementary Figure 6. **Stability of maleimide chemistry to link fluorophores to thiols of PPS core of NPs.** Size exclusion chromatography (CL6B in saline). This experiment was repeated once with similar results.

Measurement of NP vs OND cargo distribution within LN images

LN images were taken on confocal (Supplementary Figure 7, Source Data Figure S7) as previously described. Z-stack images were converted to maximum intensity projections and then separated by fluorescence channel. Using a custom image J macro an outline was drawn around the LN boundary with the free from tool in the single channel images. The image was then thresholded to zero pixel value outside of

the LN boundary and the custom script returned the coordinates of the outline and the thresholded fluorescence pixels within the LN boundary. Those coordinates were then transferred into a custom MatLab script that calculated and returned the binned minimum distance between the drawn LN boundary and the thresholded fluorescent pixels. The collected data was gathered for 24 LN samples and the difference between the NP and 3-Rhod signals was calculated and normalized to determine the bias of fluorescence towards each species along distance from the LN border.

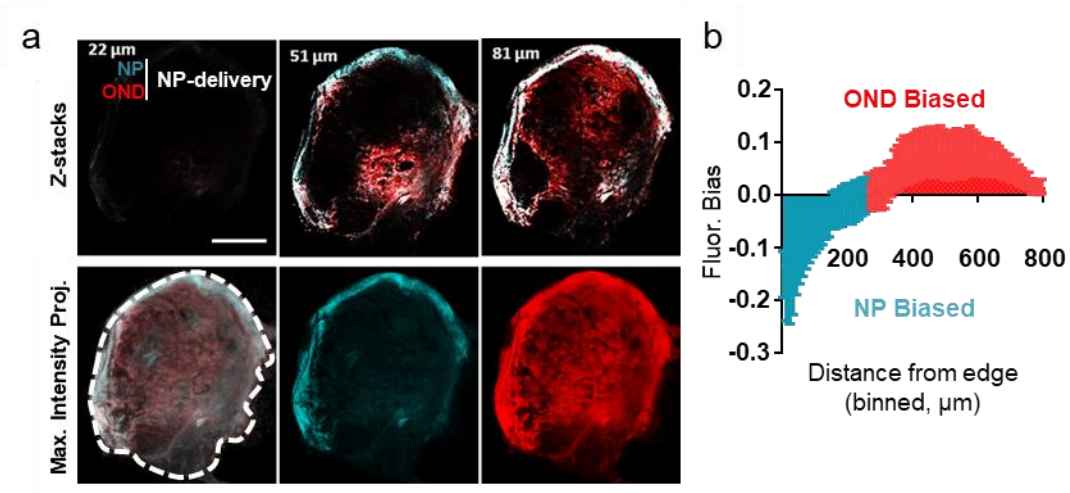

Supplementary Figure 7. Altered access by NP-OND throughout draining lymph node. a) Fluorescence microscopy of draining LN excised from C57Bl6 mouse 24 h after forelimb skin administration of: NP labeled with AF647-maleimide alone vs. (OND) NP labeled with both AF647-maleimide and **3-Rhod**. Top row = presence of NP and **3-Rhod** fluorescence at different 2-channel Z stack depths of the LN. Bottom row = Maximum intensity projection of LN. Left = 2-channel overlaid NP and OND cargo fluorescence. middle = AF647 channel; right = rhodamine channel. These images are representative of findings in three independent experiments. Scale bar = 500 µm. b) Difference in normalized pixel count for each single channel (NP vs. **3-Rhod**) vs.

distance from the outermost portion of the LN (dashed white line in panel f). Negative blue shaded area indicates NP bias; positive red shaded area indicates rhodamine bias. n=24 biological replicates per group.

Cargo encapsulation, release, and biodistribution

Cyanine5.5 carboxylic acid fluorescent dye (Cy5.5, “cargo”) (Lumiprobe, Hunt Valley, MD, USA, 27090) was dissolved in DMSO (VWR, 97063-136) at 5 mg/mL, then added to an aqueous solution of NPs at 10% v/v and mixed by inversion for 5 minutes. 100uL of Cy5.5-NP or concentration-matched free Cy5.5 were diluted to 1000uL with Milli-Q water, and a sample was taken and fluorescence and absorbance measurements were read on a BioTek Synergy H4 microplate reader (BioTek, Winooski, VT, USA) to obtain starting signal. NPs or free dye were added to 100,000 Da MWCO dialysis cups (Spectrum Chemical, New Brunswick, NJ, USA, G235035), and dialyzed against 5L of Milli-Q water with stirring. At varying time points, samples were taken and read on the microplate reader (ex.: 680nm, em.: 710nm; abs.: 695nm). Measurements were normalized to the signal from non-dialyzed “capped” Cy5.5-NPs and presented as fraction of the starting Cy5.5 signal at t=0h. Signal from PEG-containing NPs was determined to remain stable with dialysis using an iodine assay [reference Alex used in Supplementary Methods]. NP-containing samples were diluted into 200uL water and to this 50uL of 50mg/mL BaCl (Sigma Aldrich, 202738) in 1N HCl was added, followed by addition of 25uL of 9:1 20mg/mL KI:1N I2 (KI: Sigma Aldrich, 793582; I2: Alfa Aesar, Tewksbury, MA, USA, 35632). The reaction was allowed to proceed for 10 minutes after which absorbance was measured at 535 nm on a microplate reader.

NPs containing available core thiols were reacted with 10 mM AlexaFluor 488 maleimide (Thermo Fisher, A10254) overnight with stirring and cleaned of free dye using a sepharose CL-6B size exclusion chromatography column. NP fractions were combined, concentrated using 30,000 Da MWCO Amicon spin filter (Millipore Sigma, UFC903008) at 4000 x g for 30 min, and stored at 4°C until use. Stability of AF488 labeling with storage was determined by running a sample of AF488-labeled NPs through a sepharose CL-6B column and observing an absence of free dye in the appropriate fractions. Cy5.5 cargo was encapsulated into the core of AF488-labeled NPs as described above. After encapsulation, Cy5.5-NPs were cleaned of free dye and DMSO using a 7,000 Da MWCO Zeba spin desalting column (Thermo Fisher, 89892). C57BL6 mice were injected into both forearms i.d. with 30uL fresh Cy5.5-encapsulated (**Cargo**) AF488-NPs 48, 24, 12, and 6 h prior to sacrifice. Mice were sacrificed and LNs excised and stained as described. Cy5.5 (**Cargo**) and AF488 (**NP**) were measured on the AlexaFluor700 and FITC channels, respectively. Cells were gated as described above.

Virus-like Particle (VLP) Production

Virus-like particles (VLPs) derived from bacteriophage Qβ were produced as reported.[12, 13] Briefly, BL21(DE3) Escherichia coli were transformed with T7 pCDF plasmid containing Qβ coat protein and streptomycin antibiotic resistance genes. A single positive colony was selected and cultured in 50 mL SOB media containing 20 mM $MgSO_4$ and 5 mg/mL streptomycin at 37°C for 17 h. Expression flasks (500 mL) containing 20 mM $MgSO_4$ and 5 mg/mL Streptomycin were inoculated with 12 mL of

starter cultures, incubated at 37°C and absorbance measured at 600 nm. Cultures were induced with 1 mM IPTG once OD = 0.9 and incubated, shaking, at 37°C for 4 h. Cultures were pelleted, resuspended in 0.1 M KPO_4 buffer, and cells lysed by sonication for 20 min (30 sec intervals) by VirSonic 600 probe sonicator, followed by ammonium sulfate precipitation, and organic extraction with 1:1 chloroform:butanol to separate protein from cellular debris. VLPs were purified by centrifugation at 28,000 rpm in a 10-40% sucrose gradient followed by ultracentrifugation at 68,000 rpm via Beckman Coulter Optima XPN-80 ultracentrifuge.

VLP Characterization

Protein concentration of purified VLPs was determined by Bradford Assay (Coomassie reagent, absorbance 595 nm). Average particle concentration was 20 mg/mL. Particle hydrodynamic radius was determined by dynamic light scattering (Wyatt DynaPro Platereader), followed by fast protein liquid chromatography (Agilent 1260, Superose 6 10/300 GL) to assess particle purity. Molecular weight of VLP coat protein was measured by time-of-flight liquid chromatography / mass spectrometry (C3 column 2.1 x 75mm, Agilent 1260 Infinity and Agilent 6230 TOF LC/MS). Mass spectrometry data were analyzed using Agilent MassHunter Software. VLP coat protein sequence: AKLETVTLGNIGKDGKQTLVLNPRGVNPTNGVASLSQAGAVPALEKRVTVSVSQPSRN RKNYKVQVKIQNPTACTANGSCDPSVTRQAYADVTFSFTQYSTDEERAFVRTELAALL ASPLLIDAIDQLNPAY, MW 14 123 Da (PDB ID 1QBE) (Golmohammadi, *Biochemistry* 1996).

VLP-NHS ester AF647 conjugation and characterization

VLPs were covalently labeled by reacting excess VLP with NHS-ester AlexaFluor 647 at 4°C for 16 h on a rotisserie stand in the dark. VLP-AF647 conjugates were purified by size exclusion chromatography using two consecutive PD-10 columns and concentrated using 100 kDa MWCO Amicon Ultra 4 spin filter and centrifugation at 4000 x g for 20 min in 1x -/- PBS. Protein concentration was determined by Bradford assay, followed by DLS, FPLC, and TOF LC/MS to determine particle hydrodynamic radius, reaction purity, and density of dye per coat protein, respectively. Final concentration was 5.7 mg/mL of VLP-AF647.

VLP-OND3-Rhodamine Conjugation and Characterization

VLPs were thiol-activated by adding dithiothreitol (DTT) to 5 mM for 20 min at 25°C. VLPs were cleaned of DTT by running reaction on three consecutive 5mL 7 kDa MWCO Zeba columns at 1000 x g for 2 min. To install OND3-Rhodamine and maleimide-Rhodamine, reduced thiols on VLPs were immediately reacted with excess OND3-Rhod for 1 h, RT, rotisserie, in the dark. VLP conjugates were cleaned of unreacted OND-Rhod by size-exclusion chromatography using two consecutive PD-10 columns in 1x -/- PBS then concentrated to 1 mL using 100 kDa MWCO Amicon Ultra 4 spin filter and centrifugation at 4000 x g for 20 min. Final protein concentration was determined by Bradford assay, followed by DLS, FPLC, and TOF LC/MS to determine particle hydrodynamic radius, reaction purity, and density of dye per coat protein, respectively. Final concentration was 3.8 mg/mL of VLP-AF647-OND3-Rhodamine.

Stability of Maleimide linker to NP Core versus Corona Thiols

Thiol-mediated displacement of maleimide linkers is a well-described phenomenon.[14] Consistent with this, the release of rhodamine linked via a maleimide linker to NP thiols was accelerated in the presence of an added small molecule thiol (β-mercaptoethanol) (Supplementary Figure 8a,b). Use of NP core versus corona thiols presented the opportunity to explore the effects of different thiol accessibility on this process. When applied *in vivo*, fluorophore connected to PDS NP corona thiols via a maleimide demonstrated prodigious uptake in B and T cells, and slightly increased uptake in both subsets of dendritic cells (Supplementary Figure 8c). Uptake in these cells peaked at approximately two times the half-life in the presence of competitive thiols, a trend we also observed for both OND linkers (Figure 4d). In contrast, fluorophore that was tethered to the nanoparticles via core thiols showed little cellular association (Supplementary Figure 8c), consistent with all other *in vivo* experiments conducted using core thiol-tagged NP that did not use OND connectors (Figures 2 and 3, Extended Data Figures 2 and 3).

The apparent enhanced delivery from corona-thiol-maleimide conjugates was unlikely to be caused by particle instability, as Pluronic levels on NPs did not decay upon extended storage or with *in vitro* release (Supplementary Figure 6). However, when adjacent unreacted NP corona thiols were capped with N-ethylmaleimide, the apparent enhanced delivery disappeared: in this case, the amounts of fluorophores found associated with cells were low and roughly equivalent for corona-tethered vs. core-tethered maleimides (Supplementary Figure 8d).

These results suggest that uncapped thiols on the corona can engage adjacent thiol-maleimide adducts to induce intramolecular (intra-particle) retro-Michael reaction, as shown in Supplementary Figure 8e (red). This apparently occurs much more rapidly than intermolecular attack by free thiol (Figure 8e, blue) or by free thiols in the core, which may be poorly positioned or less abundant. We plan to more fully investigate this phenomenon as another potential programmable multistage release strategy. **Note** that the use of maleimide as a “noncleavable” linker as mentioned in the main text refers to cases in which dyes were conjugated to interior NP thiols, which were subsequently capped with N-ethylmaleimide.

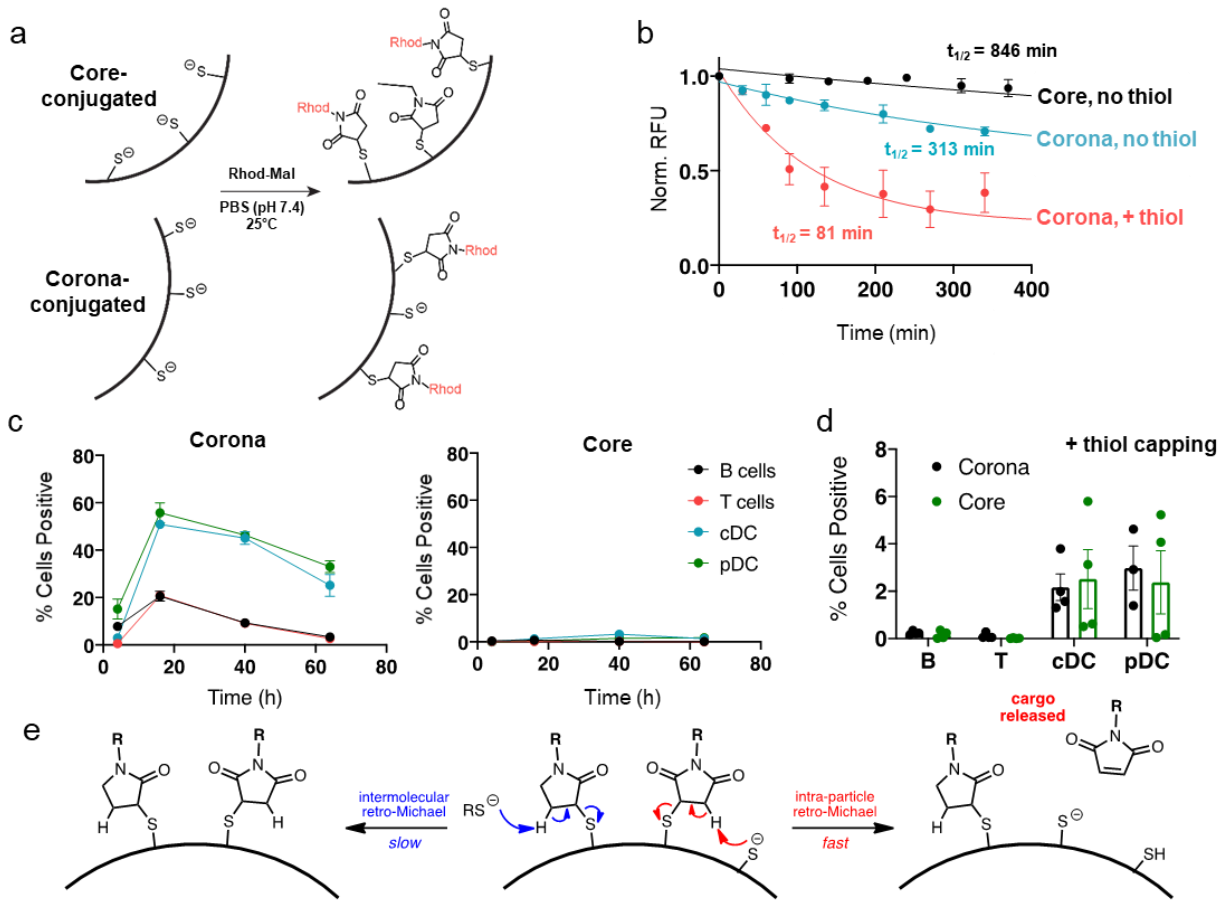

Supplementary Figure 8. Maleimide stability on external NP thiols. a) Schematic representation of the preparation of PPS or PDS PPS NP carrying Rhodamine via maleimide linker on thiols present on the NP core versus corona, respectively. b) Release curves of Rhodamine NP tethered via thiols either on the NP core or corona at 37°C, with or without the addition of β-mercaptoethanol (200mM). Data is normalized to signal of Rhodamine-maleimide conjugated to thiols in the NP core. Labels: half-lives of Rhodamine as released from NP (data is normalized to signal at t=0 within each experiment, n=3 sample replicates per time point). c) Fluorophore uptake by indicated immune cells after i.d. injection with NPs whose free thiols remained uncapped after

labelling with Rhodamine-maleimide on NP corona (corona) or NPs whose free thiols had been capped after labelling core thiols with AF647-maleimide (core), as in panel a. n=3 biological replicates per time point. d) Percent of immune cells positive for Rhodamine conjugated to the NP via maleimide linker on thiols on NP corona (black) or core (green) and capped with N-ethylmaleimide as measured by flow cytometry. n=4 biological replicates per group. e) Proposed retro-Michael reaction to eject cargo-maleimide when intermolecular thiolate groups are available. For all graphs, the columns/points and error bars represent the mean + SEM.

Synthesis and characterization of irinotecan derivatives

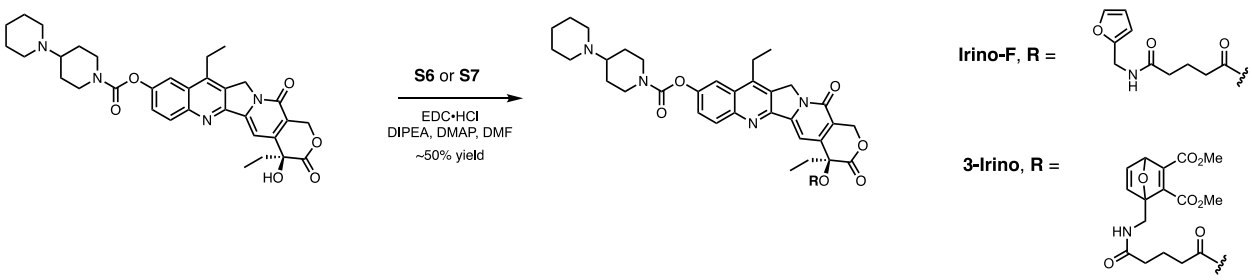

Scheme S10. Synthesis of **Irino-F** and **3-Irino** drug-OND conjugates.

Carboxylic acids **S6** or **S7** (1.2 equiv) was activated with EDC•HCl (1.2 equiv), DMAP (0.1 equiv), and iPr$_2$NEt (2.2 equiv) for 10 min in DMF followed by addition of Irinotecan HCl salt trihydrate (1.0 equiv). The reaction mixture was stirred at room temperature for 16 h. EtOAc and H_2O were added and the aqueous phase was extracted with EtOAc ($\times$2). The organic extracts were combined, dried over Na_2SO_4, filtered and concentrated *in vacuo*. The residue was purified on reversed-phase C18 column to yield **Irino-F** and **3-Irino** as yellow fluffy solids (50–60% yield).

Irino-F: ESI-HRMS calcd for $C_{43}H_{50}N_5O_9^+$ $[MH]^+$: 780.3603, found: 780.3601; ^{1}H NMR (400 MHz, DMSO-d_6), δ 9.31 (br s, 1H), 8.28 (t, 1H, J = 5 Hz), 8.18 (d, 1H, J = 8.6 Hz), 8.00 (d, 1H, J = 2.0 Hz), 7.68 (dd, 1H, J = 2.3, 9.4 Hz), 7.54 (br s, 1H), 7.02 (s, 1H), 6.35 (m, 1H), 6.18 (d, 1H, J = 3.2 Hz), 5.51 (m, 2H), 5.35 (m, 2H), 4.36–4.50 (m, 2H), 4.15–4.29 (m, 4H), 3.40–3.53 (m, 3H), 3.10–3.23 (m, 3H), 2.92–3.05 (m, 3H), 2.05–2.23 (m, 6H), 1.84–1.93 (m, 2H), 1.65–1.82 (m, 7H), 1.44 (m, 1H), 1.29 (t, 3H, J = 7.5 Hz), 0.92 (t, 3H, J = 7.8 Hz).

3-Irino: ESI-HRMS calcd for $C_{49}H_{56}N_5O_{13}^+$ $[MH]^+$: 922.3869, found: 922.3885; ^{1}H NMR (500 MHz, DMSO-d_6), δ 9.14 (br s, 1H), 8.19 (d, 1H, *J* = 9.3 Hz), 8.07 (m, 1H), 8.00 (d, 1H, *J* = 2.5 Hz), 7.69 (dd, 1H, *J* = 2.5, 9.3 Hz), 7.31 (ddd, 1H, *J* = 1.9, 5.3, 11.8 Hz), 7.11 (t, 1H, *J* = 4.9 Hz), 7.03 (d, 1H, *J* = 1.7 Hz), 5.70 (dd, 1H, *J* = 1.8 Hz), 5.49–5.55 (br m, 2H), 5.33–5.40 (br m, 2H), 4.37–4.50 (m, 1H), 4.18–4.27 (m, 1H), 3.88–4.01 (m, 2H), 3.77–3.85 (m, 1H), 3.72 (d, 3H, *J* = 4.76 Hz), 3.71 (s, 3H), 3.10–3.27 (m, 4H), 2.90–3.09 (m, 4H), 2.07–2.23 (m, 6H), 1.85–1.95 (m, 2H), 1.62–1.84 (m, 7H), 1.45 (m, 1H), 1.30 (t, 3H, *J* = 7.4 Hz), 1.25 (br s, 1H), 0.93 (t, 3H, *J* = 7.5 Hz).

In vitro testing of furan-modified irinotecan toxicity on splenocytes

C57BL6 mouse spleens were excised and processed for splenocytes following well-known literature procedures.[11, 15, 16] 1M splenocytes were platted in (Iscove's Modified Dulbecco's Media) IMDM media in round bottom 96 well plates in duplicate for each concentration of drug tested. Furan-modified irinotecan was dissolved in 5% DMSO/PBS and then added to the wells to reach the final concentration listed in the manuscript. The cells were incubated at 37°C and 5% CO_2 for 24 h. Cell death (Extended Data Figure 4) and marker staining was performed using flow cytometry. The

cells were first blocked with 2.4G2, followed by Live/Dead staining using Zombie Aqua (1:100), and subsequent all staining: CD11c – BV421 (1:80), B220 – BV650 (1:40), CD3 – BV711 (1:80), and CD11b – AF700 (1:80), with washing in between each step. Subsequently, cells were in 2% PFA for 15 min before washing and resuspension in FACS buffer (2% albumin solution in 1x PBS). Samples were run on a BD Fortessa flow cytometer. Cells were gated according to the following markers: B – B220+ CD3- CD11b- and PDC – B220+ CD11c+.

Release studies of NP-OND-CpG

NP-OND-CpG purified from Sepharose CL6B column was incubated in a 37°C water bath and aliquots were withdrawn at three time points (0, 24 and 72 h). The collected samples were passed through a CL6B column followed by collection of the NP-OND-CpG and the Furan-CpG fractions. The fractions were analyzed on LCMS (Figure S10), CpG was measured using GelRed staining, and NP were measured using Iodine staining.

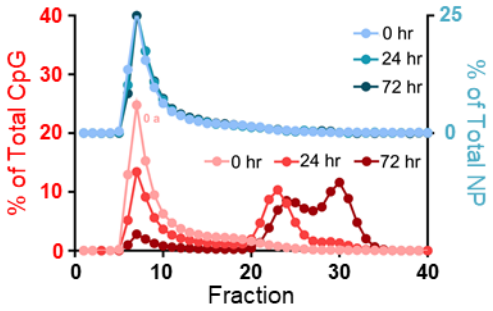

time (h)	species	% of total CpG
0	NP-CpG	100
24	NP-CpG	51
24	**CpG-F**	49
72	NP-CpG	11
72	**CpG-F**	89

Supplementary Figure 9. CpG release from NP-OND system. Left, Size-exclusion chromatography (CL6B column) of solutions containing NP-OND-CpG particles at 37°C at the indicated time points; elution around fraction 8 is characteristic of NPs; later

fractions contain released molecules. CpG was detected using GelRed staining and NPS were detected using iodine staining. Right, Quantitation of CpG release from left panel. This experiment was repeated once with similar results. For all graphs, the columns/points and error bars represent the mean + SEM.

dLN-specific immunomodulatory effects from i.d. injection of CpG

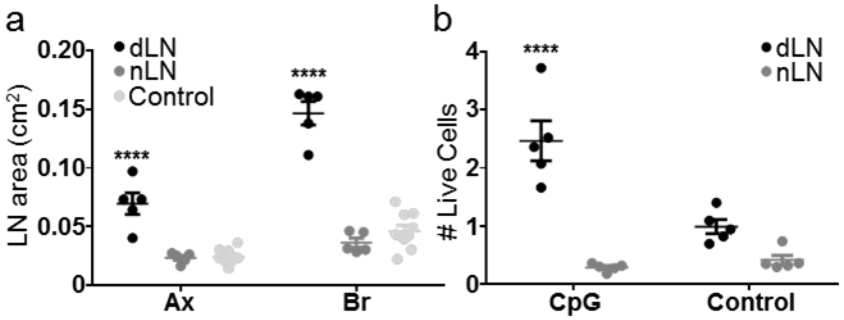

Supplementary Figure 10. Response to intradermally administered CpG only occurs in LNs draining the site of injection (dLN) and not in the contralateral LNs (nLN). a) LN area for both axillary and brachial LNs 24 hr after CpG (1 µg) treatment (dLN and nLN) or saline controls (Control). n=5 biological replicates per group. b) Number of live LN cells 24 h after CpG treatment. n=5 biological replicates per group. For all graphs, the columns/points and error bars represent the mean + SEM. Statistics were performed by two-way ANOVA with Tukey's multiple comparisons test. ****=p<.0001, ***=p<.005, *=p<.05.

CpG systemic biodistribution

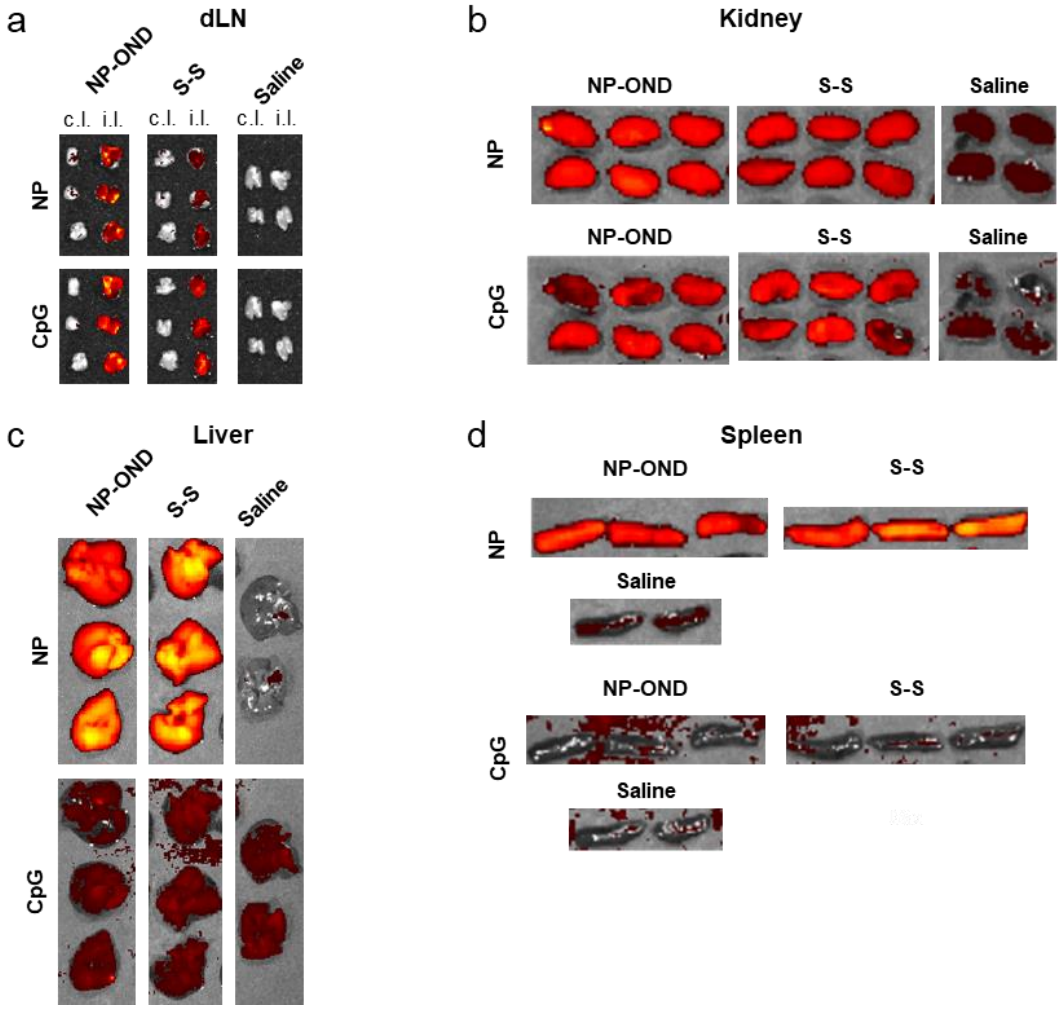

Supplementary Figure 11. Supplementary Figure 15. CpG delivered cargo released via OND exhibits low systemic bioavailability. A total of 1 ug of CpG was administered in each formulation. Animals were sacrificed 24 h post injection and tissues were imaged using IVIS. Units are Radiant Efficiency. a) dLN. b) Kidney. c) Liver. d) Spleen. Total CpG dose, 1 ug. (c.l. = non-draining contralateral lymph node; i.l. = draining inguinal lymph node; NP-OND = pluronic-PPS nanoparticle decorated with CpG via OND connector, as described in the text and designated NP-OND-CpG in Figure 5; S-S = pluronic-PPS nanoparticle decorated with CpG via disulfide connector;

NP = observation of dye attached to the nanoparticle; CpG = observation of dye attached to oligonucleotide.) This experiment was repeated once with similar results.

EL4 lymphoma model

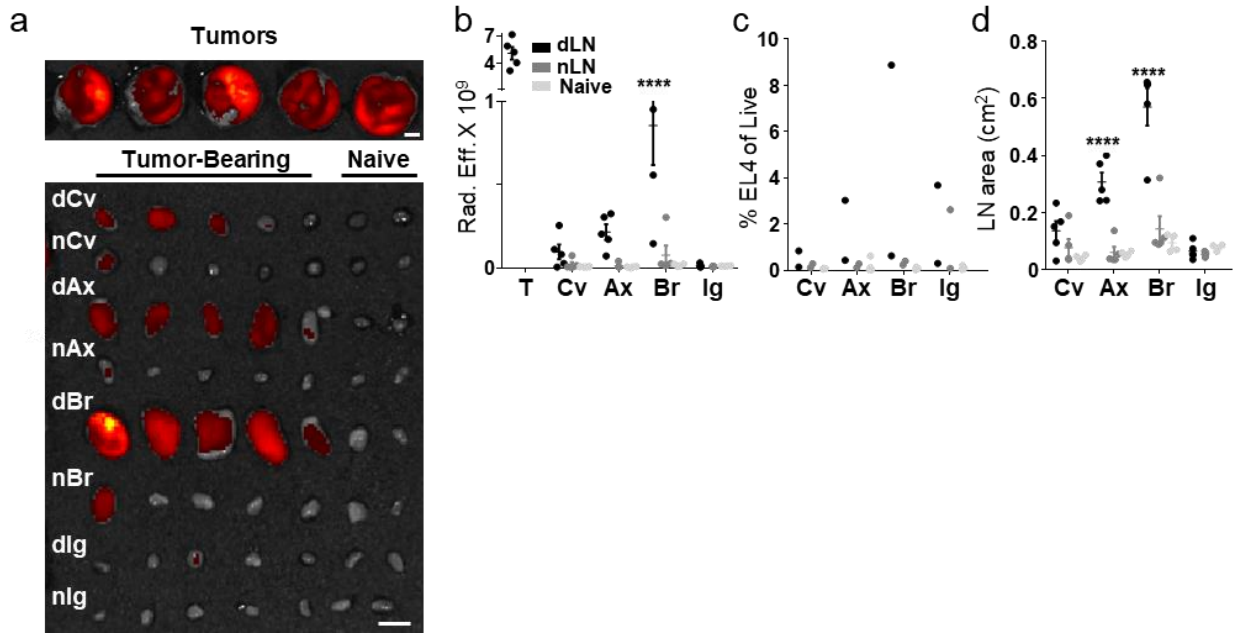

Supplementary Figure 12. **EL4 LN lymphoma model.** a) Representative IVIS images of tumors from C57Bl6 mice implanted with 250k EL4-GFP cells in the left dorsal skin. (Top) Primary tumors from 5 mice. (Bottom) Resected LNs draining (d) and contralateral (n) to the implantation site from tumor-bearing (n=5) or naïve (n=2) mice. Cv = cervical, Ax = axillary, Br = brachial, Ig = inguinal. GFP fluorescence is false-colored red. b) Quantification of IVIS images demonstrating the presence EL4-GFP cells in the dLN with increasing values in dLN closer to the primary tumor. n=5 biological replicates per group. c) Percent of total live LN cells CD3+GFP+TCRVβ12+ (EL4-GFP cells). n=2 biological replicates per group. d) Area of dLN and nLN in tumor bearing mice with both side LNs pooled from control mice. n=5 biological replicates per treatment group. For all

graphs, the columns/points and error bars represent the mean + SEM. Statistics were performed by two-way ANOVA with Tukey's multiple comparisons test. ****=p<.0001, ***=p<.005, *=p<.05.

Gating strategy for EL4-GFP cells in dLN

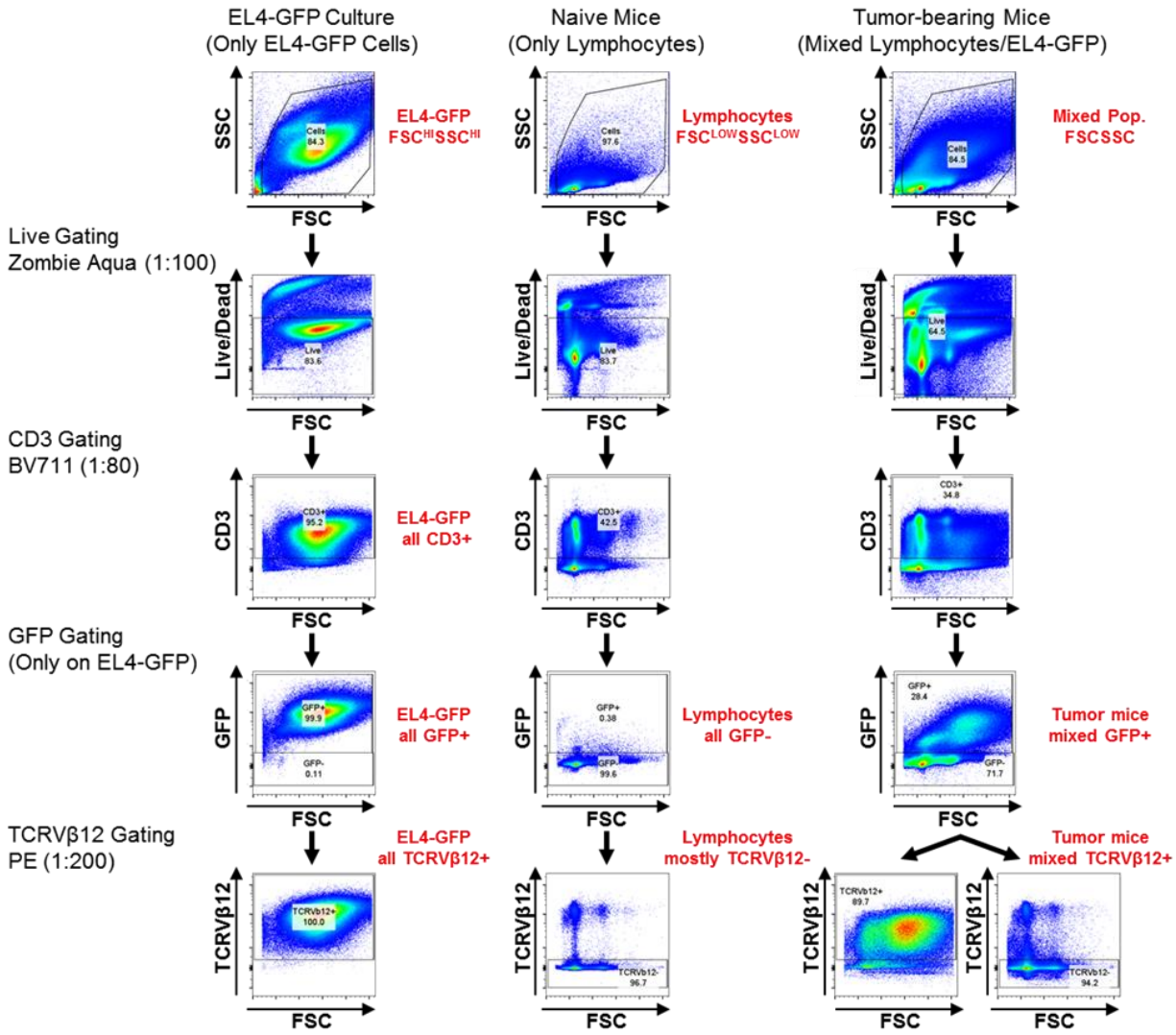

Supplementary Figure 13. Flow cytometry gating strategy for EL4-GFP cells in LNs. EL4-GFP cells are larger in size than lymphocytes, nearly 100% CD3+, 100% GFP+, and 100% TCRVβ12+. Lymphocytes from mechanically strained LNs are a

heterogenous mixture of CD3+ and CD3- cells, with all CD3+ being GFP- and TCRVβ12- (97%). Within the dLN of a tumor-bearing mouse both cell types are evident within the FSC/SSC dot plot and the EL4-GFP cells can be distinguished from the C57Bl6 mice CD3+ cells by GFP and TCRVβ12. For each gating the fluorophore and dilution (per 1M cells/100µL) is listed.

Immunohistochemistry

Flash frozen EL4 (parental or GFP expressing) tumors and EL4 LNs were cut into 5-µm thick sections and mounted on glass slides. Slides were rinsed with 0.1% Tween 20 in PBS with calcium and magnesium and incubated for 1 h at room temperature with 10% Normal Donkey Serum (MilliporeSigma™ Calbiochem™, 5664605ML, San Diego, CA) in PBS with calcium and magnesium for protein blocking. Slides were rinsed after protein blocking in 0.1% Tween 20 in PBS with calcium and magnesium prior to overnight treatment at 4°C with mouse monoclonal anti-TCRVβ12 (Abcam, ab171114, 1:50, Cambridge, MA) antibody. EL4-GFP tumors were also incubated with AlexaFluor 488 rabbit polyclonal anti-GFP tag antibody (Invitrogen, A-21242, 1:300, Grand Island, NT, USA) in addition to monoclonal anti-TCRVβ12. The following day, slides were rinsed with 0.1% Tween 20 in PBS with calcium and magnesium and treated with AlexaFluor 647 goat anti-mouse IgG2b (Invitrogen, A-21311, 1:200, Grand Island, NT, USA) for 1 h at room temperature. Slides were mounted with VECTASHIELD® mounting media (Vector Laboratories, H-1000, Burlingame, CA) and imaged using a Zeiss LSM 780 confocal microscope system.

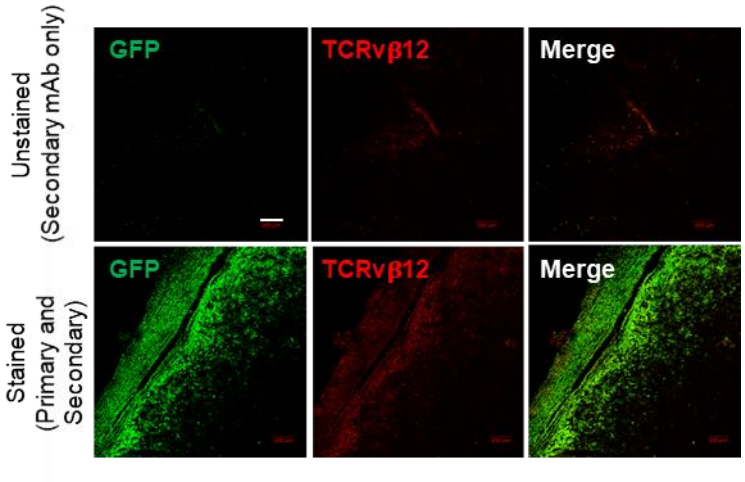

Supplementary Figure 14. **TCRVβ12 mAb staining of EL4 cells.** Left, Fluorescent signal in unstained (top) and from Rb α-GFP-AlexaFluor488 antibody stained (bottom) EL4-GFP skin tumors. Middle, Fluorescent AF647 signal from secondary only (top) and Ms α-Ms TCRVβ12 monoclonal antibody stained (bottom) EL4-GFP skin tumors. Right, Merged fluorescence from GFP and TCRVβ12 stains. Scale bar (white, upper left panel) = 200 µm. This experiment was repeated once with similar results.

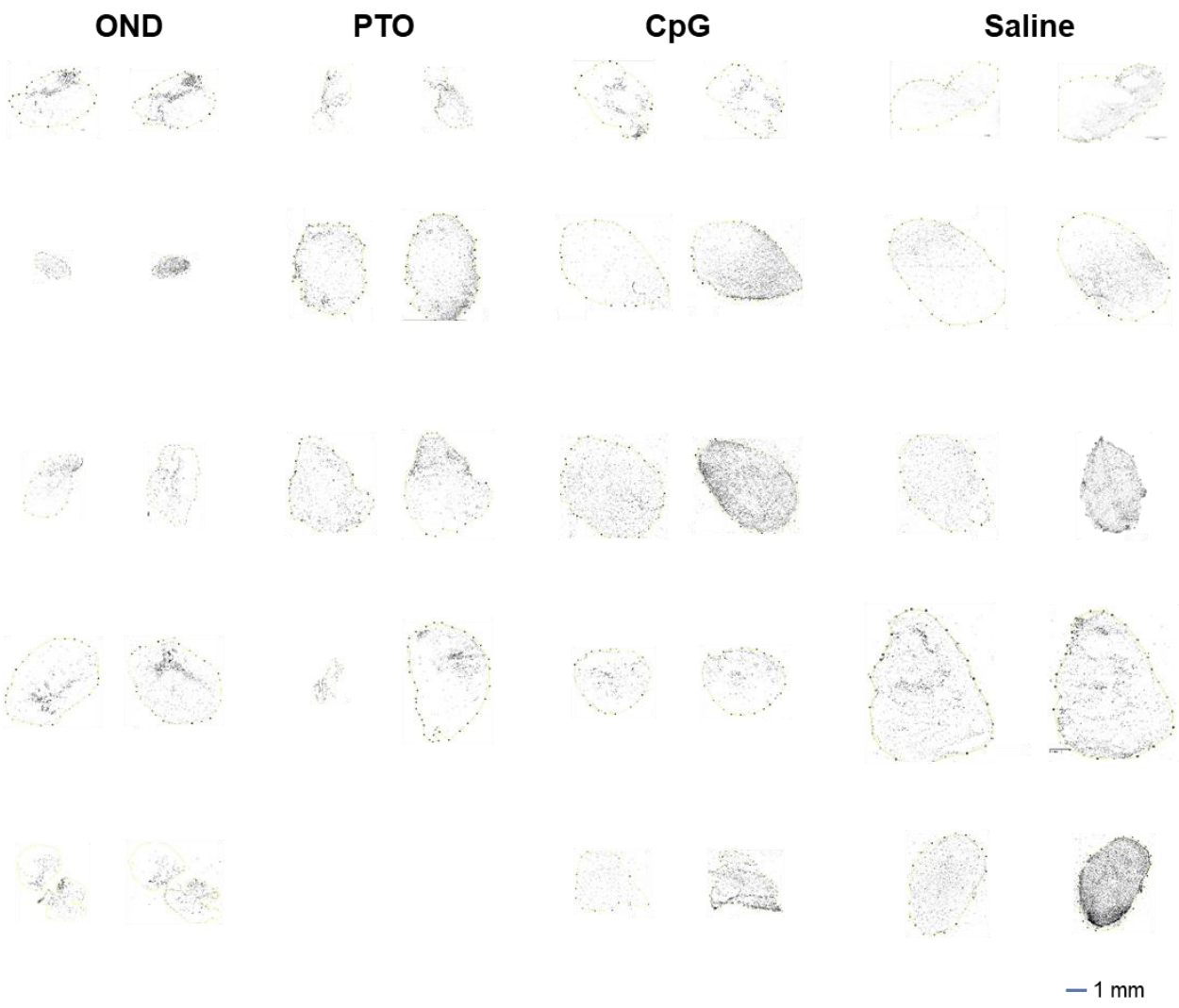

Supplementary Figure 15. Immunohistochemistry samples staining for EL4 using TCRVβ12 epitope. Left column for each group, control TCRVβ12 staining images of 5 µm LN slices from EL4 tumor experiment using only secondary antibody against TCRVβ12. Right column for each group, experimental TCRVβ12 staining images of 5 µm LN slices from EL4 tumor experiment using TCRVβ12 primary antibody. Scale bar (blue, lower right) = 1 mm. This experiment was repeated once with similar results.

EL4 primary tumor growth curves

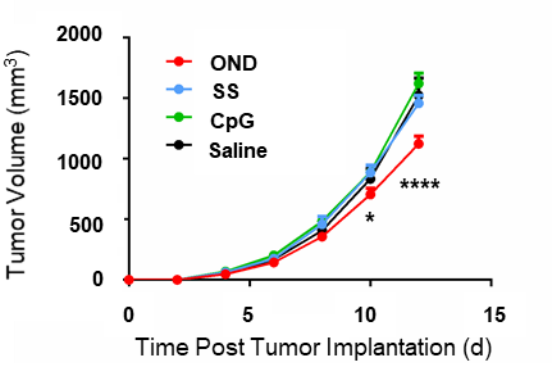

Supplementary Figure 16. **EL4 primary tumor growth.** Ellipsoid tumor volume over time. n=5 biological replicates per group. For all graphs, the columns/points and error bars represent the mean + SEM. Statistics were performed by ordinary one-way ANOVA with Tukey's multiple comparisons test. ****=p<.0001, ***=p<.005, *=p<.05.

References

1. Mitkin, O.D., Wan, Y., Kurchan, A.N. & Kutateladze, A.G. Synthesis of dithiane-based photolabile molecular systems. *Synthesis* **112**, 1133-1142 (2001).
2. van der Vlies, A.J., O'Neil, C.P., Hasegawa, U., Hammond, N. & Hubbell, J.A. Synthesis of pyridyl disulfide-functionalized nanoparticles for conjugating thiol-containing small molecules, peptides, and proteins. *Bioconjug Chem* **21**, 653-662 (2010).
3. Higginson, C.J., Eno, M.R., Khan, S., Cameron, M.D. & Finn, M.G. Albumin-Oxanorbornadiene Conjugates Formed ex Vivo for the Extended Circulation of Hydrophilic Cargo. *ACS chemical biology* **11**, 2320-2327 (2016).
4. Higginson, C.J., Kim, S.Y., Pelaez-Fernandez, M., Fernandez-Nieves, A. & Finn, M.G. Modular degradable hydrogels based on thiol-reactive oxanorbornadiene linkers. *J Am Chem Soc* **137**, 4984-4987 (2015).
5. Kislukhin, A.A., Higginson, C.J., Hong, V.P. & Finn, M.G. Degradable conjugates from oxanorbornadiene reagents. *J Am Chem Soc* **134**, 6491-6497 (2012).
6. Hong, V., Presolski, S.I., Ma, C. & Finn, M.G. Analysis and optimization of copper-catalyzed azide-alkyne cycloaddition for bioconjugation. *Angewandte Chemie (International ed. in English)* **48**, 9879-9883 (2009).
7. Nguyen, T. & Francis, M.B. Practical Synthetic Route to Functionalized Rhodamine Dyes. *Organic Letters* **5**, 3245-3248 (2003).
8. Sivakumar, K. et al. A Fluorogenic 1,3-Dipolar Cycloaddition Reaction of 3-Azidocoumarins and Acetylenes. *Organic Letters* **6**, 4603-4606 (2004).

9. Yu, D., Zhao, Q., Kandimalla, E.R. & Agrawal, S. Accessible 5′-end of CpG-containing Phosphorothioate Oligodeoxynucleotides is essential for immunostimulatory activity. *Bioorganic & Medicinal Chemistry Letters* **10**, 2585-2588 (2000).
10. Phelps, E.A., Templeman, K.L., Thule, P.M. & Garcia, A.J. Engineered VEGF-releasing PEG-MAL hydrogel for pancreatic islet vascularization. *Drug delivery and translational research* **5**, 125-136 (2015).
11. Thomas, S.N., Vokali, E., Lund, A.W., Hubbell, J.A. & Swartz, M.A. Targeting the tumor-draining lymph node with adjuvanted nanoparticles reshapes the anti-tumor immune response. *Biomaterials* **35**, 814-824 (2014).
12. Fiedler, J.D. et al. Engineered mutations change the structure and stability of a virus-like particle. *Biomacromolecules* **13**, 2339-2348 (2012).
13. Fiedler, J.D., Brown, S.D., Lau, J.L. & Finn, M.G. RNA-directed packaging of enzymes within virus-like particles. *Angewandte Chemie (International ed. in English)* **49**, 9648-9651 (2010).
14. Baldwin, A.D. & Kiick, K.L. Tunable degradation of maleimide-thiol adducts in reducing environments. *Bioconjug Chem* **22**, 1946-1953 (2011).
15. Lund, A.W. et al. VEGF-C promotes immune tolerance in B16 melanomas and cross-presentation of tumor antigen by lymph node lymphatics. *Cell Rep* **1**, 191-199 (2012).
16. Thomas, S.N. et al. Impaired humoral immunity and tolerance in K14-VEGFR-3-Ig mice that lack dermal lymphatic drainage. *Journal of immunology (Baltimore, Md. : 1950)* **189**, 2181-2190 (2012).

Characterization of NP-OND-Dn conjugation and fragmentation rates

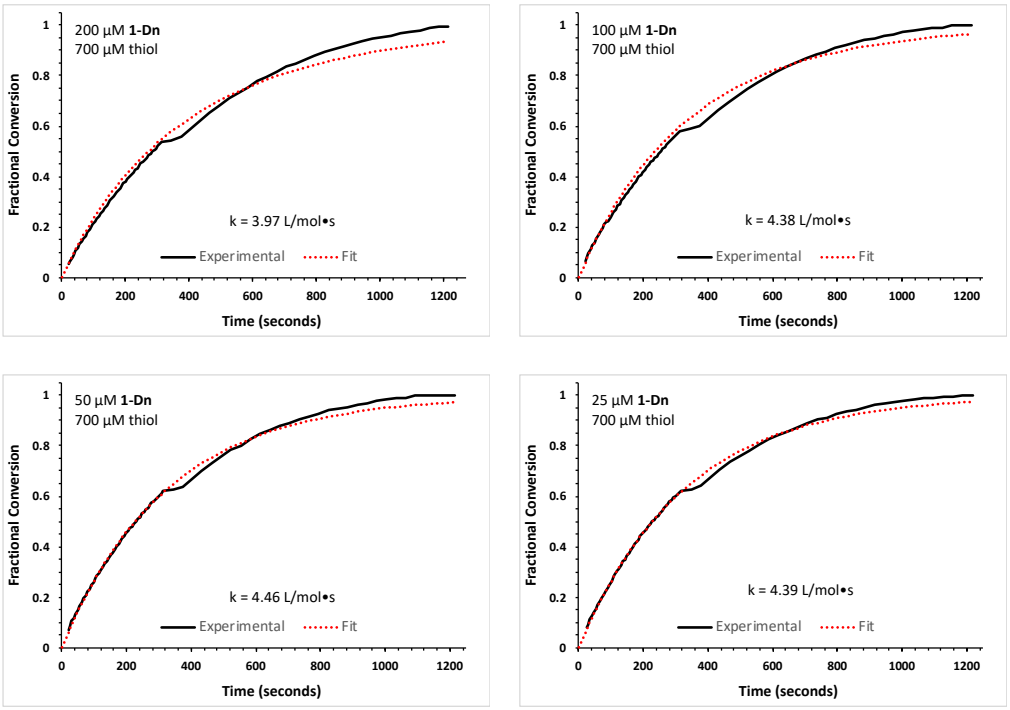

Supplementary Data Figure S1. Conjugate addition between NP core thiols and fluorogenic reagent **1-Dn** at room temperature. Concentration of electrophile and thiol, and rate constant for best fit are shown. This experiment was repeated once with similar results.

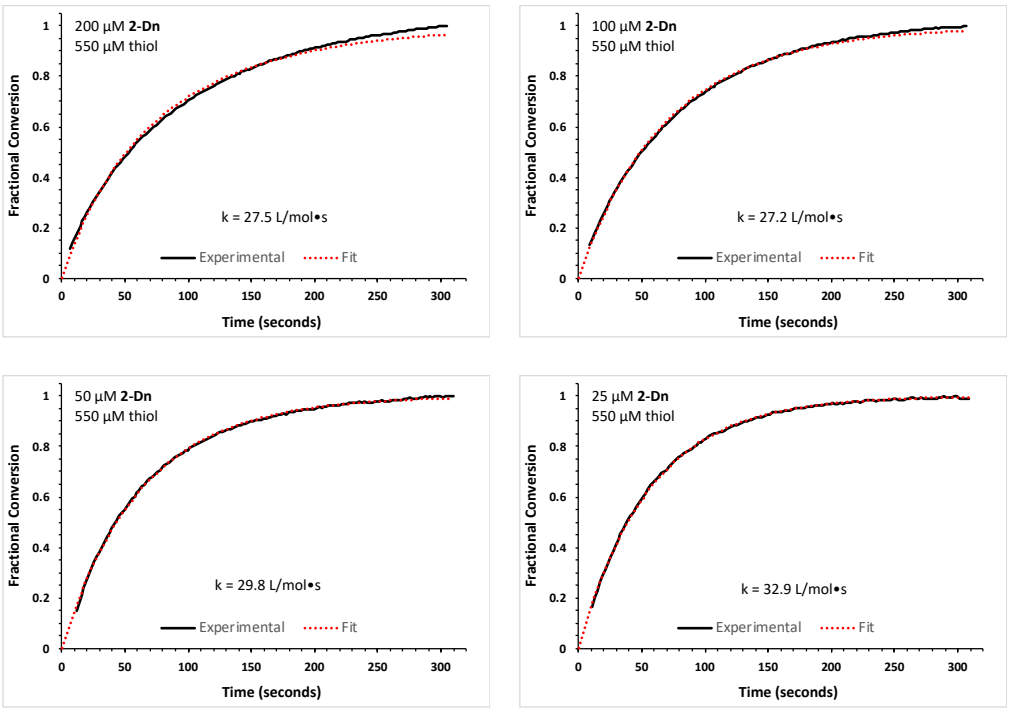

Supplementary Data Figure S2. Conjugate addition between NP core thiols and fluorogenic reagent **2-Dn** at room temperature. Concentration of electrophile and thiol, and rate constant for best fit are shown. This experiment was repeated once with similar results.

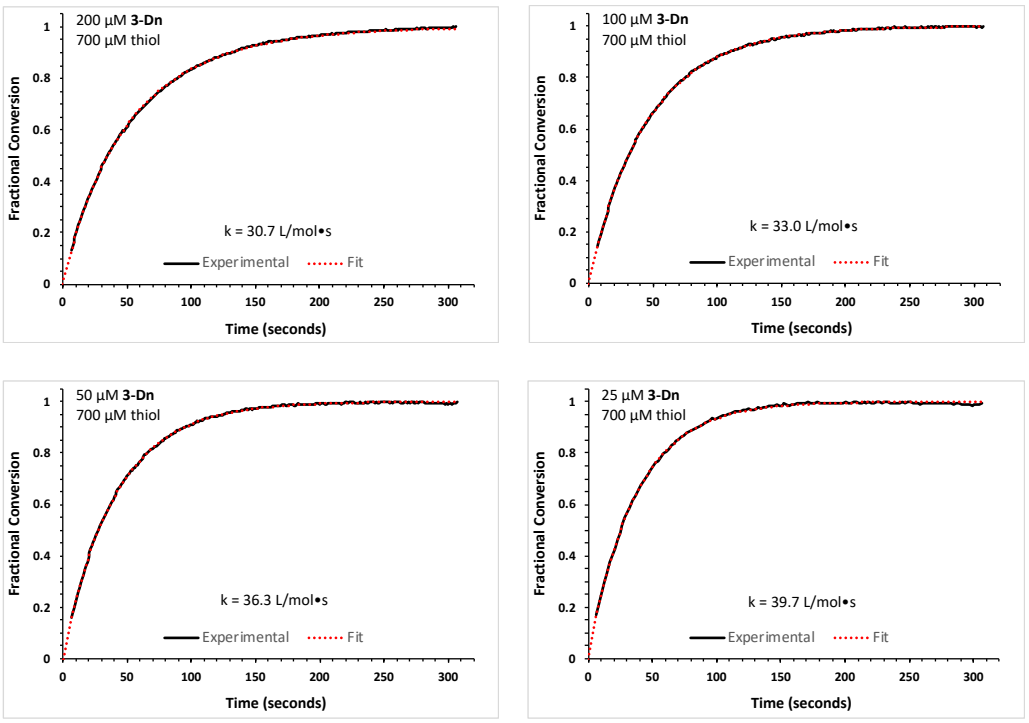

Supplementary Data Figure S3. Conjugate addition between NP core thiols and fluorogenic reagent **3-Dn** at room temperature. Concentration of electrophile and thiol, and rate constant for best fit are shown. This experiment was repeated once with similar results.

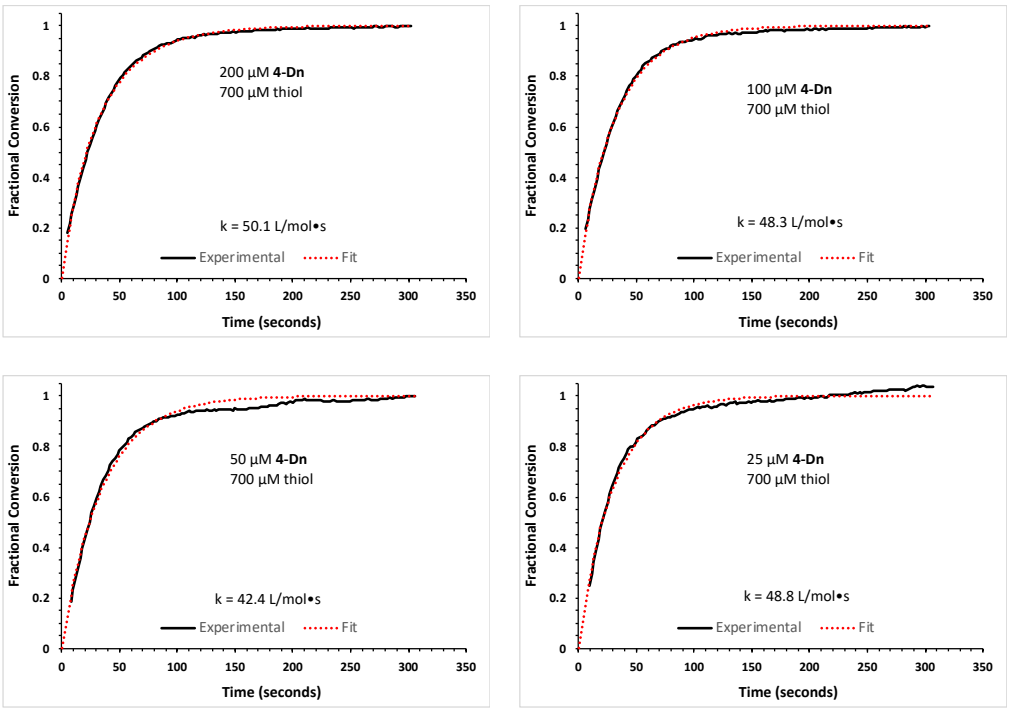

Supplementary Data Figure S4. Conjugate addition between NP core thiols and fluorogenic reagent **4-Dn** at room temperature. Concentration of electrophile and thiol, and rate constant for best fit are shown. This experiment was repeated once with similar results.

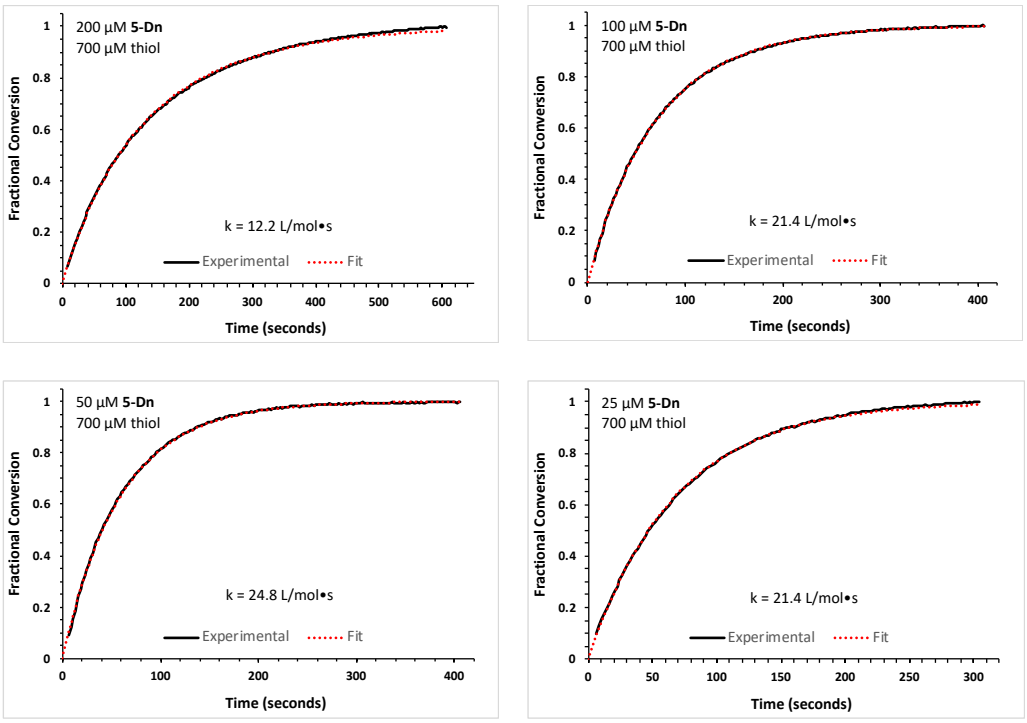

Supplementary Data Figure S5. Conjugate addition between NP core thiols and fluorogenic reagent **5-Dn** at room temperature. Concentration of electrophile and thiol, and rate constant for best fit are shown. This experiment was repeated once with similar results.

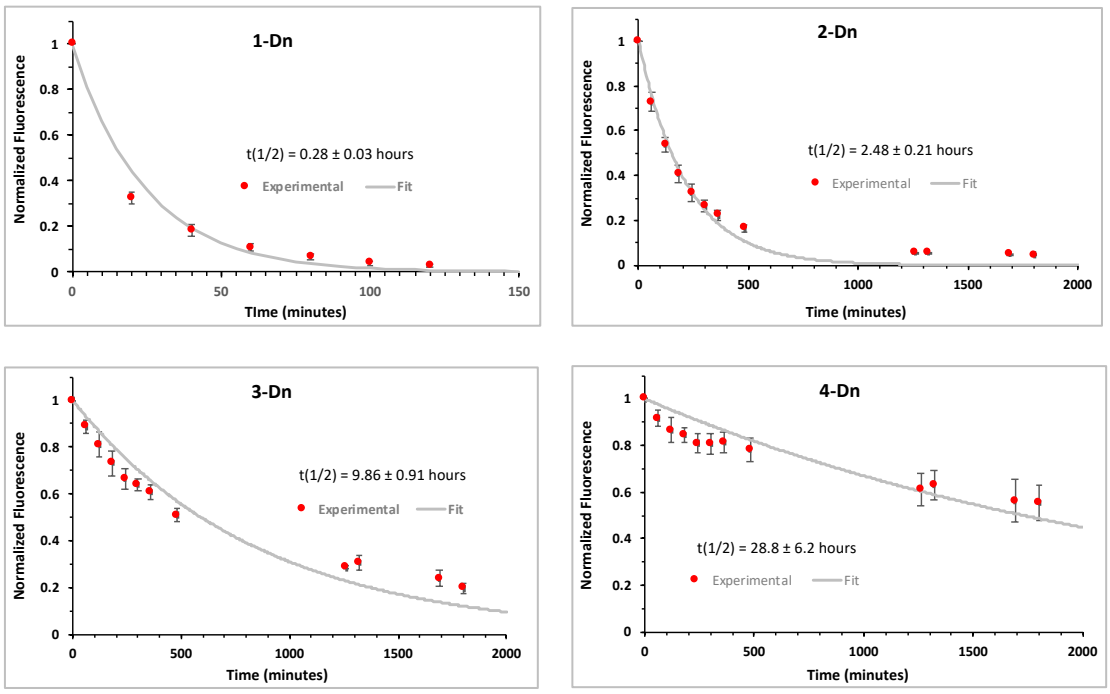

Supplementary Data Figure S6. Retro-Diels-Alder fragmentation and cargo release profiles from NP-OND-Dn conjugates prepared with OND electrophiles **1-Dn**, **2-Dn**, **3-Dn**, and **4-Dn**. This experiment was repeated once with similar results. n=3 samples per group.

Measurement of NP vs OND cargo distribution within LN images

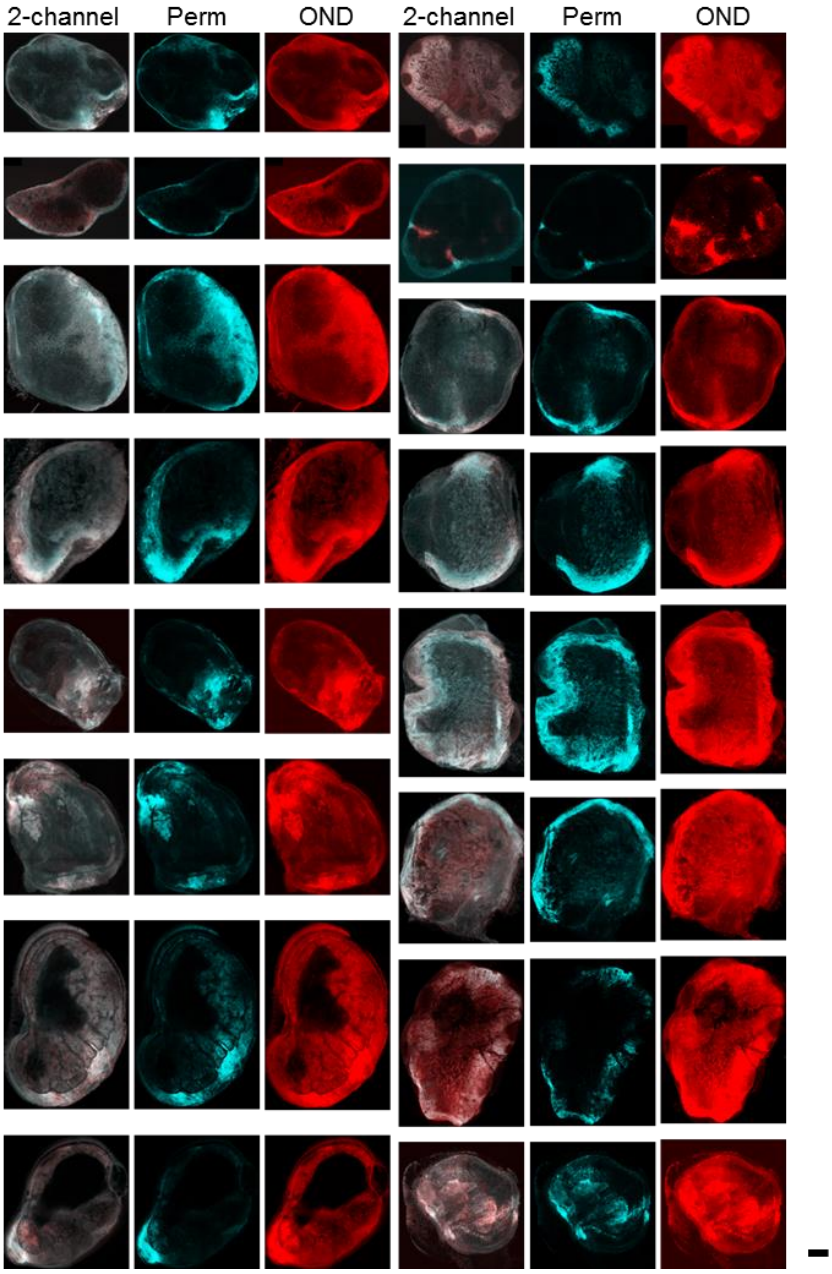

Supplementary Data Figure S7. LN fluorescence spatial distribution. LN confocal images are converted to maximum intensity projections of all Z stacks. Images are separated from 2-channel overlaid into (NP) NP labeled with AlexaFluor647 via non-cleavable linker and (OND) **3-Rhod** fluorescence images. Black bar = 500 μm. These images are representative of findings in three independent experiments.

PDS NP stability

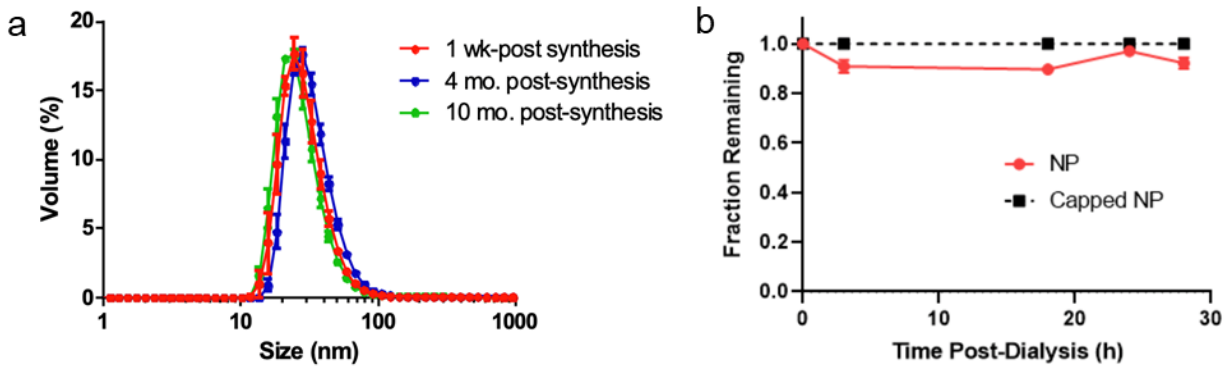

Supplementary Data Figure S8. PDS-NP size and Pluronic content is sustained with storage and in dialysis. a) Overlaid DLS traces of different storage times. n=3 samples per group. b) Calculation of the PDS capping over time. n=3 samples per group. For all graphs, the columns/points and error bars represent the mean + SEM.

Release studies of NP-OND-CpG

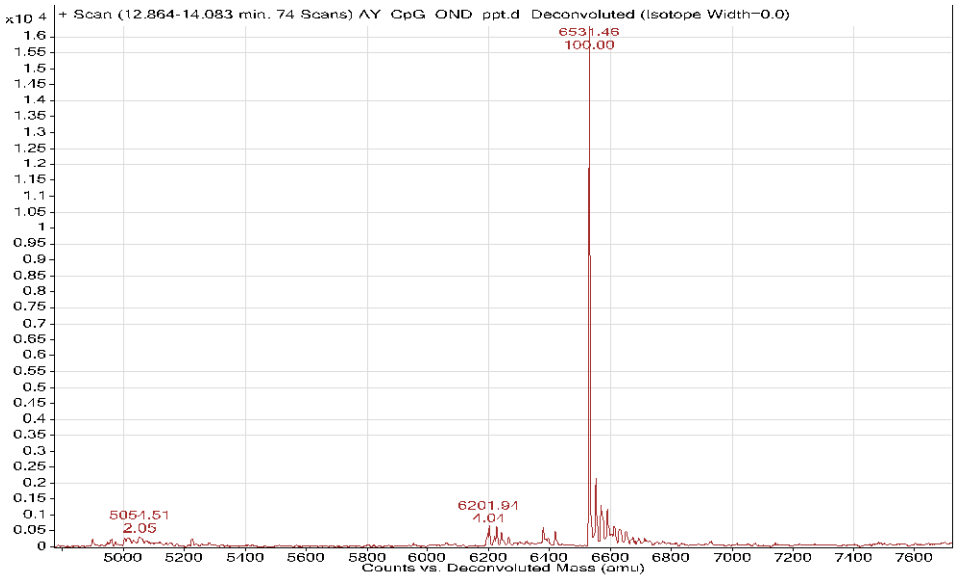

OND-CpG

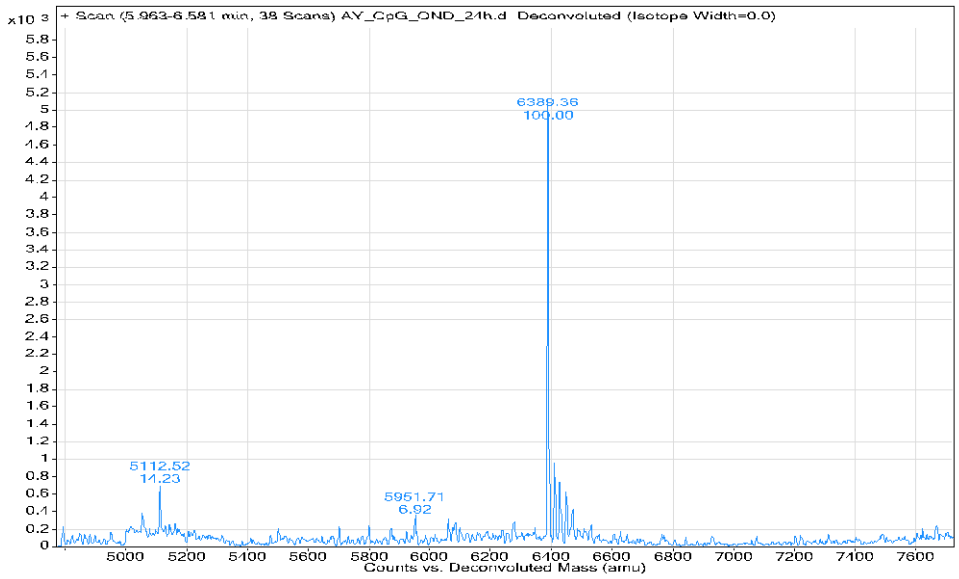

Furan-CpG

Supplementary Data Figure S9. Deconvoluted MS spectra of OND-CpG (top) and the released Furan-CpG (bottom) from NP after 24 hours incubation. LCMS conditions: Buffer A (0.1% NH4OAc in H_2O, pH 7.4), Buffer B (MeCN only), ESI-TOF (positive mode). This experiment was repeated once with similar results.

Graphical NMR spectra

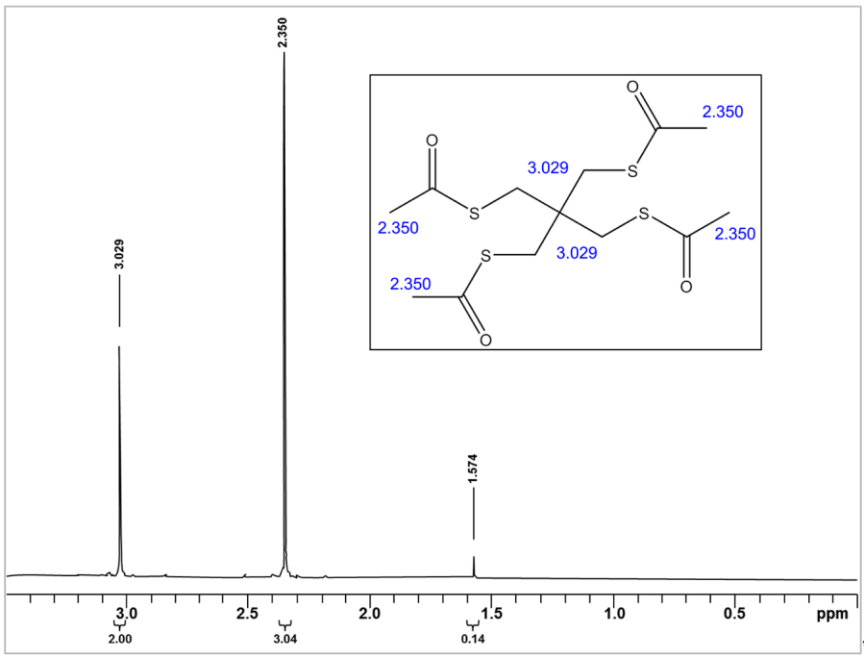

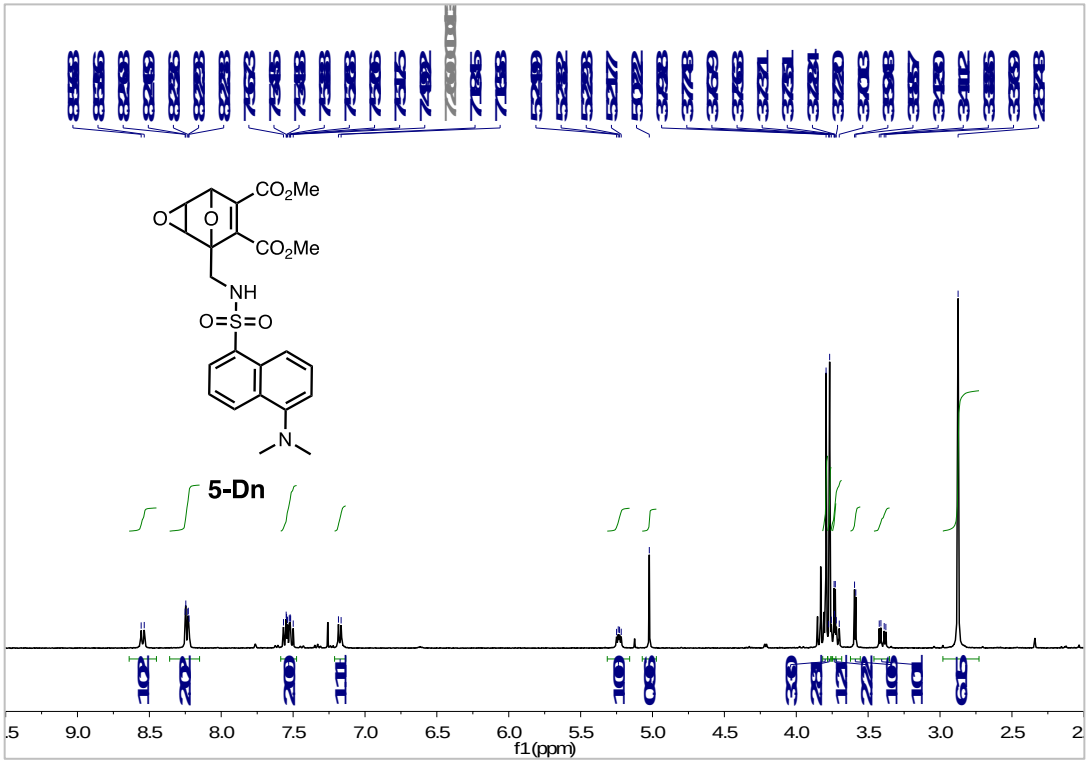

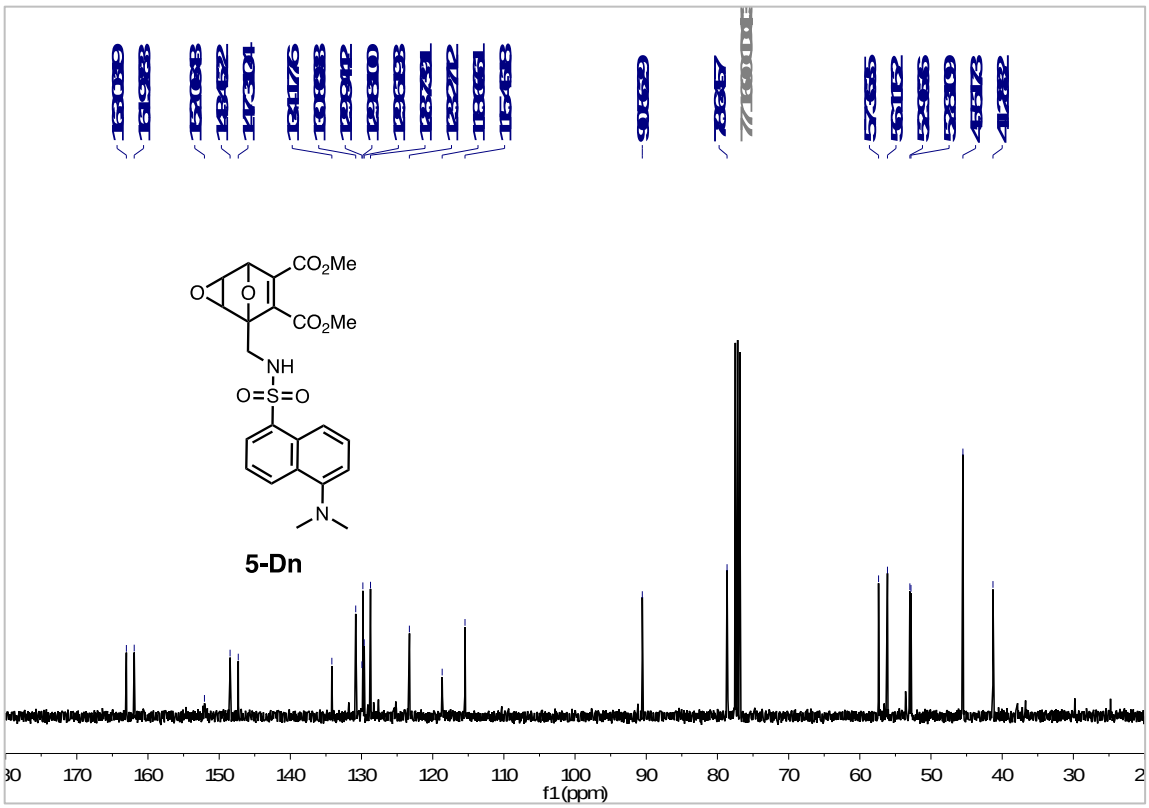
CO2Me
CO2Me
NH
O=S=O
N
5-Dn
f1(ppm)

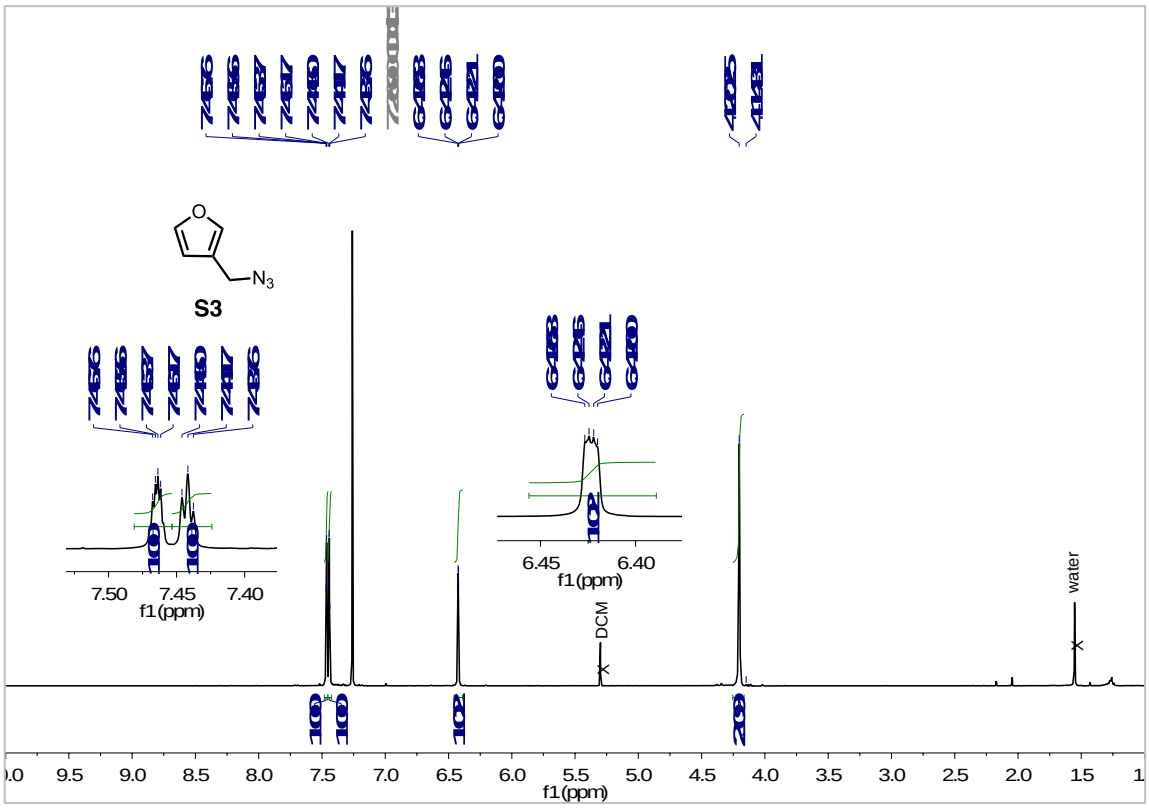
N3
S3
7.50
7.45
7.40
6.45
6.40
DCM
water
f1(ppm)

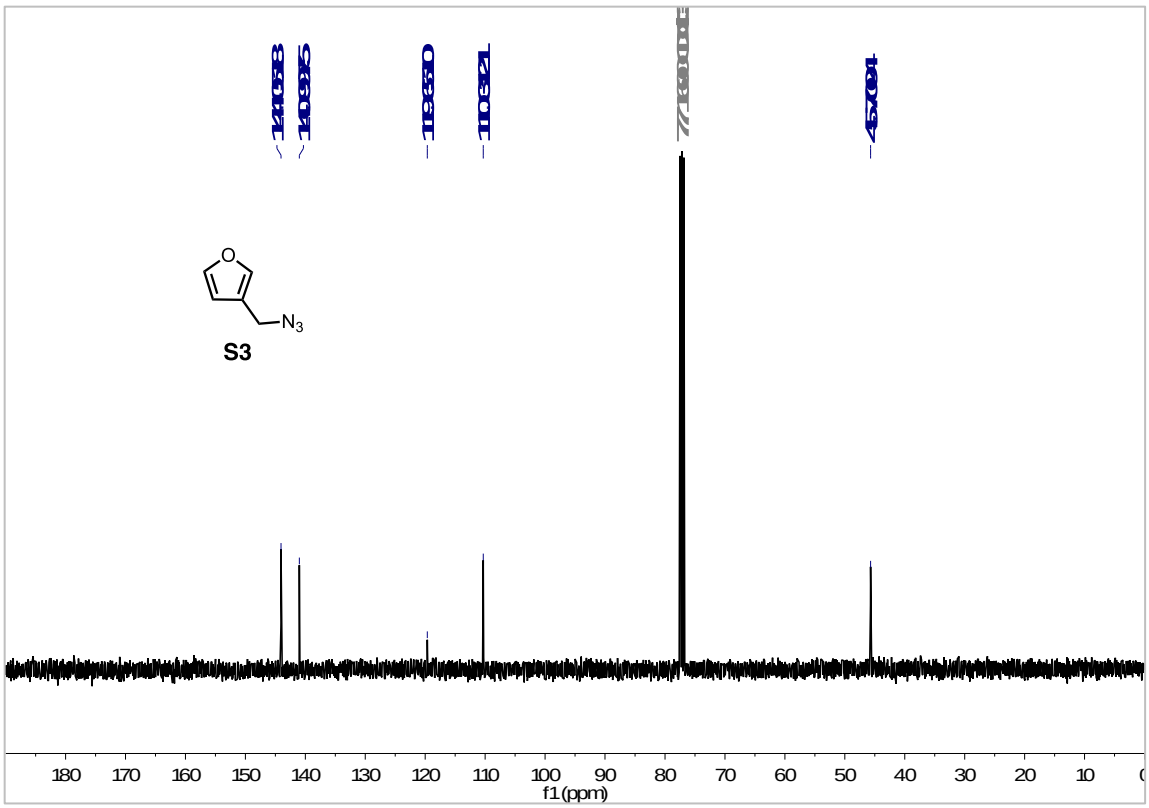
S3
f1 (ppm)

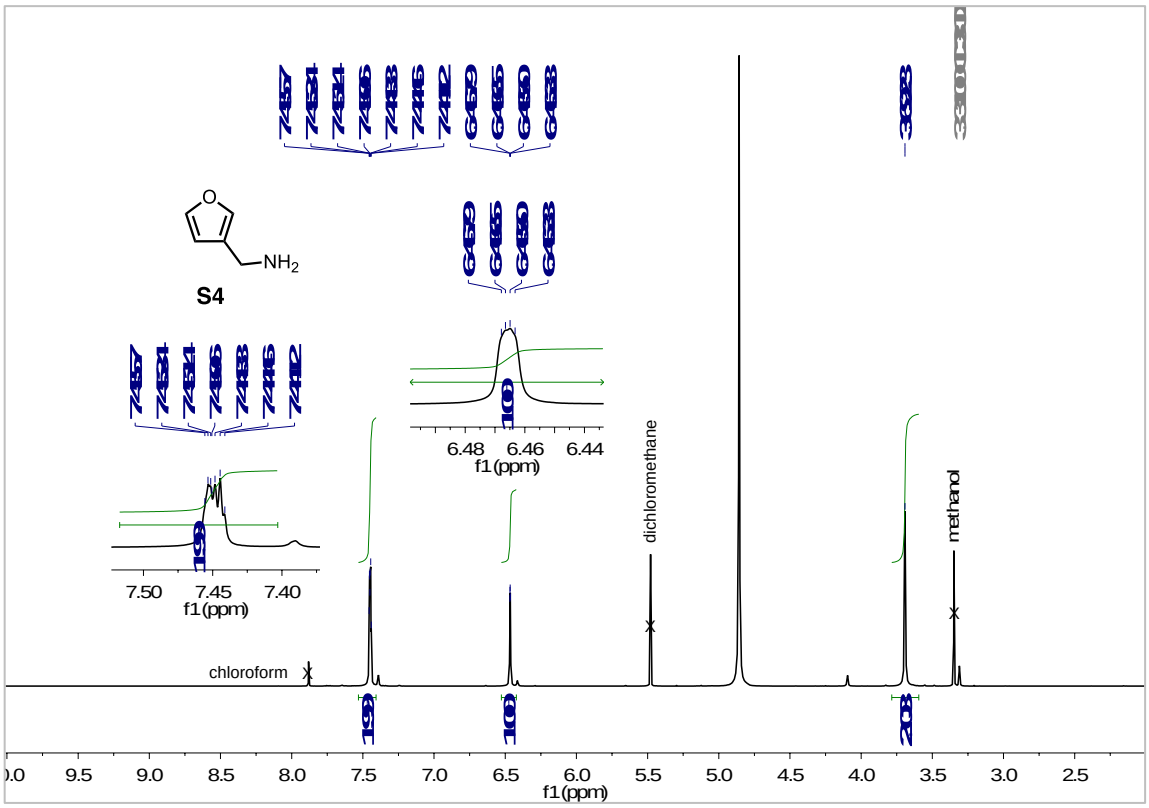
S4
chloroform
dichloromethane
methanol
f1 (ppm)

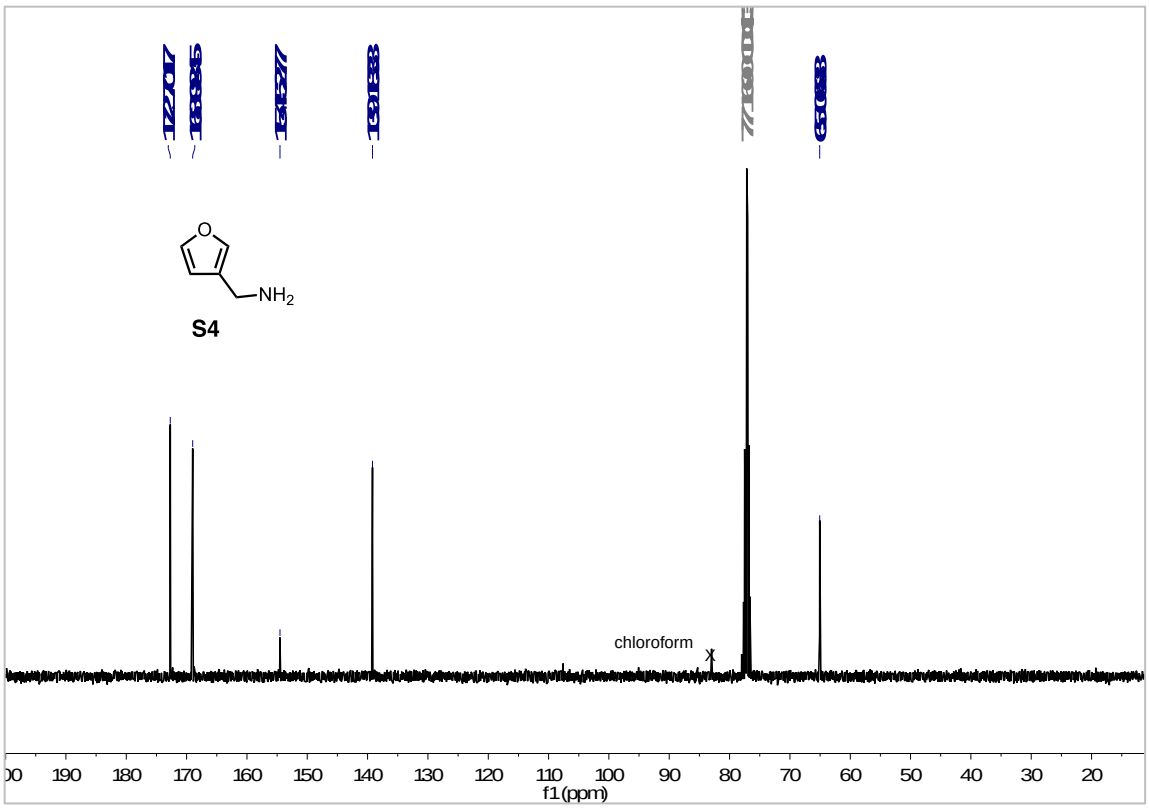
S4
chloroform
f1 (ppm)

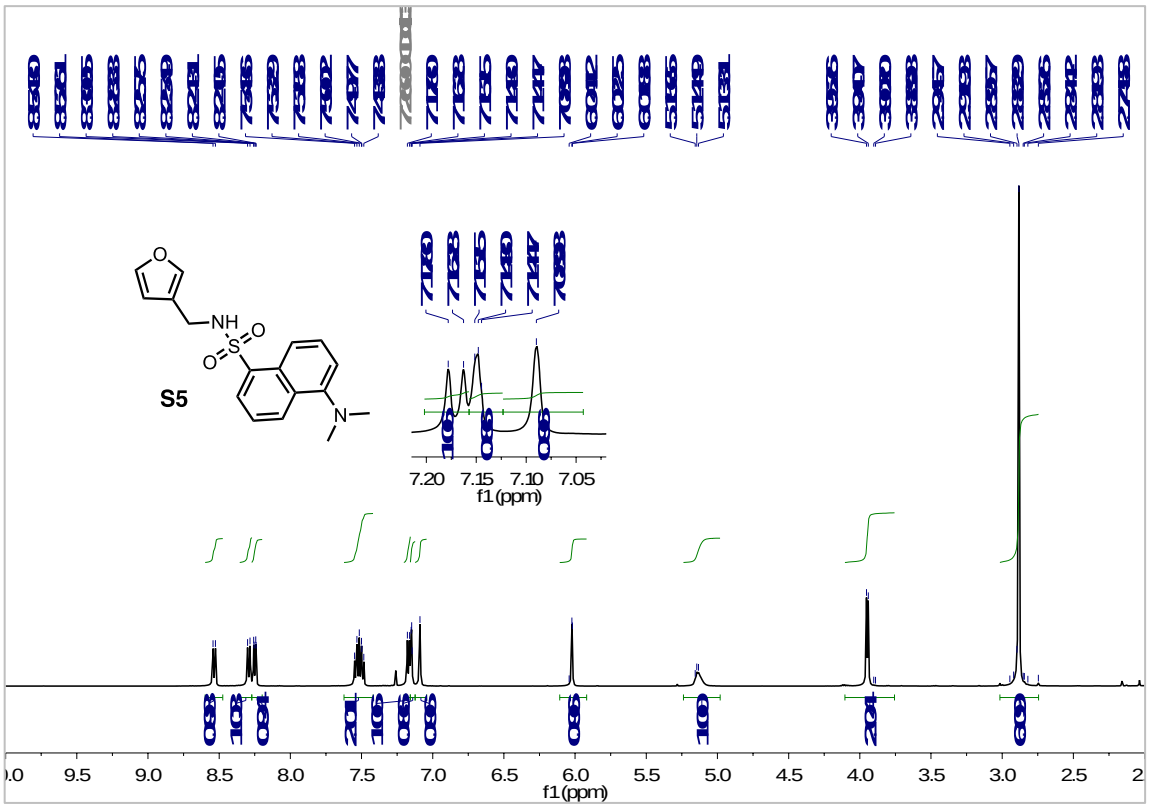
S5
f1 (ppm)

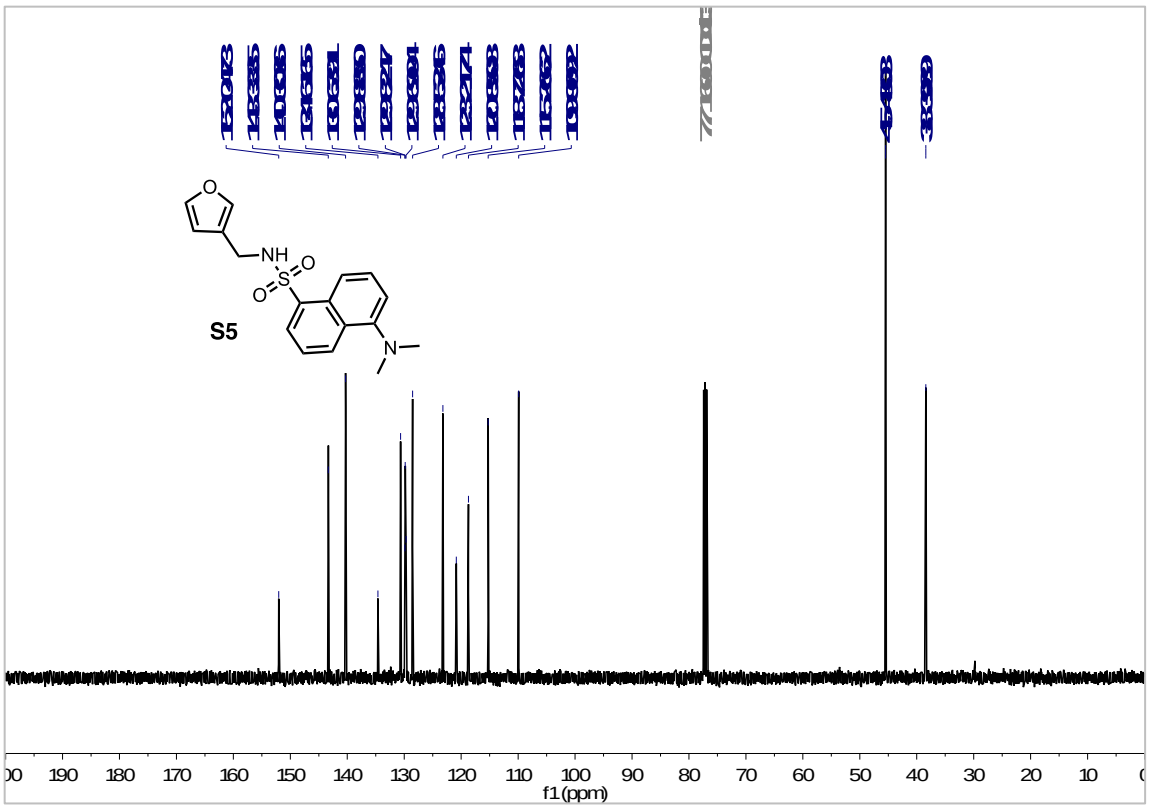
S5
f1(ppm)

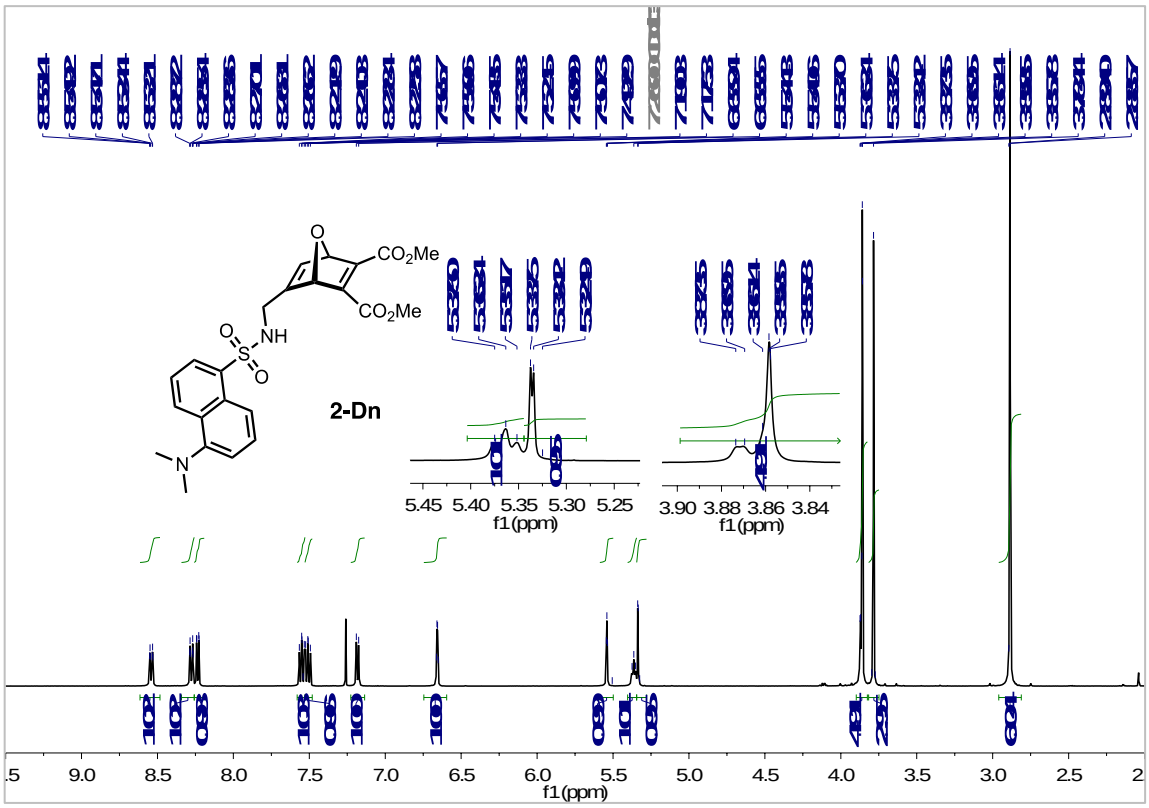
2-Dn
f1(ppm)
f1(ppm)
f1(ppm)

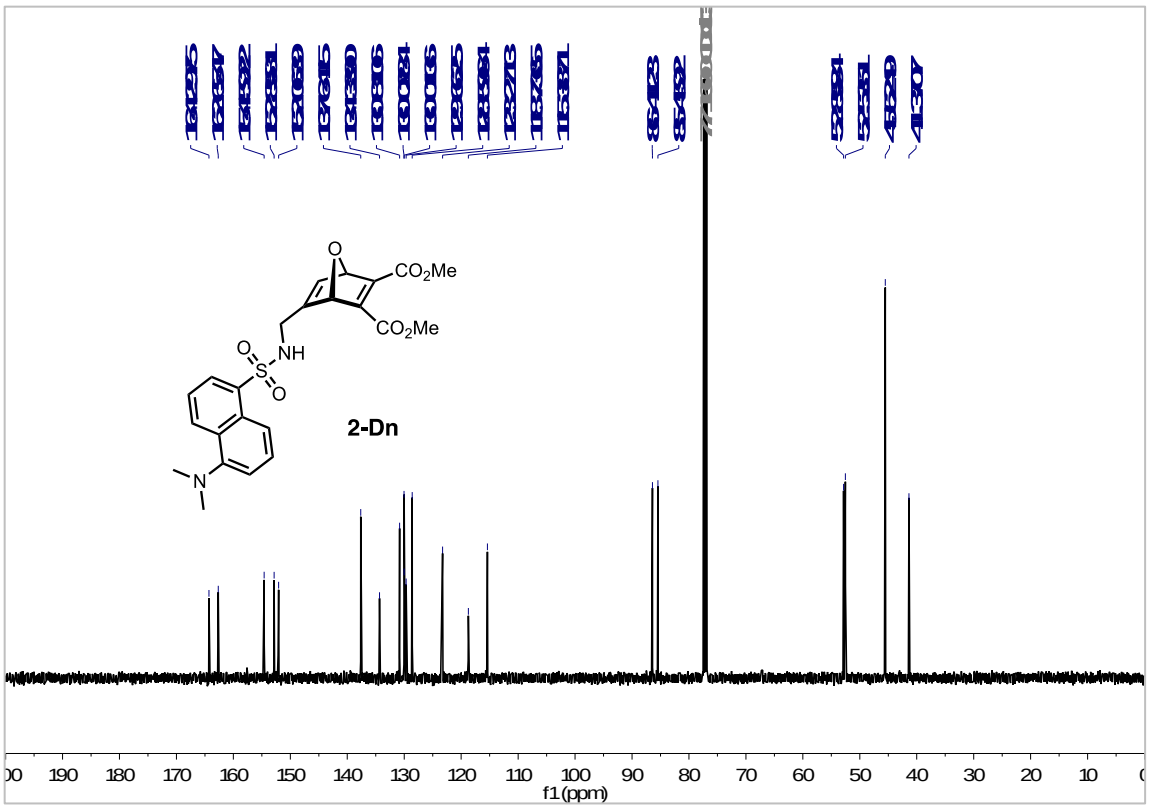
CO2Me
CO2Me
O
NH
S
O
O
N
2-Dn
f1 (ppm)

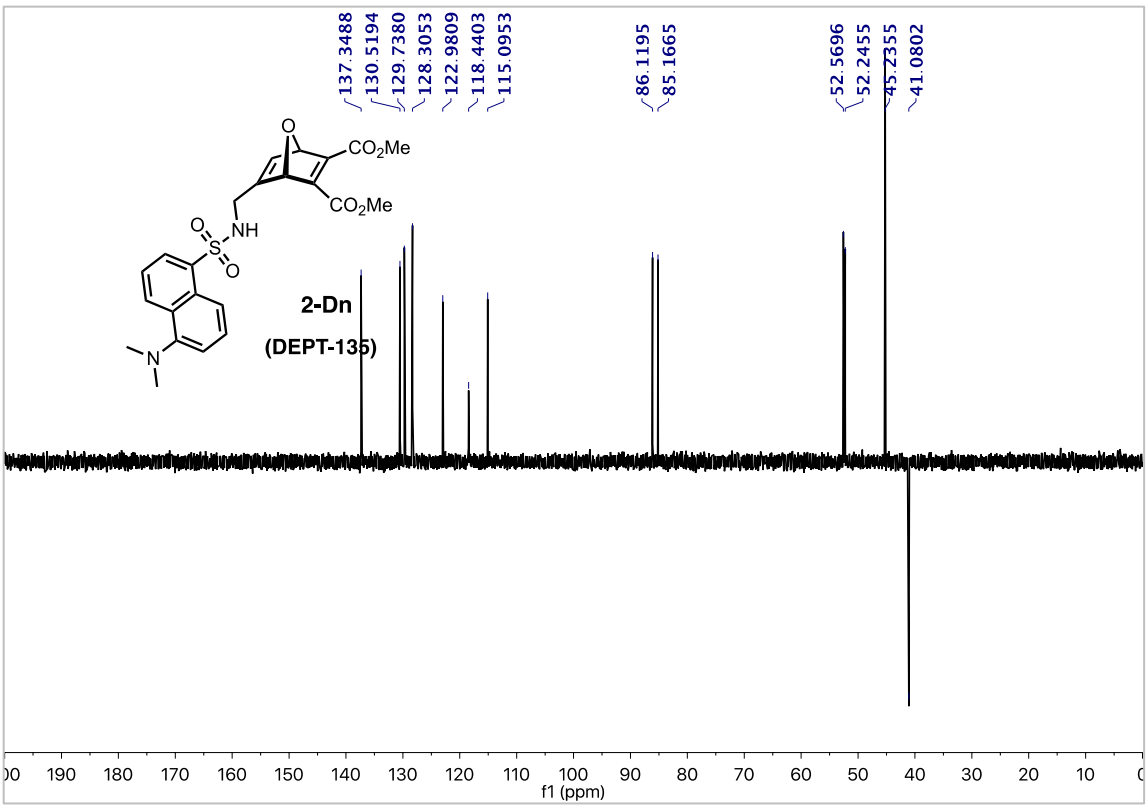
137.3488
130.5194
129.7380
128.3053
122.9809
118.4403
115.0953
86.1195
85.1665
52.5696
52.2455
45.2355
41.0802
CO2Me
CO2Me
NH
2-Dn
(DEPT-135)
f1 (ppm)

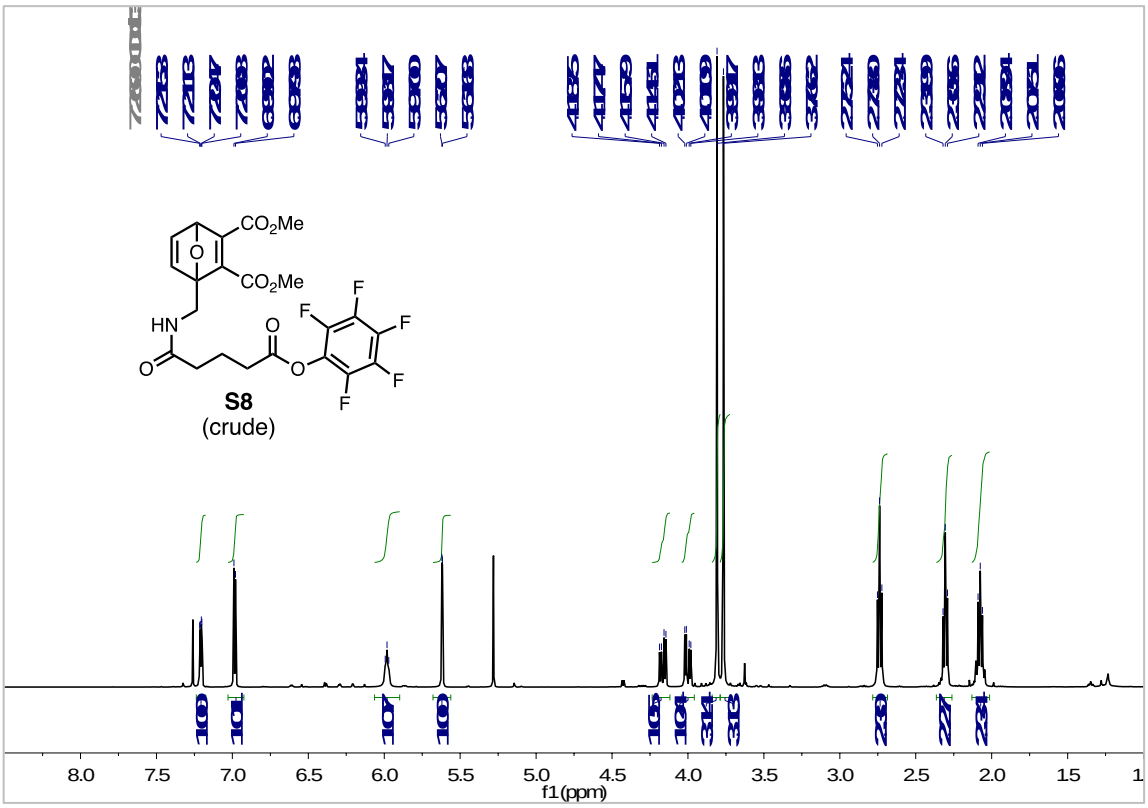
CO2Me
CO2Me
HN
F
S8
(crude)
f1(ppm)

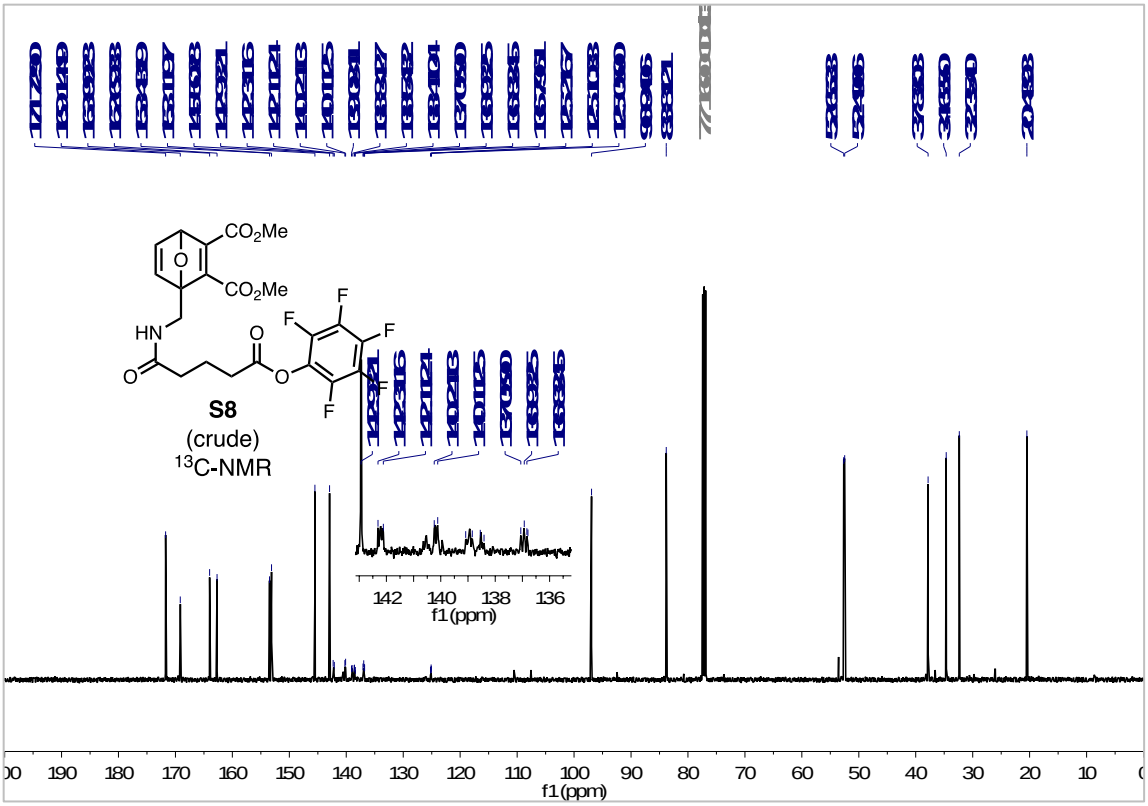
S8
(crude)
^{13}C-NMR
f1 (ppm)

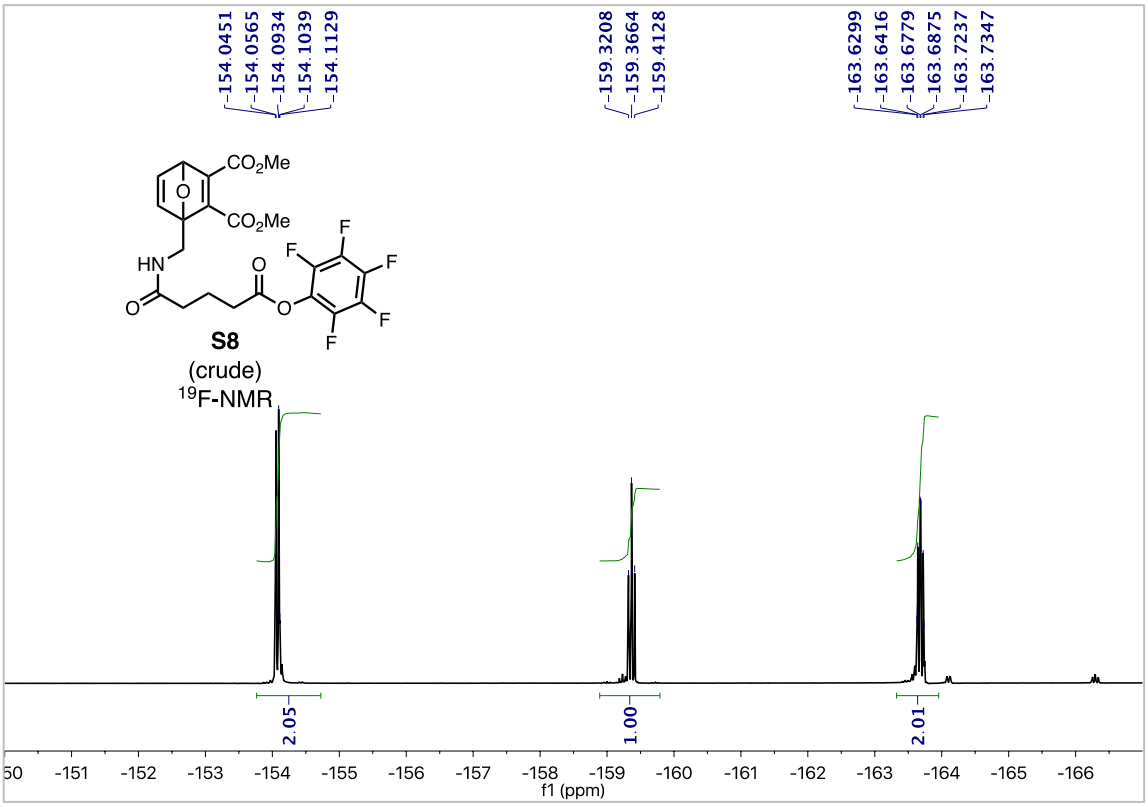
S8
(crude)
^{19}F-NMR
2.05
1.00
2.01
f1 (ppm)

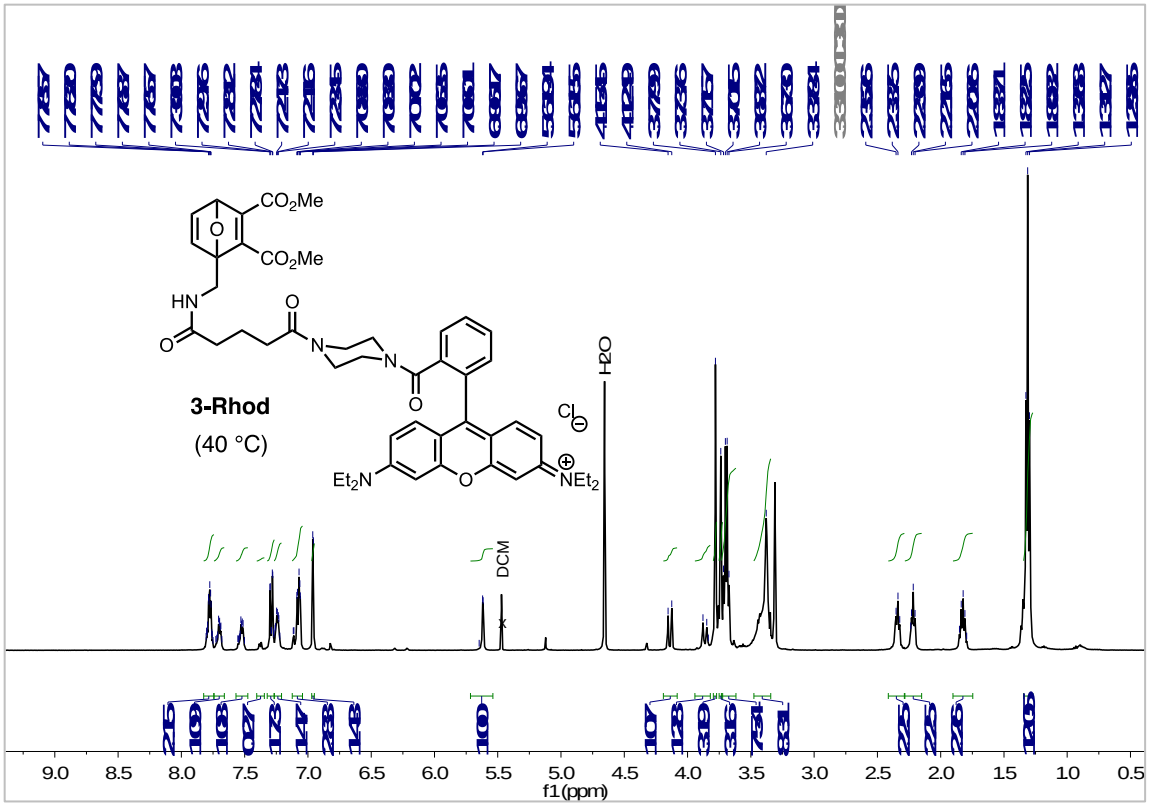
3-Rhod
(40 °C)
DCM
H2O
f1(ppm)

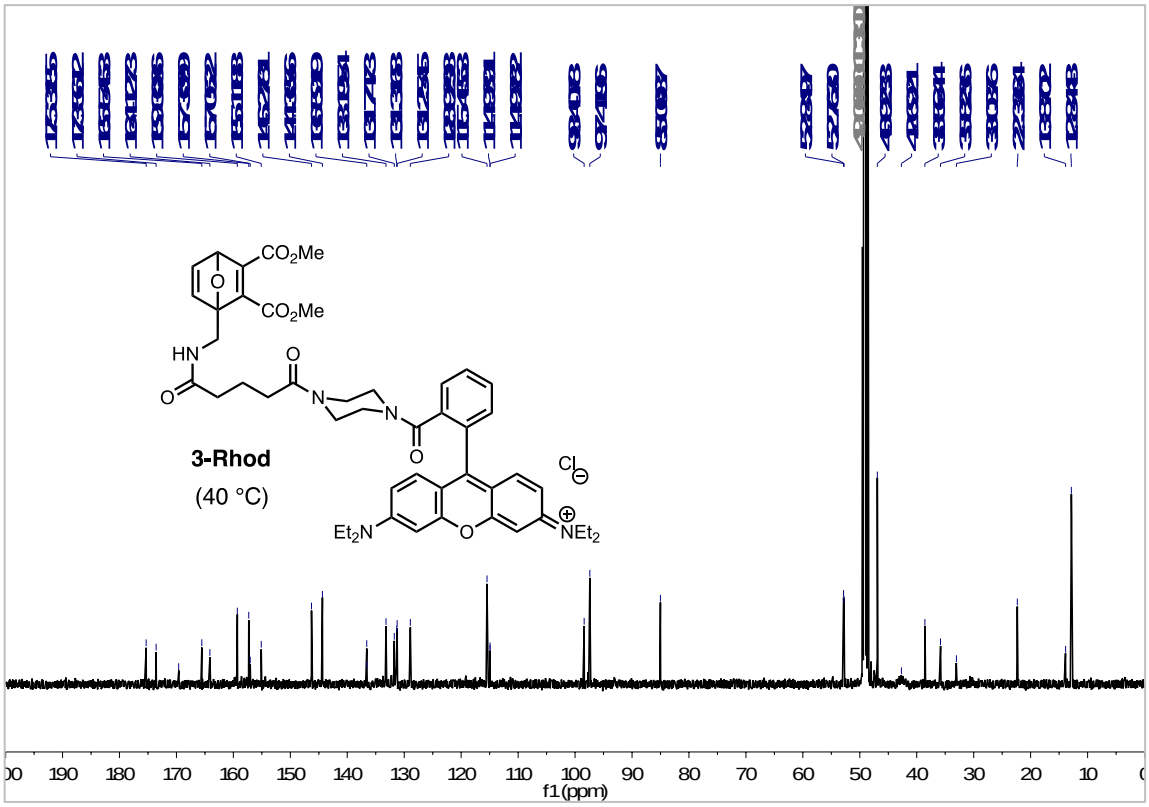
3-Rhod
(40 °C)
f1(ppm)

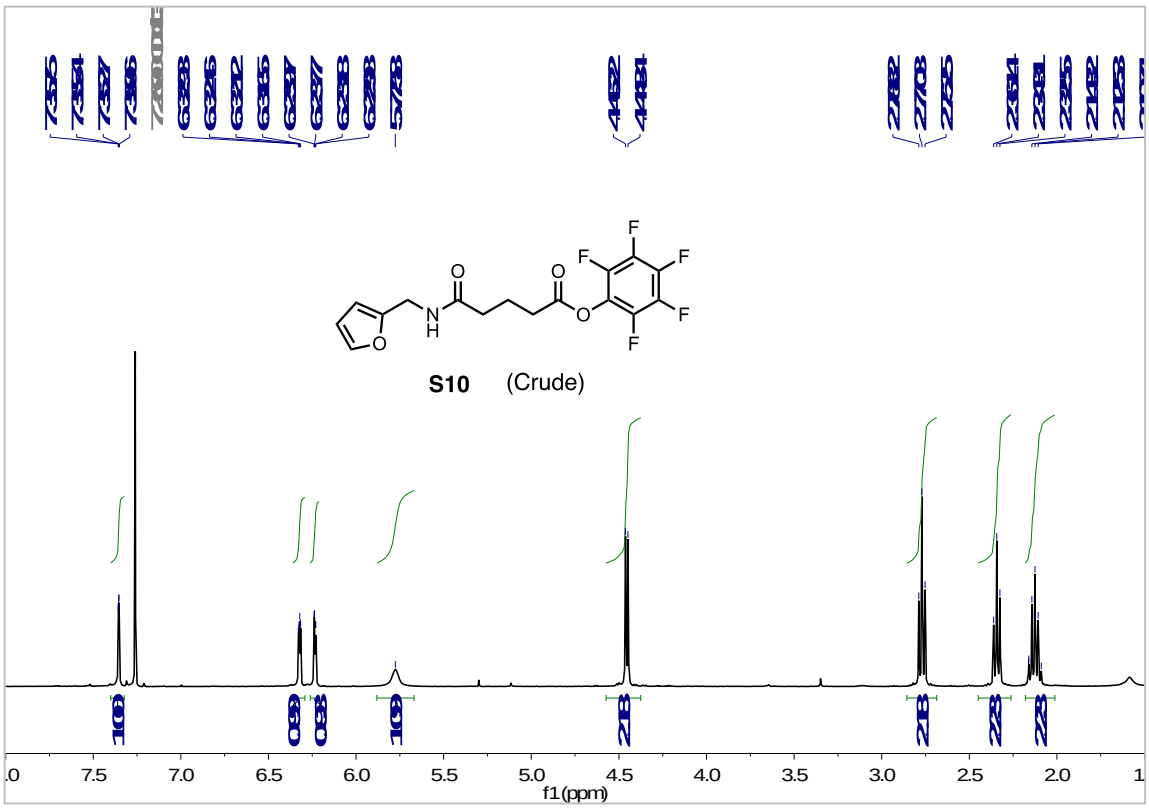
S10 (Crude)
f1(ppm)

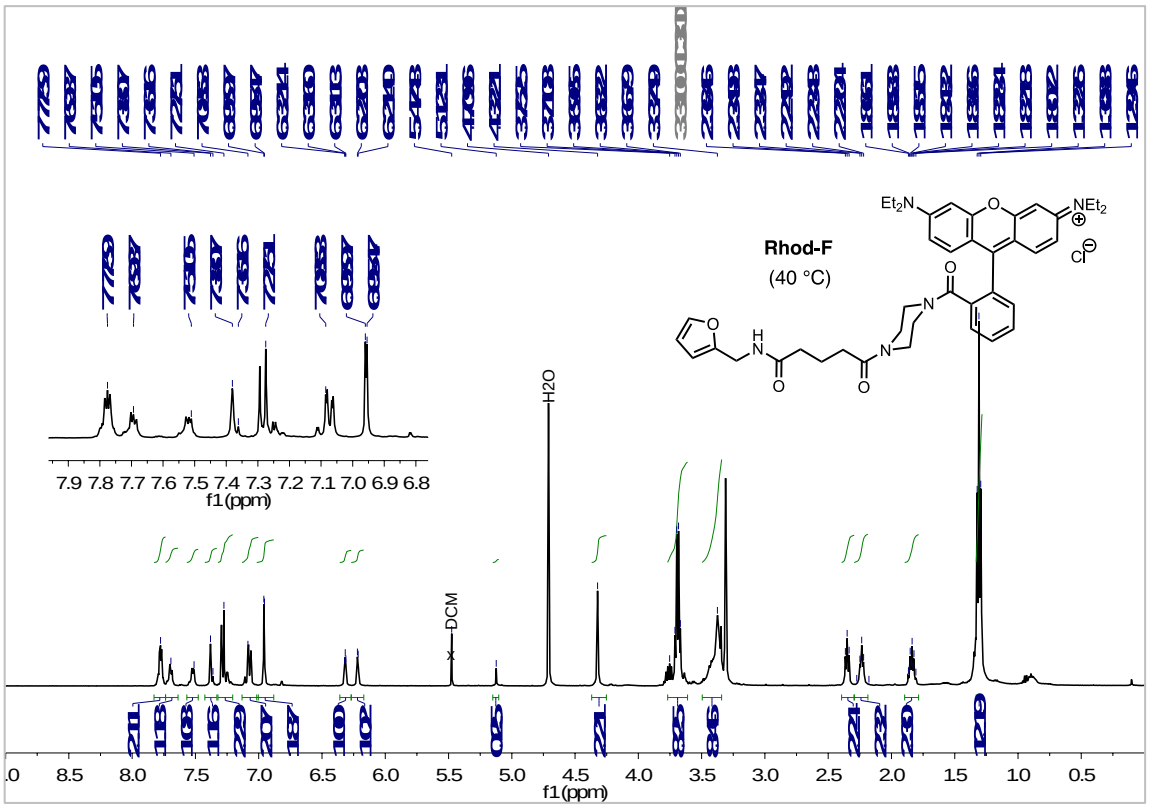
Rhod-F
(40 °C)
H2O
DCM
f1(ppm)

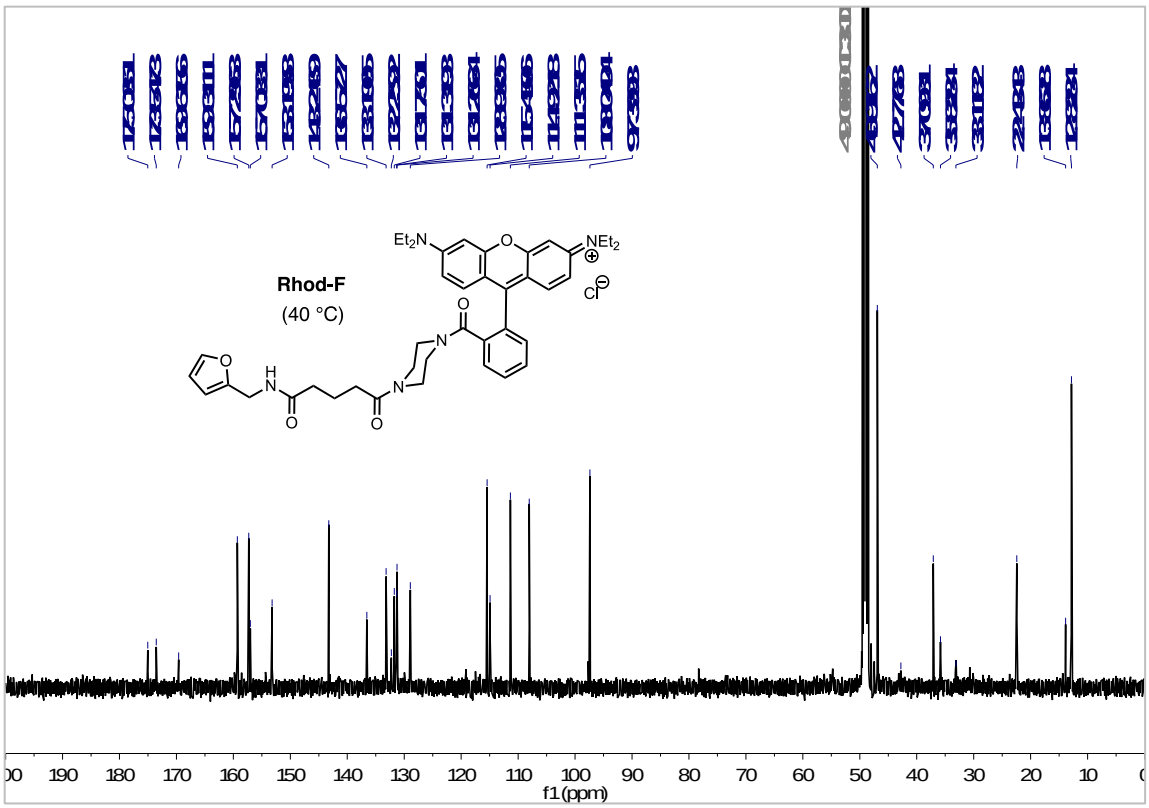
Rhod-F
(40 °C)
f1(ppm)

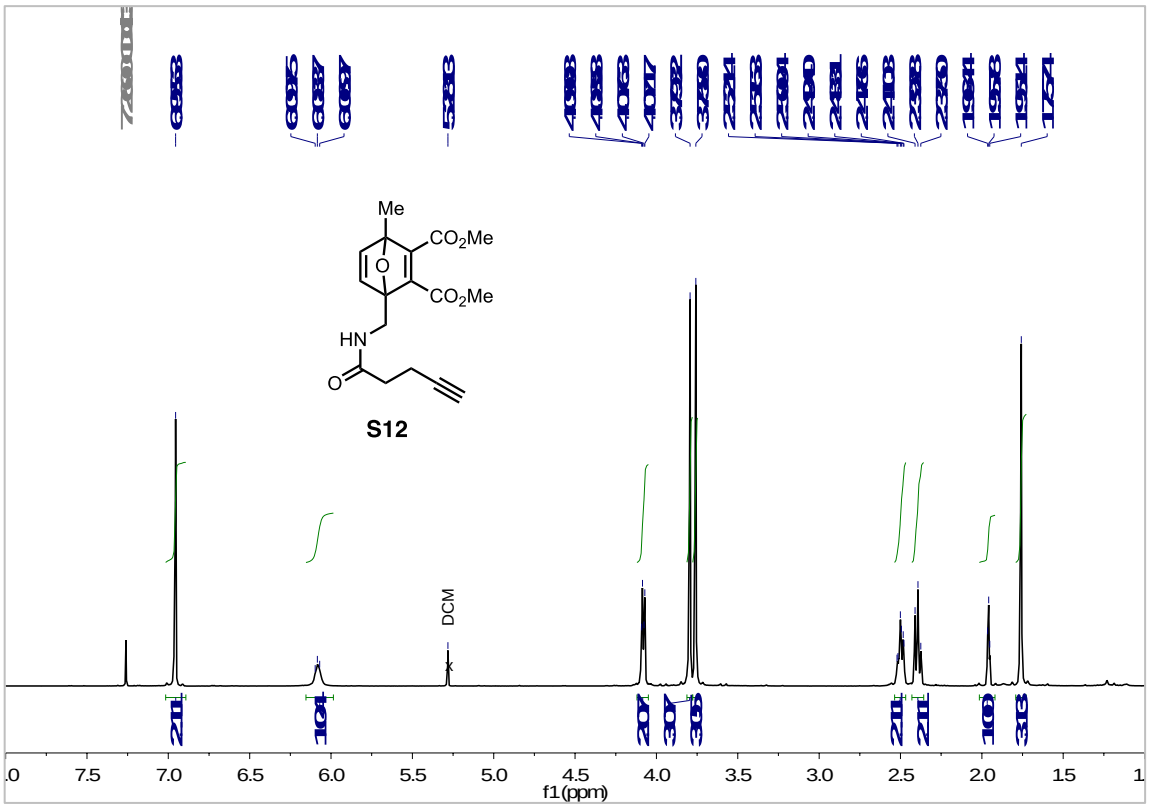
S12
DCM
f1(ppm)

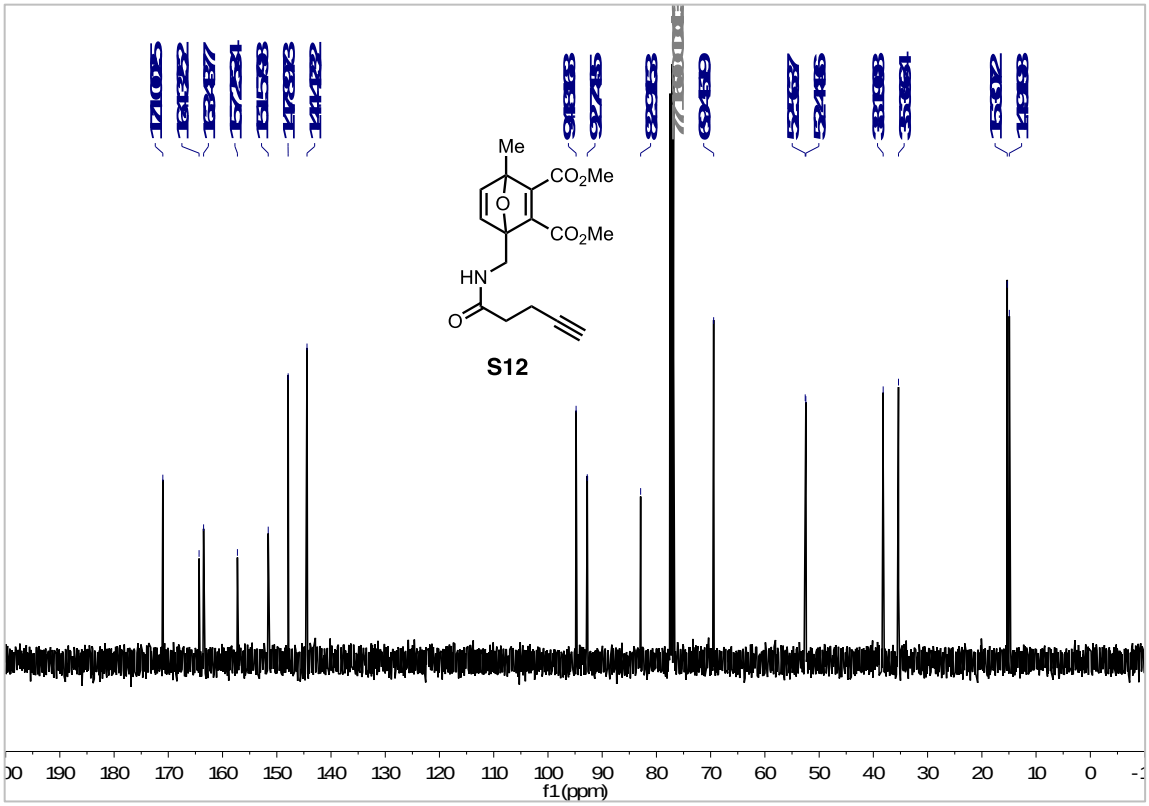
Me
CO2Me
CO2Me
HN
O
S12
f1 (ppm)

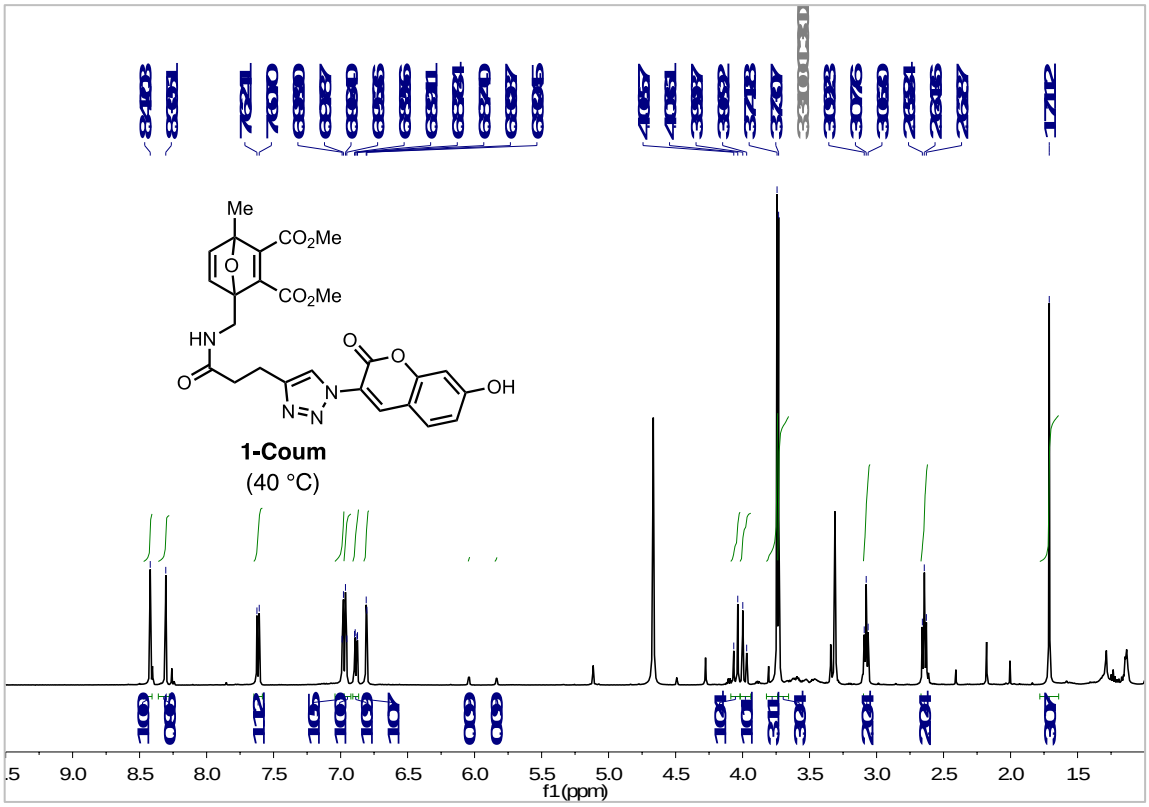
Me
CO2Me
CO2Me
HN
O
N
N
OH
1-Coum
(40 °C)
f1 (ppm)

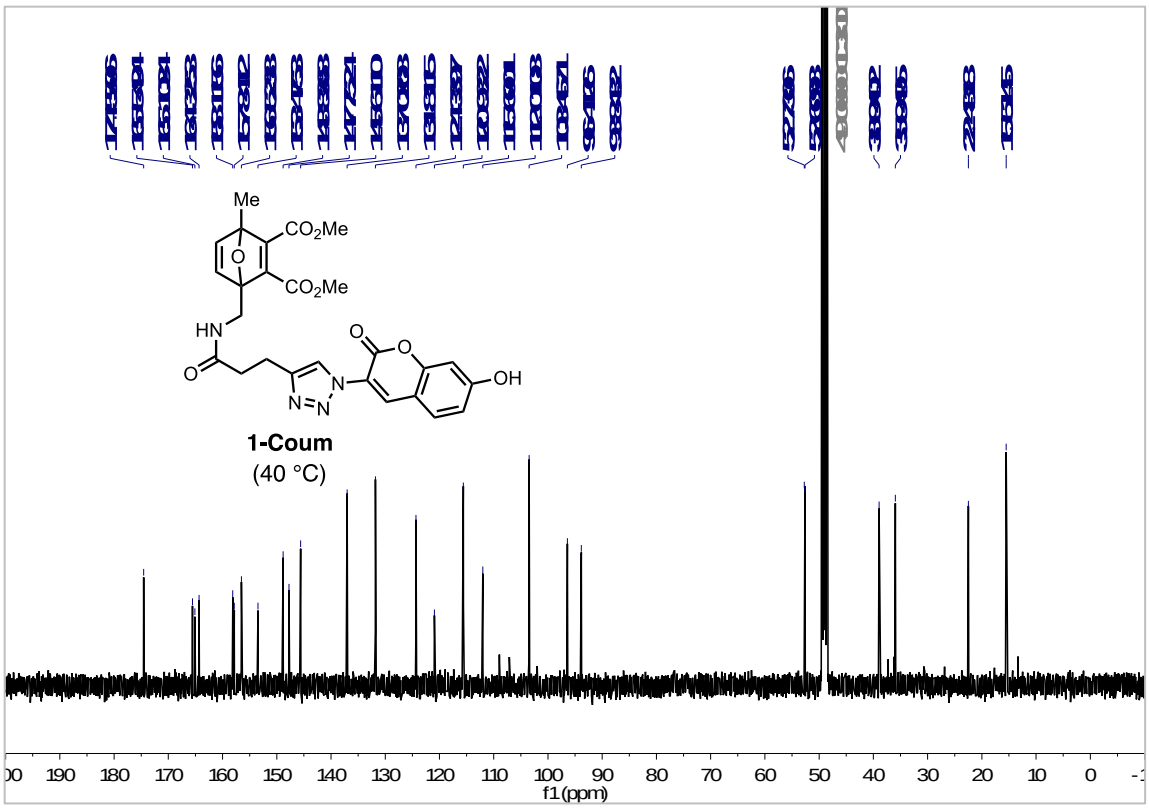
Me
CO2Me
CO2Me
O
HN
O
O
O
N
N=N
OH
1-Coum
(40 °C)
f1 (ppm)